Model-Predictive Control for Alleviating Transmission Overloads and Voltage Collapse in Large-Scale Electric Power Systems

by

Jonathon A. Martin

A dissertation submitted in partial fulfillment
of the requirements for the degree of
Doctor of Philosophy
(Electrical Engineering: Systems)
in the University of Michigan
2017

Doctoral Committee:

Professor Ian A. Hiskens, Chair
Professor Daniel Kirschen, University of Washington
Assistant Professor Johanna Mathieu
Professor Pascal R. Van Hentenryck

Jonathon A. Martin

jandrewm@umich.edu

ORCID iD: 0000-0003-0611-7624

Dedication

To Amanda.

For causing me to smile when I need it most.

For sharing my excitement when I learn something new.

For encouraging me to reach my goals.

Acknowledgements

I am immensely grateful to all the family, friends, mentors, and teachers who have influenced my educational journey. Their support, encouragement, and guidance provided the motivation and confidence to pursue this milestone work.

I would like to thank my research advisor Professor Ian Hiskens for his willingness to take me on as a member of his team. His direction, leadership, and technical insight provided a path for investigating the topics discussed in this work. His care as a mentor provided the confidence to venture down that path.

I am also grateful to the members of my committee, Professors Daniel Kirschen, Johanna Mathieu, and Pascal Van Hentenryck. Their suggestions and feedback strengthened and honed my studies. I appreciate their willingness to join this endeavor and offer their unique insights.

I must also thank Professor Mads Almassalkhi for his pioneering work in this project. His high-quality investigation of these model-predictive control ideas during his doctoral degree provided the strong foundation upon which my work develops.

I have been exceedingly blessed with educators who have demonstrated excellence and passion in their teaching at all stages of my academic journey. Numerous instructors have taken time outside outside the classroom to shape my development as an individual. They have taught me the value of connecting ideas in the classroom to real-world issues. They have instilled a commitment to life-long learning.

I am also very thankful for my parents Nelson and Carol Martin for their love and support. From the beginning, they directed my energy toward constructive ends, and taught me the value of the relationships I would develop along my educational journey.

Many more specific individuals certainly deserve appreciation for the role they have played in my reaching this point. While I cannot list them all here, I can acknowledge that the ideas here resulted from many fruitful conversations. Additionally, the grit and determination to continue searching for answers in the face of obstacles is due to the network of support surrounding me.

Lastly, I am grateful to the Department of Energy and National Science Foundation for providing the financial means to pursue this work.

Table of Contents

List of Tables

List of Figures

Abstract

Emergency control in electric power systems requires rapid identification and implementation of corrective actions. Typically, system operators have performed this service while relying on rules-of-thumb and predetermined control sequences with limited decision support tools. Automatic control schemes offer the potential to improve this process by quickly analyzing large, complex problems to identify the most effective actions. Model-predictive control (MPC) is one such scheme which has a strong record of success in the process industry and has begun receiving attention in power systems applications.

Incorporating flexibility into the MPC model using energy storage and temperature-based transmission line limits has shown promising results for relieving transmission overloads on small networks with linear active power models. Separately, MPC has demonstrated its capabilities in correcting transformer-driven voltage collapse behaviors. However, a comprehensive solution combines both aspects into a single controller formulation with knowledge of active and reactive power and voltage magnitude and angle. Additionally, most power system networks are large and result in computationally challenging problem formulations. This work considers these practical limitations and suggests techniques to enable an MPC process capable of operating reliably in the real-world.

A new linear controller model is proposed which considers voltage magnitude and angle and both active and reactive power. The new model provides greater accuracy when predicting system behavior and better identifies the actual control needs of the system. The problem size is reduced by limiting the model to only those devices which are significantly affected by the emergency conditions. The new approach is shown to identify controls more rapidly and better suppresses undesirable thermal behavior on overloaded transmission lines while avoiding potential voltage collapse situations.

Chapter 1

Introduction

1.1 Motivation

Access to affordable, dependable electricity has become a basic assumption in industrial nations. Daily life depends on electricity to operate smoothly, and any disruptions to the electric supply significantly influence all parts of the economy [3]. This condition implies great risk in the case of failure, but it also implies amplified benefits resulting from improvements in cost and reliability.

Power system operation respects this risk/reward tradeoff by balancing two key features, economy and reliability. Legacy power systems emphasized reliability as utilities coordinated generation, networks, and loads [4]. Recent shifts toward market-based operation have enhanced the economy of the electricity supply but strained the ease of ensuring reliability [4]. This conflict creates a rich environment for ongoing research and development, especially as the energy supply transitions from large centralized sources to smaller distributed sources.

Computation, communication, and sensing technologies have also experienced massive improvements, enabling calculations to occur more rapidly. This reduces errors by shifting analysis closer to real-time and using measured conditions rather than predicted conditions. Computing advances also enable more complex modeling calculations which better match reality. Combining these improvements enhances control fidelity which boosts both economy and reliability through more accurate operation of the network.

Leveraging these technological changes to improve power system economy and reliability motivated this work. Through funding provided by the Advanced Research Projects Agency - Energy (ARPA-E), a joint project with University of Michigan and University of Washington was developed to investigate potential benefits of positioning energy in the electric grid both geographically and temporally using energy storage. A

technique to site and size potential energy storage devices was developed to reduce transmission congestion and operating costs. Once proposed devices were added to the network, operational features were investigated to validate and assess the economic and reliability implications. A tri-level approach was proposed to provide unit commitment, economic dispatch, and corrective control while considering the temporal characteristics of energy storage to provide reliable, low-cost operation of the network [5].

The work presented here continues the development of the corrective control process based on *Model-Predictive Control* (MPC) theory. By redispatching traditional and renewable generation, energy storage, demand response, and voltage regulation, MPC seeks to relieve thermal rating overloads on transmission lines and unacceptable voltage deviations resulting from network contingencies while respecting devices limits and the physics of power flow in an electric power system. These dynamic processes require several minutes to reach steady-state conditions, enabling the use of a centralized control framework.

The initial formulation of this controller was based on a simplified linear model of the power flow equations which ignored voltage magnitude and reactive power [6, 7]. Early testing also only considered small networks [8]. This work has extended the controller design to account for voltage magnitude and reactive power and to consider the application challenges that arise with implementation on large networks. Ultimately, this practical control process unlocks flexibility in power systems inaccessible to a human operator. While the work here assumes automatic operation it could also be adapted to provide decision support to a human operator pursuing the same objective of restoring a power system to a secure operating condition. This analysis has opened up a variety of interesting research questions, some of which are investigated here.

1.2 Background

Understanding the basics of current power system operation highlights how this research expands on current practice. No single operational standard is applied universally in power systems. *Regional Transmission Organizations* (RTOs) each have developed their own best practices and methods based on decades of practical experience. Although inefficiencies exist in these best practices, most of the ideas have been shown to work quite well. Even without a detailed operational standard, many common characteristics can be identified as different RTOs must satisfy similar requirements and regulations.

1.2.1 Power System Security

One common characteristic in power system operation is the emphasis of reliability first and economy second. Much of the equipment used to operate the grid is very expensive and difficult to replace. Significant catastrophic failure of this equipment could cripple regional economies as replacement can take months [9].

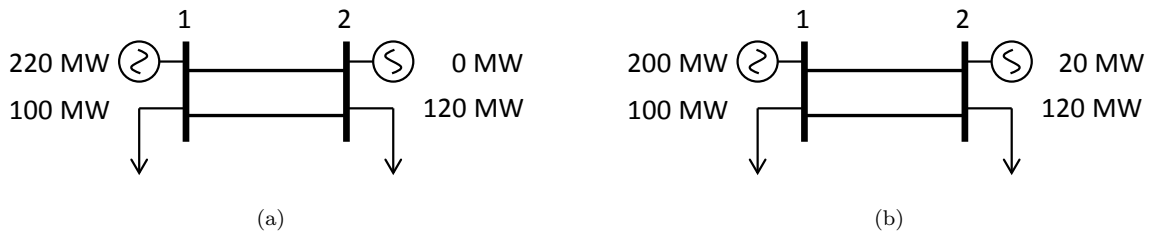

Figure 1.1: The generation dispatch minimizes costs while ensuring N-1 reliability. (a) Cheapest unreliable solution requires transmission of 120 MW. (b) Cheapest reliable solution requires transmission of 100 MW.

Common engineering practice in this type of situation incorporates safety factors into the design. Reasonable failure methods are considered during the design process and the final solution is created to exceed the minimal requirements for safe operation by some safety factor margin. In power systems, allowable voltage ranges are specified at different points in the network to protect equipment from undo stress. Similarly, power ratings are defined to keep equipment from overheating and losing important structural material properties. This system is also operated so that the loss of any single network element (e.g. transmission line, transformer, generator) will not harm the system. This has come to be known as the N-1 reliability standard.

While this safety factor concept is vitally important, the implementation method has some flexibility. Traditionally, N-1 reliability is implemented through preventive measures. When scheduling generation to meet the forecasted demand, the potential contingencies are also considered. The power dispatch is scheduled so that any single contingency (i.e. the loss of a single network element) will not violate the predetermined voltage and power limits. This allows the system to continue operating securely without intervention if one of the considered contingencies occurs. However, this added security may increase the cost of the energy provided.

Example: cost of security

The added cost of security is easily demonstrated through a simple example. Consider a lossless two bus network shown in Figure 1.1. The two generators must be scheduled to supply the system loads while satisfying reliability requirements. The loads at buses 1 and 2 demand 100 MW and 120 MW, respectively. Either generator could individually satisfy the total demand, but they use different fuel sources. Generator 1 provides energy at \$50/MWhr and Generator 2 costs \$70/MWhr. The cheapest possible dispatch is shown in Figure 1.1a where Generator 1 supplies the entire load at a cost of

$$50\left[\frac{\$}{MWhr}\right] * 220[MW] = 11,000\left[\frac{\$}{hr}\right]. \tag{1.1}$$

However, preventive N-1 reliability requires a dispatch that can handle losing one of transmission lines without requiring adjustments. Each of the two lines is individually rated to carry 100 MW. If one of the lines is lost under the dispatch of Figure 1.1a, the other line would be carrying 120 MW of power and exceed its rating by 20 MW. Therefore, 20 MW of generation must be shifted to the more expensive Generator 2 for a total cost of

$$50\left[\frac{\$}{MWhr}\right] * 200[MW] + 70\left[\frac{\$}{MWhr}\right] * 20[MW] = 11,400\left[\frac{\$}{hr}\right]. \tag{1.2}$$

Under this preventive dispatch, shown in Figure 1.1b, only 100 MW is transmitted across the network. The added cost for this security is \$400/hr, a 3.6% increase over the insecure case.

Alternatively, N-1 security could also be achieved through a corrective strategy instead of a preventive one. Transmission lines possess thermal inertia which allows them to experience power overloads for short periods of time before reaching unsafe temperatures. In this example, both lines have a 30 minute short-term emergency rating of 120 MW. This means they can carry 120 MW of power for 30 minutes before they must return to their normal 100 MW rating. Generator 2 is able to change its power output by 40 MW/hr and is willing to provide reserve capacity at \$5/MW to ensure that the line loading is reduced by 20 MW within 30 minutes.

The system is then dispatched as shown in Figure 1.1a but with Generator 2 guaranteeing 20 MW of standby capacity each hour if it is needed for a total cost of

$$50\left[\frac{\$}{MWhr}\right] * 220[MW] + 5\left[\frac{\$}{MW}\right] * 20\left[\frac{MW}{hr}\right] = 11,100\left[\frac{\$}{hr}\right]. \tag{1.3}$$

Under this approach, the security adds a cost of \$100/hr, a 0.9% increase over the insecure case. Using a corrective rather than preventive strategy results in a savings of \$300/hr or 2.6% with the same guarantee that the system will operate without damaging equipment or disrupting consumers following the loss of a transmission line.

When implemented on a realistic system, these incremental cost improvements can have a significant impact. Modern dispatch software has the ability to schedule markets using some combination of preventive and corrective measures, but the vast majority of operation occurs in preventive mode [10]. PJM, a major RTO in the Northeast United States, estimates that preventive N-1 security adds millions of dollars in costs annually. However, the probability that one of these contingencies occurs while requiring a more expensive dispatch to satisfy limits is less than 0.05% [11]. With such a low probability of contingent events occurring, corrective control strategies become desirable as long as they operate reliably when called upon.

To attain these cost savings, PJM has implemented a corrective strategy for specific transmission lines in its network. However, very stringent requirements must be met before a line can be controlled in this way. For example, more than enough reserve must be available and generators must have a strong track record of successfully providing reserves as required. Additionally, lines operating at very high voltages, over 345 kV, are not eligible for this type of control as they are more critical to the network [11].

Consequences of insecure operation

The ratings and limits describing safe operating regions in power systems are defined by two main considerations, protective device operation and the dynamic response to network disturbances. Protective devices (e.g. relays, fuses, and circuit breakers) are primarily designed to protect physical equipment from damage. Operation of these devices typically results in equipment being abruptly disconnected from the rest of the system. System dynamics are based on the physical properties of the network. After a disruption, states fluctuate over time until reaching a new equilibrium. This equilibrium may cause protective devices to operate and initiate new fluctuations. Ratings and limits are designed to prevent the system from reaching these undesirable equilibria.

In some cases, operating outside of limit specifications could cause a single disturbance to initiate a cascade of events eventually leading to black-outs in portions or all of the network. In the example of the previous section, operating at the insecure dispatch and losing a transmission line causes an overload on the remaining line. If the overload is sustained long enough, the line will overheat. A protective relay may sense high temperatures and disconnect the line, or the line may sag until it short-circuits on vegetation and is disconnected by an over-current relay. At this point, the load is no longer connected to generation and black-out occurs. Though great care is taken to avoid these types of situations, cascading outages occasionally occur. For example, the 2003 black-out in the Northeast United States initiated in the Midwest and propagated eastward [12]. The repercussions of this event were costly with restoration taking up to four days and total expenses including lost revenue estimated in the range of $4-10 Billion [12].

Voltage control is also a common consideration when defining power system limits. To enable active power flow throughout the network, reactive power must be available to regulate voltages. Generators are significant suppliers of voltage support and reactive power, and it is important that they maintain sufficient reactive power reserves to continue regulating voltages as conditions change. However in heavy load situations, losing a transmission line or generator can cause losses to increase and voltages to drop. Transformers may begin adjusting their taps to restore load voltages which decreases transmission voltages further. As generators attempt to maintain their voltage setpoints, their reactive power reserves are exhausted and their voltages begin to drop. Eventually, voltages drop so low that protective relays disconnect generation from the rest of

the network and black-out occurs.

Regardless of the mechanism driving system instability, losing power in large portions of a network can be costly. By responding to a situation quickly and appropriately, the cascading sequence can be broken. MPC is well-equipped to achieve this goal by predicting system behavior and selecting control actions which return the system to a safe operating region.

1.2.2 Power System Dispatch

As previously mentioned, the first priority in power system operation is security with a secondary emphasis toward economy. RTOs require that generation and control devices be ready when they are needed, and therefore advance planning is necessary to ensure that generator operators are aware of their upcoming responsibilities. The dispatch planning process used in the PJM RTO provides a good picture of the common practices applied in many power systems.

Two markets exist in PJM to procure the energy and control capabilities necessary to operate the electric grid. The first market is a day-ahead market which covers the estimated needs for the following day. Generators offer bids to supply energy and reserves at certain costs for each hour of the upcoming day. Load forecasts are used by PJM to determine how much generation and reserve is required at each hour and schedules the least-cost generation capable of satisfying the load while respecting network constraints [13].

The second market is the real-time balancing market. This market accounts for differences from the day-ahead dispatch due to inaccurate load forecasts, unexpected failures, or unavailable generation and clears every five minutes during the operating day [13]. It is within this timeframe that corrective control strategies are determined and applied.

Two main dispatch engines guide real-time operation. An intermediate-time security constrained economic dispatch program estimates the system behavior over the next one to two hours. A real-time security constrained economic dispatch program then determines finalized schedules 10 to 20 minutes into the future which track the trajectory defined by the Intermediate-Time program [14]. Any deviations away from this schedule are determined by fast-acting, closed-loop regulation controls and operator identified adjustments.

Improving the decision-making process for deviations away from the real-time dispatch is the focus of this work. Several specific opportunities for advancement have been identified. First, models which better capture the flexibility and capability of network resources are desired. Second, volatility in the dispatch signals being sent to generators should be reduced [14]. MPC provides a useful framework in which both of these goals can be addressed.

1.2.3 Previous Work

As mentioned in Section 1.2.1, maintaining voltages and power flows within acceptable ranges are reliability goals of steady-state power system operation. Although previous work exists in both of these areas, flexible techniques designed to operate in real-time have traditionally considered each goal individually. A summary of each of these bodies of work is provided as a context for the present analysis.

Voltage control

Voltage control and reactive power management began receiving increased attention during the 1970s and 1980s. Long-distance bulk power transfers started testing the limits of existing transmission practices and more sophisticated voltage control techniques were sought to address this challenge. Local voltage control devices were coordinated to more effectively achieve system-wide objectives. In [15], real-time optimization of generator voltage setpoints, tap-changing transformers, and reactive compensation devices was applied to minimize voltage violations and system losses. Similarly, secondary voltage control schemes started considering interarea interactions [16] and coordinated under-voltage load shedding [17] to achieve better performance. These strategies largely ignored the interactions between active and reactive power and a need for more precise automatic control techniques remained an open need [18].

As optimal power flow formulations began to account for both active and reactive power, the modern security-constrained economic dispatch process was born. In addition to correcting voltage violations, these algorithms started considering the economic impact of attaining a secure solution [19]. However, as mentioned in Section 1.2.2, methods to better capture system flexibility and future behavior continue to be opportunities for improvement.

One control technique which is well suited to handle a variety of system conditions while considering future behavior is MPC. It also provides a systematic approach to resolving discrepancies arising from the use of linear models for controlling nonlinear systems [20, 21]. MPC uses an internal (approximate) model of the system to predict behavior and establish an optimal control sequence. The control actions from the first step of this sequence are implemented on the actual system. Subsequent measurement of the resulting system behavior provides the initial conditions for MPC to again predict behavior and recalculate an optimal control sequence. The feedback inherent in the repetition of this process allows MPC to control a broad range of devices while effectively satisfying a multi-period constrained optimal power flow problem.

After demonstrating its potential in the process industry, MPC began appearing in the power systems literature to address dynamic voltage control challenges. One of the earliest investigations was presented in [22]. The method used search-based techniques and detailed nonlinear and discrete system models to

determine appropriate settings for automatic voltage regulators, tap-changing transformers, and load shedding during a voltage emergency. Similar follow-up studies are also presented in [23, 24]. Since that time, subsequent works have applied techniques from MPC to address rapid voltage control in an online setting.

Trajectory sensitivities emerged as a popular technique to predict the future behavior of the system. Under this approach, a nominal trajectory is determined for the system, and linear sensitivities describe how control changes cause the system to deviate from this trajectory [25]. In [26], Zima *et al.* develop an open-loop voltage protection scheme using trajectory sensitivities to determine a single set of control inputs which are fixed over the entire prediction horizon. They adapt this method to operate in a closed-loop MPC manner in [27]. In [28], trajectory sensitivities are used to identify nondisruptive load shedding controls to improve voltage stability. Automatic voltage regulator adjustment and load shedding are used as voltage controls in [29], and the trajectory sensitivity model is compared against other integration techniques. Voltage control using MPC and trajectory sensitivities is investigated in [30] with capacitor switching as the control actuator.

In addition to using trajectory sensitivities, other detailed formulations of MPC have also been used to correct voltage concerns. Instead of using search-tree solution techniques as was done in [22, 23], the authors of [31] use an interior-point method to solve a nonlinear problem formulation. However, they forego standard load and tap-changing transformer models and instead use a linear load recovery model to drive the system dynamics. While this model is somewhat inaccurate, it is sufficient to direct MPC toward secure corrective actions. This observation that highly detailed models within MPC may be unnecessary matches the findings of [29]. However, the models employed must sufficiently identify the key drivers of instability in order for MPC to respond appropriately.

Alternative formulations based on the strategy of MPC have also been proposed. A protection scheme with bi-level static and dynamic optimization but which ignores the voltage recovery dynamics is proposed in [32]. In [33], loads are assumed to reach their fully recovered state and the controls selected by MPC are scaled to account for the recovery process. A distributed control process similar to MPC is described in [34].

Transmission limits

Transmission limits are typically defined to avoid unsafe heating of transmission lines. Resistive losses dissipate energy as heat in the conductor material and can cause unsafe reduction of line clearance due to sagging as the material heats and expands. When determining transmission line ratings, ambient assumptions are biased toward warmer, low-wind conditions to produce a conservative rating. Some utilities define ratings for a variety of ambient conditions so that less conservative ratings can be selected at the time of operation [11].

This strategy of updating transmission line ratings based on actual ambient conditions is known as

dynamic line rating. The wind speed and air temperature around transmission line conductors can provide significant cooling effects for the conductor material [1]. Cooler ambient conditions allow more current to flow along the conductor without causing unsafe sagging. This effectively increases the transmission capacity and can relieve congestion without requiring expensive transmission upgrades. The methods and technology needed for tracking ambient conditions and line temperatures have existed for several decades [35] and continue to improve [36, 37].

Emergency ratings are also defined to indicate the severity of control effort required if the normal operating limit of the transmission line is violated. For example, PJM specifies three ratings for every line: normal, emergency, and load dump. Violations of the normal and emergency limits must be corrected in 15 minutes, but load shedding may only be used if the emergency rating is exceeded. Exceeding the load dump limit must be resolved within five minutes or load shedding is initiated to reduce the line's load [11].

Typical control actions to correct a line flow overload include adjustment of phase-shifting transformers, line or shunt switching, generator redispatch, and load shedding. These controls are identified by the operator with the help of dispatching software which determines new operating targets for the system and sensitivity factors which describe the impact of control actions on the overloaded line.

The development of tools to identify corrective actions has been of interest for several decades. These algorithms must be capable of considering a variety of control devices while operating quickly and reliably [38], and have traditionally been divided between power redispatch [39–42] and transmission switching [43–45]. The binary nature of switching actions requires mixed-integer models which are difficult to solve in real-time for large networks. In contrast, linear models offer straightforward implementation for large-scale systems but must be carefully designed to accurately represent power system nonlinearities [46, 47].

Early investigations into the use of MPC for relieving thermal overloading of transmission lines were undertaken in [48, 49]. To return line currents to within their long-term ratings following a contingency, MPC regulated the angle on phase-shifting transformers, redispatched generation, and shed load as a last resort. The study found that both the length of the prediction horizon and the accuracy of the network model can have an appreciable influence on the ability of MPC to meet its control objectives.

The work presented in [50] further expanded on these ideas by incorporating a temperature-based model of transmission lines [51, 52]. Enforcing a temperature limit on a transmission line while considering actual ambient conditions provides greater flexibility than the conservative assumptions typically used in device ratings. Employing a temperature model of transmission lines is possible using existing dynamic line rating technologies. The authors of [50] pointed out that moving to a temperature-based model of transmission line loading reduces the likelihood of incorrect operation of the control scheme.

The shift toward distributed renewable generation and energy storage technologies motivated further

investigation of MPC-based cascade mitigation. In [6–8], brief temperature overloads were relieved using energy storage and curtailment of renewables in addition to the control measures utilized in [48, 50]. These works demonstrated the ability of MPC to prevent cascading overloads in small test networks. To do so, they made use of a linear DC power flow formulation.

Explicit MPC

One of the challenges of MPC is the need to solve an optimization problem in real-time. This time constraint motivated Explicit MPC techniques which partition the state space into distinct regions and precompute a control law for each operating region [53]. These results are stored in a lookup table and can be accessed quickly at run-time instead of solving the optimization problem online. Unfortunately, realistic power systems are quite large and require high-dimension optimal programs. As the number of states and constraints grow, the lookup tables grow rapidly which causes implementation challenges [53].

Additionally, power system models such as power flow and device models are constrained nonlinear systems. This motivates the use of Explicit Nonlinear MPC techniques [54]. Including the network configuration as a parameter in the problem further expands the problem dimension as all possible contingencies and operating conditions must be included in the problem formulation. For this reason, Explicit MPC is not examined in this work. Instead, the nonlinear system model is linearized whenever MPC operates and the resulting optimization problem is solved in real-time. Model reduction techniques are applied to simplify the solution process and satisfy run-time requirements.

1.3 Contributions

The work presented here expands on the previous literature in several ways. First, the previously separated control objectives of avoiding voltage collapse and thermal transmission line overloads are combined into a single controller formulation. Though voltage concerns are primarily associated with reactive power and transmission line flows with active power, control actions taken to address one concern can have important impacts on the other. Incorporating both phenomena into a single corrective control formulation identifies more appropriate control actions over the range of possible operating conditions and contingencies.

Second, this work investigates methods of balancing accuracy and simplicity within the internal model of MPC. The linear formulation is expanded to more accurately describe off-nominal power system conditions. It incorporates updated descriptions of voltage magnitude and angle, active and reactive power, transmission losses, and transformer tap-changing dynamics. Specifically, a linear relaxation relating transmission losses to voltage magnitude and angle is introduced and justified with eigenanalysis.

During an emergency situation in a power system, the off-nominal conditions can have a meaningful impact on the system behavior. Accounting for them reduces the chance that the controller will be unrealistically optimistic or pessimistic about the future behavior of the system [48]. If the controller is too optimistic, it may not act quickly enough to avoid detrimental behavior. If the controller is too pessimistic, it may enact expensive control actions which are not actually necessary. This work pursues accuracy in the prediction of future behavior while avoiding complex nonlinear models which significantly increase the computational burden.

Third, performance on real-world networks is examined. As these networks can be quite large, a technique is proposed to improve computational performance by limiting the internal model to critical elements.

Previous testing of MPC in power systems was limited to small networks of less than 100 buses. This kept problem formulations small by requiring only a few constraints and variables and reduced the computational complexity. Realistic power system networks typically have thousands of buses with many individual generators and loads. However, explicitly modeling all these network components may not be necessary to achieve satisfactory control in emergency situations. Specifically, during a thermal overload event a relatively small number of lines are close to their limits, and a limited number of control actions will have meaningful ability to resolve the situation. Any network components outside of these groups will operate normally and can be condensed in the controller model.

The specific contributions presented in this work can be summarized as follows:

- The control objectives of correcting voltage instability and resolving thermal transmission overloads are combined in a comprehensive model-predictive control strategy.
- Case-studies demonstrating the controller's ability to effectively resolve voltage instability and thermal overloads are presented and discussed.
- Linear power flow constraints are updated to relate active and reactive power to voltage magnitude and angle using the Jacobian of the AC power flow equations.
- Generator models are updated to linearly approximate nonlinear power capability regions.
- Load models are updated to linearly account for voltage sensitivity.
- A linear loss model is introduced for individual transmission lines which describes local nonlinearity while considering changes in both voltage magnitude and angle.
- The Hessian matrix of the transmission line loss equation is proven to have exactly two positive eigenvalues when expressed in terms of voltage magnitude and angle over realistic operating voltages. This characteristic is exploited to motivate a convex approximation of losses.

- A linear model of transformer tap-changing dynamics is incorporated into the controller formulation.
- Control feasibility is demonstrated on a realistic network with over $4,000$ buses.
- A strategy for condensing the constraint formulation and improving computational speed while limiting control detriment on large networks is presented.

1.4 Basic Theories

1.4.1 Model-Predictive Control

The term MPC does not refer to a specific control strategy but rather to a group of strategies which utilize a process model to find a control sequence over a specified horizon by minimizing an objective function [20]. If the horizon is finite or the model imperfect, the strategy is repeated as time progresses and new information becomes available.

This work considers a finite horizon with M discrete intervals of duration T_s. At a given discrete time instance, l, the MPC process is initiated to determine the behavior of some states[1], $x[k|l]$ for $k \in \{1, \ldots, M\}$, driven by controls, $u[k|l]$ for $k \in \{0, \ldots, M-1\}$. The notation $x[k|l]$ represents the modeled states at time $l+k$ given an initiation of the model at time l. The first control in the sequence, $u[0|l]$, is implemented on the physical system. When new system measurements for the states become available at the next discrete time instance, $l+1$, the process is repeated to find the new control sequence, $u[k|l+1]$ for $k \in \{0, \ldots, M-1\}$. Since the MPC process is repeated at every discrete time instance, the notation of l becomes somewhat unnecessary and cumbersome as it is typically evident from context. In this work, the notation $u[k]$ will be used as a shorthand for $u[k|l]$.

The proposed MPC strategy repeatedly solves a form of multi-period optimal power flow that considers slower dynamic processes associated with transmission line conductor temperature, transformer tap-changing, energy storage state-of-charge, and ramp-limited generation. For such processes, a controller response rate on the order of one minute is sufficient. Sub-second voltage and generator transients are significantly faster than the time constants of these slower processes. It is assumed fast transients are stabilized by standard closed-loop controls (e.g. generator automatic voltage regulators and power system stabilizers) and are ignored in the MPC model.

Figure 1.2 outlines the MPC control strategy. At time l, all measurements necessary to model the network, z_l^{meas}, are provided to the controller. These measurements include voltages, generation, storage state-of-charge, device operating states, network configuration, transmission line temperatures, and the most recent

[1] It is assumed that states are observable and can be measured.

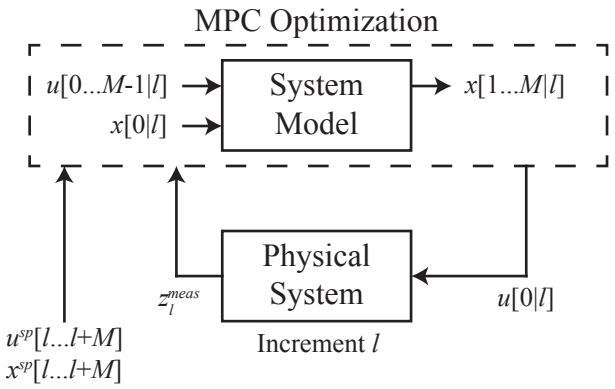

Figure 1.2: Overview of MPC strategy.

load and renewable forecasts. This information is obtained from SCADA/PMU measurements and state estimation[2], and determines the initial value of the system state, $x[0|l]$. MPC then builds an optimization problem to determine a control sequence, $u[0 \dots M-1|l]$, over a horizon of M time-steps while considering its effects on states, $x[1 \dots M|l]$, using a model of the network. The controls are selected to track scheduled set-point values[3] for both the controls, $u^{sp}[l \dots l+M-1]$, and states, $x^{sp}[l+1 \dots l+M]$, over the prediction horizon. Once an optimal control sequence is identified, the controls from the first step in the sequence, $u[0|l]$, are applied to the physical system in a step-wise manner with constant step-width T_s, giving $u(t) := u[0|l]$ for $t \in [(l)T_s, (l+1)T_s)$. The physical system responds to the controls as time advances from l to $l+1$, and the process repeats when new system measurements, z_{l+1}^{meas}, become available.

The MPC strategy extends naturally to power system applications due to its compatibility with present economic dispatch techniques. The MPC formulation presented in this work operates every minute whereas traditional security-constrained economic dispatch programs operate every five minutes [55, 56]. In the PJM and NYISO networks, severe overloads exceeding the load dump or short-term emergency ratings, respectively, must be resolved within five minutes [55, 57] to prevent tripping of a transmission line which can further exacerbate the problem. MPC identifies an optimal response within this time-frame while considering future effects of the control actions and minimizing deviations from the economic dispatch. In this way, the proposed controller assumes the role of a system operator responding to thermal rating and voltage magnitude concerns in real time while seeking to maintain, as best possible, the economic schedule.

[2]The time delays inherent in SCADA and state estimation (less than 60 seconds [55]) can be ignored as they are small relative to the time constants of the dynamic processes considered in this MPC formulation.

[3]These scheduled values are typically established by economic dispatch.

1.4.2 Optimal Program Formulation

The optimal control problem solved within MPC is a *quadratic program* (QP). A high level summary of the network model embedded in the program is provided in (1.4).

$$\begin{aligned} \text{minimize} \quad & \text{Deviation from economic dispatch} \\ s.t. \quad & \text{Generator constraints} \\ & \text{Renewable constraints} \\ & \text{Load constraints} \\ & \text{Storage constraints} \\ & \text{Power flow constraints} \\ & \text{Transformer constraints} \\ & \text{Thermal constraints.} \end{aligned} \tag{1.4}$$

As a QP, the objective function is quadratic while the constraints are linear. The program considers time-coupled behavior to predict the power system response over the interval $[l, l+M]$. The system dynamics are discretized using forward Euler with sample time T_s. A more detailed discussion of each problem component (objective, variables, constraints) is presented in the following sections.

The implementation of (1.4) in this work is similar to that of [6–8] but with the model extended to incorporate voltage magnitudes and reactive power. These extensions only slightly change the generator and load constraints, and both terms also appear in the objective. More significant changes occur in the power flow, transformer, and thermal constraints and these will be discussed in greater detail in Chapter 3.

1.4.3 Objective and Variables

The objective of (1.4) is to minimize the cost of corrective actions which deviate from a prespecified dispatch while resolving power system limit violations. The objective function has the form,

$$\left\|x[M] - x^{sp}[M]\right\|_{P_M} + \sum_{k=0}^{M-1} \left(\left\|x[k] - x^{sp}[k]\right\|_P + \left\|u[k] - u^{sp}[k]\right\|_R \right). \tag{1.5}$$

The notation $\|y\|_P$ represents the quadratic function $y^\top P y$. The weighting matrices P_M, P, and R are positive definite with larger weights applied to P_M than P to provide flexibility throughout the horizon while encouraging the controller to return to the prespecified dispatch by the end of the prediction horizon.

The internal model of MPC primarily tracks changes from the measured conditions at the start of the

prediction horizon. For clarity, variables associated with these changes include a Δ symbol. Not all variables included in the constraints of (1.4) appear in the objective function (1.5). Many are internal variables necessary to model the behavior of the various network elements. They will be introduced as the constraints of (1.4) are further clarified. The state variables $x[k]$ that appear in the objective function are:

- $\Delta\hat{T}_{ij}$: Relaxed temperature overload on line ij, [°C]
- Δp_{Gn}: Active power output of generator n, [pu]
- Δq_{Gn}: Reactive power output of generator n, [pu]
- Δq_{Rn}: Reactive power output of renewable n, [pu]
- E_n: Energy in storage device n, [pu-hr]
- U_n^+, U_n^-: Over (under)-voltage violation at bus n, [%]
- Δa_{ij}: Tap magnitude of tap-changing transformer ij, [pu]
- $\Delta\psi_{ij}$: Phase angle of phase-shifting transformer ij, [rad].

The control variables $u[k]$ are:

- dp_{Gn}: Change in active power of generator n, [pu]
- Δp_{Rn}^{cur}: Active power curtailment of renewable n, [pu]
- Δp_{Dn}^{red}: Active power reduction of load n, [pu]
- $p_{Sc,n}$: Charging power of storage device n, [pu]
- $p_{Sd,n}$: Discharging power of storage device n, [pu]
- U_{ij}^{ref}: Reference voltage of voltage-regulating transformer ij, [%]
- q_{ij}^{ref}: Reference reactive power flow of reactive-regulating transformer ij, [pu]
- p_{ij}^{ref}: Reference active power flow of active-regulating transformer ij, [pu]

1.4.4 Device Constraints

Traditional generator constraints

Within (1.4), generators are modeled as power sources with ramp-rate limits on their active power production. As such, their active power output is governed by a simple discretized dynamic equation in combination with

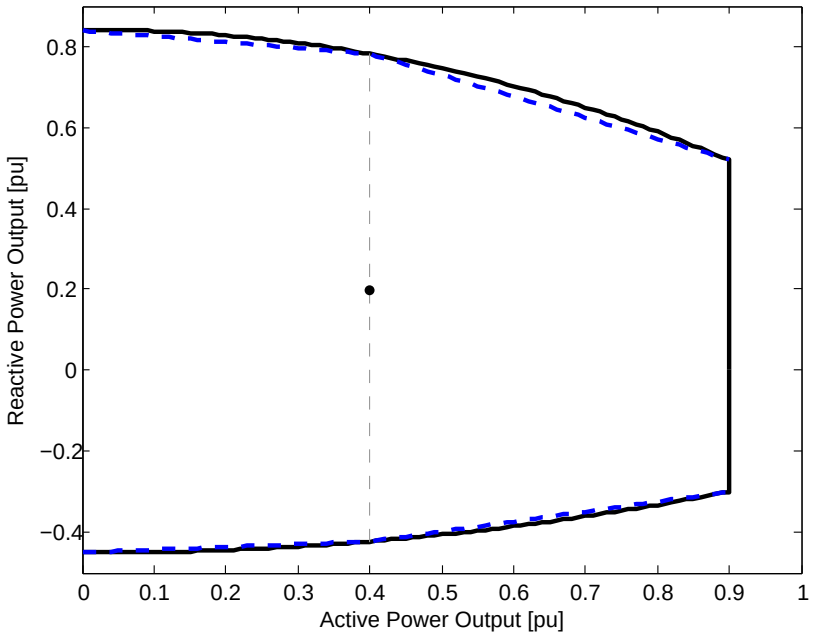

Figure 1.3: The acceptable operating range of a generator is specified in terms of its active and reactive power output. The output capabilities are bounded by the solid black curve. Two piecewise linear segments approximate each of the nonlinear boundaries within MPC (shown by the dashed blue lines). The dot represents a possible measured operating condition at the start of the prediction horizon.

operating limits on the active and reactive power outputs:

$$\Delta p_{Gn}[k+1] = \Delta p_{Gn}[k] + dp_{Gn}[k], \tag{1.6a}$$

$$\Delta p_{Gn}[0] = 0, \tag{1.6b}$$

$$dp_{Gn}^{min}[k] \leq dp_{Gn}[k] \leq dp_{Gn}^{max}[k], \tag{1.6c}$$

$$\Delta p_{Gn}^{min}[k] \leq \Delta p_{Gn}[k] \leq \Delta p_{Gn}^{max}[k], \tag{1.6d}$$

$$\Delta p_{Gn}^{min}[M] \leq \Delta p_{Gn}[M] \leq \Delta p_{Gn}^{max}[M], \tag{1.6e}$$

$$\Delta q_{Gn}[k] \geq \omega_{Gn}^{min,i} \Delta p_{Gn}[k] + \nu_{Gn}^{min}, \tag{1.6f}$$

$$\Delta q_{Gn}[k] \leq \omega_{Gn}^{max,i} \Delta p_{Gn}[k] + \nu_{Gn}^{max}, \tag{1.6g}$$

for $k \in \{0, \ldots, M-1\}$ and $i \in \{1, 2\}$.

Equations (1.6a) and (1.6c) ensure that generator active power output does not change more quickly than its ramp-rate limits permit, (1.6b) initializes the generator output to its measured value at the start of the prediction horizon, and (1.6d)-(1.6e) maintain the active power within its limits.

Equations (1.6f) and (1.6g) enforce lower and upper limits on the reactive power output. The coefficients ω and ν are defined in (1.7). The power output of a generator is limited by its voltage and current ratings

on the stator and rotor. These ratings often specify a "D"-shaped acceptable operating region in terms of active and reactive power. Figure 1.3 shows this region bounded by the solid black curves. The powers are normalized in terms of the machine MVA rating.

The piecewise linear constraints given in (1.6f) and (1.6g) are shown by the dashed blue lines in Figure 1.3. They approximate the nonlinear boundary of the acceptable operating range and are defined based on the measured operating conditions at the start of the prediction horizon. For example, in Figure 1.3 the measured active power output at the start of the prediction horizon p_{Gn}^{meas} is at 0.4 pu and the measured reactive power output q_{Gn}^{meas} is at 0.2 pu and is represented by the dot. These measured conditions determine the intersection of the two linear segments.

The coefficients ω and ν are defined as,

$$\omega_{Gn}^{min,1} = \frac{\mathcal{Q}_{Gn}^{min}(p_{Gn}^{meas}) - \mathcal{Q}_{Gn}^{min}(0)}{p_{Gn}^{meas}}, \tag{1.7a}$$

$$\omega_{Gn}^{min,2} = \frac{\mathcal{Q}_{Gn}^{min}(p_{Gn}^{max}) - \mathcal{Q}_{Gn}^{min}(p_{Gn}^{meas})}{p_{Gn}^{max} - p_{Gn}^{meas}}, \tag{1.7b}$$

$$\nu_{Gn}^{min} = \mathcal{Q}_{Gn}^{min}(p_{Gn}^{meas}) - q_{Gn}^{meas}, \tag{1.7c}$$

$$\omega_{Gn}^{max,1} = \frac{\mathcal{Q}_{Gn}^{max}(p_{Gn}^{meas}) - \mathcal{Q}_{Gn}^{max}(0)}{p_{Gn}^{meas}}, \tag{1.7d}$$

$$\omega_{Gn}^{max,2} = \frac{\mathcal{Q}_{Gn}^{max}(p_{Gn}^{max}) - \mathcal{Q}_{Gn}^{max}(p_{Gn}^{meas})}{p_{Gn}^{max} - p_{Gn}^{meas}}, \tag{1.7e}$$

$$\nu_{Gn}^{max} = \mathcal{Q}_{Gn}^{max}(p_{Gn}^{meas}) - q_{Gn}^{meas}, \tag{1.7f}$$

with $\mathcal{Q}_{Gn}^{min}(\cdot)$ and $\mathcal{Q}_{Gn}^{max}(\cdot)$ representing the respective nonlinear boundary functions of the lower and upper reactive power limits in terms of active power.

The objective function includes a small penalty on changes in a generator's reactive power output relative to the output measured at the start of the prediction horizon. This improves the convergence characteristics of the QP by identifying a unique reactive power allocation when multiple sources are located at the same bus.

Renewable generator constraints

Renewable generators are capable of providing reactive power support but only have the ability to curtail their active power output:

$$\Delta p_{Rn}^{nom}[k] = \Delta p_{Rn}[k] + \Delta p_{Rn}^{cur}[k], \tag{1.8a}$$

$$0 \leq p_{Rn}^{cur,meas}[k] + \Delta p_{Rn}^{cur}[k] \leq p_{Rn}^{nom}[k], \tag{1.8b}$$

$$\Delta q_{Rn}[k] \geq \omega_{Rn}^{min,i} \Delta p_{Rn}[k] + \nu_{Rn}^{min}, \tag{1.8c}$$

$$\Delta q_{Rn}[k] \leq \omega_{Rn}^{max,i} \Delta p_{Rn}[k] + \nu_{Rn}^{max}, \tag{1.8d}$$

for $k \in \{0, \ldots, M-1\}$ and $i \in \{1, 2\}$.

In (1.8a), the output of the renewable source, p_{Rn}, plus any curtailment, p_{Rn}^{cur}, must equal the nominal forecast, p_{Rn}^{nom}. Curtailment remains within limits due to (1.8b). The reactive power remains within its limits through constraints (1.8c)-(1.8d). The process for defining the terms ω and ν is the same as that used for traditional generators.

No ramp rate limits are enforced on renewable generators since their output can typically change very rapidly. Additionally, the forecast is assumed to be perfect in this analysis. Uncertainty in the renewable forecast could be an alternative contingency or disturbance which the controller must address but is not investigated here.

Load constraints

Loads consume power at a fixed power factor and can be reduced if necessary. Additionally, the power consumed by loads is usually voltage dependent, and modeling this behavior is especially important in voltage collapse scenarios. The load model within MPC is expressed:

$$\Delta p_{Dn}[k] = \mathcal{PU}_{Dn}(U_n^{meas})(\Delta p_{Dn}^{nom}[k] - \Delta p_{Dn}^{red}[k]) + (p_{Dn}^{nom}[0] - p_{Dn}^{red,meas}) \frac{\partial \mathcal{PU}_{Dn}}{\partial U_n} \Delta U_n[k], \tag{1.9a}$$

$$\Delta q_{Dn}[k] = \mathcal{QU}_{Dn}(U_n^{meas})(\Delta q_{Dn}^{nom}[k] - \Delta q_{Dn}^{red}[k]) + (q_{Dn}^{nom}[0] - q_{Dn}^{red,meas}) \frac{\partial \mathcal{QU}_{Dn}}{\partial U_n} \Delta U_n[k], \tag{1.9b}$$

$$0 = q_{Dn}^{nom}[k] \Delta p_{Dn}^{red}[k] - p_{Dn}^{nom}[k] \Delta q_{Dn}^{red}[k], \tag{1.9c}$$

$$0 \leq p_{Dn}^{red,meas} + \Delta p_{Dn}^{red}[k] \leq p_{Dn}^{nom}[k], \tag{1.9d}$$

$$0 \leq q_{Dn}^{red,meas} + \Delta q_{Dn}^{red}[k] \leq q_{Dn}^{nom}[k], \tag{1.9e}$$

for $k \in \{0, \ldots, M-1\}$.

Constraints (1.9a) and (1.9b) are linearizations of the more accurate nonlinear model relating power demand, load reduction, and voltage sensitivity,

$$p_{Dn} = (p_{Dn}^{nom} - p_{Dn}^{red})\mathcal{PU}_{Dn}(U_n), \tag{1.10a}$$

$$q_{Dn} = (q_{Dn}^{nom} - q_{Dn}^{red})\mathcal{QU}_{Dn}(U_n). \tag{1.10b}$$

The expressions $\mathcal{PU}_{Dn}(U_n)$ and $\mathcal{QU}_{Dn}(U_n)$ respectively describe how the voltage magnitude U_n influences the active power and reactive power of the load. They are normalized so that $\mathcal{PU}_{Dn}(1) = \mathcal{QU}_{Dn}(1) = 1$. The nominal active and reactive powers, p_{Dn}^{nom} and q_{Dn}^{nom}, are available from load forecasts which are assumed to be perfect. Reductions in power from these forecasts (possibly through demand response programs) are represented by p_{Dn}^{red} and q_{Dn}^{red}. The net active power and reactive power demands of the load are represented by p_{Dn} and q_{Dn}, respectively.

Equation (1.9c) ensures that demand response actions adjust both the active and reactive power in proportion to the nominal power factor. Demand response capability limits are enforced by (1.9d)-(1.9e).

Storage constraints

Storage devices are limited-energy devices:

$$E_n[k+1] = E_n[k] + T_s\eta_{c,n}p_{Sc,n}[k] - \frac{T_s}{\eta_{d,n}}p_{Sd,n}[k], \tag{1.11a}$$

$$E_n[0] = E_n^{meas}, \tag{1.11b}$$

$$\Delta p_{Sn}[k] = p_{Sc,n}[k] - p_{Sd,n}[k] - p_{Sn}^{meas}, \tag{1.11c}$$

$$0 = p_{Sc,n}[k]p_{Sd,n}[k], \tag{1.11d}$$

$$0 \leq p_{Sc,n}[k] \leq p_{Sc,n}^{rate}, \tag{1.11e}$$

$$0 \leq p_{Sd,n}[k] \leq p_{Sd,n}^{rate}, \tag{1.11f}$$

$$0 \leq E_n[k] \leq E_n^{rate}, \tag{1.11g}$$

$$0 \leq E_n[M] \leq E_n^{rate}, \tag{1.11h}$$

for $k \in \{0, \ldots, M-1\}$.

The relationship between energy, charging, and discharging in a storage device is established by (1.11a). The charging and discharging efficiencies, $\eta_{c,n}$ and $\eta_{d,n}$ respectively, describe the losses in the energy conversion process. The energy is initialized to its measured value using (1.11b). The net power demand of storage, p_{Sn}, is given by (1.11c). The complementarity condition of (1.11d) eliminates simultaneous charging and

discharging. It is relaxed into a linear formulation using the approximation described in Appendix A of [7]. The power and energy capability limits of the device are enforced by (1.11e)-(1.11h).

Part of the benefits achieved by the MPC process are due to its ability to affect the charging or discharging state of energy storage devices. Typically, system operators have limited or no control over the power output of storage devices [56], but utilizing the flexibility of these devices can provide valuable alternative control possibilities.

Chapter 2

Linearly Modeling Losses with Voltage Magnitude and Angle

This chapter proposes a new piecewise-linear transmission line loss model which utilizes information about voltage magnitudes. The new model is compared against the piecewise-linear model used in [6–8] which only considers voltage angles and against a standard first-order Taylor expansion of the line loss function. The proposed technique better captures the true loss behavior over the prediction horizon of MPC than the two alternative methods. The majority of this chapter was first published in [58].

2.1 Transmission Line Power Loss

Power loss in a transmission line is due to the resistive properties of the conductor. As current flows through the line, these resistive effects cause energy to be dissipated as heat. The power loss can be expressed in terms of current and resistance as $P = R|I|^2$ or in terms of voltage and conductance as $P = G|V|^2$. Since the formulation of (1.4) contains voltage information, the latter specification is used in this analysis.

Network voltages are expressed in polar coordinates, $V = Ue^{\mathbf{j}\delta}$. Therefore, calculating the squared magnitude of the voltage difference across a transmission line is an application of the law of cosines,

$$P_{ij}^{loss} = g_{ij} \left| V_i - V_j \right|^2, \tag{2.1a}$$

$$= g_{ij} \left(U_i^2 + U_j^2 - 2U_i U_j \cos(\delta_{ij}) \right). \tag{2.1b}$$

The term $\delta_{ij} = \delta_i - \delta_j$ in (2.1b) is the voltage angle difference across the line and is a linear transformation of

variables which allows the loss equation to be expressed in terms of three variables: U_i, U_j, and δ_{ij}. Equation (2.1b) can be represented condensely as $\mathcal{P}_{ij}^{loss}(x)$ with $x = [U_i, U_j, \delta_{ij}]^\top$.

If voltage magnitudes are assumed to remain at unity with small angle differences, as is the case in the DC power flow approximation, (2.1b) can be simplified to a simple quadratic equation in a single variable,

$$P_{ij}^{loss} = g_{ij}\left(U_i^2 + U_j^2 - 2U_iU_j\cos(\delta_{ij})\right), \tag{2.2a}$$

$$\approx g_{ij}\left(2 - 2\cos(\delta_{ij})\right), \qquad U \approx 1 \tag{2.2b}$$

$$\approx g_{ij}\left(\delta_{ij}^2\right). \qquad 1 - \cos\delta_{ij} \approx \frac{\delta_{ij}^2}{2} \tag{2.2c}$$

Under this approach, the loss function is convex and a piecewise-linear approximation can be used to implement (2.2c) with linear constraints [7, 59]. This model (referred to as DC-PWL) is able to capture the important nonlinear behavior of losses when voltage angles change significantly, but ignores the influence of off-nominal voltage magnitudes.

An alternative loss model can be defined to incorporate the effects of voltage magnitudes. A first-order Taylor expansion of (2.1b) is easily implemented in a linear framework while considering voltage magnitudes,

$$\mathcal{P}_{ij}^{loss}(x_0 + \Delta x) \approx \mathcal{P}_{ij}^{loss}(x_0) + \left(\frac{\partial \mathcal{P}_{ij}^{loss}(x_0)}{\partial x}\right)^\top \Delta x. \tag{2.3}$$

Unfortunately, this approach (referred to as AC-LIN) does not capture the nonlinear behavior of the loss function when voltage conditions change significantly.

Ideally, a loss model would incorporate the beneficial aspects of both approaches to provide a higher accuracy prediction that is effective over a range of voltage conditions. Including voltage magnitudes increases the model dimension from one to three. Any piecewise-linear approximation will therefore grow very rapidly in size as the number of linear segments is increased. Additionally, the loss equation must be convex for the approximation to remain accurate without the use of integer variables to enforce adjacency conditions.

Over the years, a wide variety of loss modeling techniques have been proposed. Nonlinear techniques are fundamentally better suited to describing loss behavior. If expressed in rectangular voltage coordinates, losses are quadratic and can be specified with a cone constraint [60]. Conic [61, 62] and piecewise-linear [63, 64] formulations have also been proposed with voltages in polar coordinates to describe changes in voltage angle. To capture the influence of voltage magnitudes on losses, first-order [65] and second-order [66] Taylor expansions have been utilized. Unfortunately, the first-order model misses the nonlinear behavior and the second-order model utilizes quadratic constraints [66].

A relaxation method which captures the nonlinearity of transmission line losses when voltages are ex-

pressed in polar coordinates is presented in the rest of this chapter. It will be shown that an appropriately chosen set of linear inequality constraints can provide a convex relaxation that (locally) achieves an accurate description of transmission line losses. Given the nonconvexity of losses when voltages are expressed in polar form, care must be taken when formulating the linear inequality constraints so that accuracy is preserved.

2.2 Proposed Loss Model in Polar Voltage Coordinates

The proposed loss modeling approach is motivated by applications such as (1.4) where the following requirements must be satisfied:

1. applicable within a linear constraint environment,
2. voltages are expressed in polar form (magnitudes and angles),
3. tight around a given base voltage condition,
4. describe losses for a specific line.

None of the loss modelling approaches listed in Section 2.1 meet this specification except the first-order Taylor-series expansion, but it fails to adequately capture the nonlinear behavior of the loss equation.

Since transmission line losses are nonlinear in terms of voltage magnitudes and angles, the first requirement necessitates the use of a relaxation underbounding the true nonlinear relationship. This condition also eliminates the use of quadratic constraint formulations. The second requirement excludes methods which only account for voltage angle differences but ignore the effects of voltage magnitude changes. The third requirement assumes the availability of a base voltage profile. The fourth requirement rules out methods that only compute total system losses.

The approach developed here meets all four requirements and affords greater accuracy than a simple linearization. Given base voltages (in polar coordinates) for the end buses of a transmission line, the first step is to linearize the loss equation at that voltage condition. The second step is to choose several nearby sets of end-bus voltages and linearize the loss equation at each of those additional voltage conditions. Each of the linearizations is relaxed into an inequality constraint and together they provide an underbound for the loss model. The process for selecting the additional sets of voltages is discussed below.

2.2.1 Forming a Set of Linear Relaxations

The main objective in forming a relaxation using a set of linear inequalities is to approximate a nonlinear constraint while using a linear solver. The linear approximation must provide a balance between simplicity

and accuracy.

Every constraint added to a set of linear inequalities increases the associated computation. Building a large set of linear inequalities to approximate a nonlinear function may achieve high accuracy but will increase solution time. The improvement in accuracy may not justify the increased computational complexity. Fewer constraints which are well selected may achieve similar accuracy while maintaining simplicity. Furthermore, linear inequality constraints that are not located in a relevant region of the solution space, and so are never binding, should be avoided. They add to the computational cost but contribute nothing to solution quality.

Consider a set of linear inequalities that is obtained by linearizing a nonlinear function at a number of points. Each linear constraint provides the most accurate estimate of the nonlinear function around its linearization point, and therefore should be binding in the vicinity of that point. For example, assume that linear inequalities are generated at the points, $x_i,\ i = 1, ..., n$, and form an approximation which seeks to underbound a nonlinear function f. The resulting piecewise linear approximation of f returns the value,

$$f^{app}(x) = \max_{i \in \{1,...,n\}} \Big\{ f(x_i) + \frac{\partial f}{\partial x}(x_i)(x - x_i) \Big\}. \tag{2.4}$$

If the i-th constraint is binding then at the point x_i, (2.4) becomes $f^{app}(x_i) = f(x_i)$ which describes the best possible underbound of the true nonlinear function. This situation is illustrated in Figure 2.1a. However, if the linearization around the point x_i is not the binding constraint then,

$$f^{app}(x_i) = f(x_j) + \frac{\partial f}{\partial x}(x_j)(x_i - x_j) > f(x_i), \tag{2.5}$$

for some $j \neq i$. This can occur if the function is nonconvex between x_i and x_j, with Figure 2.1b providing an illustration. Examining the second-order Taylor-series expansion around x_j with $\Delta x = x_i - x_j$ offers further insight,

$$f(x_i) = f(x_j) + \frac{\partial f}{\partial x}(x_j)\Delta x + \tfrac{1}{2}\Delta x^\top \frac{\partial^2 f}{\partial x^2}(x_j)\Delta x + \text{h.o.t.} \tag{2.6}$$

The error in the approximation, $f^{app}(x_i) - f(x_i) > 0$, will occur when,

$$\tfrac{1}{2}\Delta x^\top \frac{\partial^2 f}{\partial x^2}(x_j)\Delta x + \text{h.o.t.} < 0. \tag{2.7}$$

Assuming that the higher order terms are negligible, the error will be present when the second-order term in the Taylor-series expansion around x_j is negative along the path between x_i and x_j, implying concavity of f between x_i and x_j. If the function is convex on this interval then the error will not be present and the linearization at x_i will be tight.

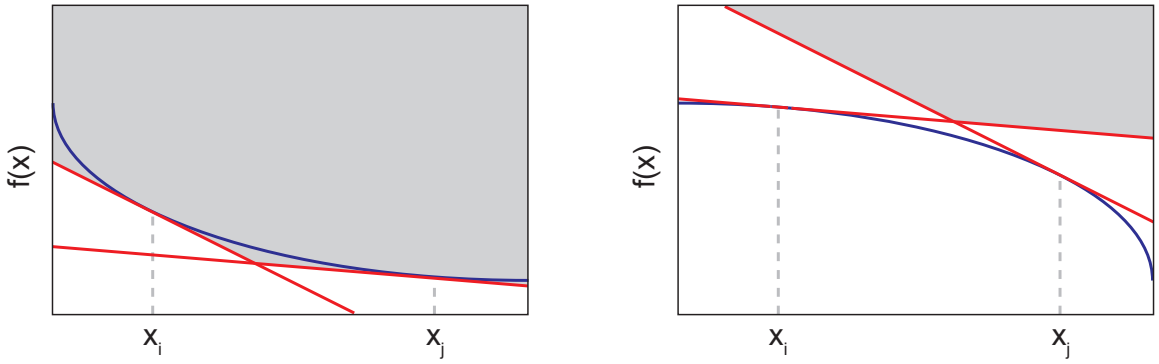

(a) (b)

Figure 2.1: A set of linear inequality relaxations underbounds a convex function but not a concave function. (a) Linear relaxation of a convex function. (b) Inaccurate linear relaxation of a concave function.

The loss function is convex in some directions and concave in others when expressed in polar voltage coordinates. The next section quantifies this claim and discusses the handling of this nonuniform behavior when building a set of linear inequalities.

2.2.2 Convexity of the Loss Equation in Polar Voltage Coordinates

To gain a better understanding of the behavior of the loss function expressed in (2.1b), a second-order Taylor-series expansion can be formed by ignoring the higher-order terms in (2.6),

$$\mathcal{P}_{ij}^{loss}(x+\Delta x) \approx \mathcal{P}_{ij}^{loss}(x) + \nabla_x \mathcal{P}_{ij}^{loss}(x)^\top \Delta x + \Delta x^\top \frac{\nabla_{xx}^2 \mathcal{P}_{ij}^{loss}(x)}{2} \Delta x, \tag{2.8}$$

where $x \equiv [U_i \; U_j \; \delta_{ij}]^\top$. The gradient is given by,

$$\nabla_x \mathcal{P}_{ij}^{loss}(x) = 2g_{ij} \begin{bmatrix} U_i - U_j \cos(\delta_{ij}) \\ U_j - U_i \cos(\delta_{ij}) \\ U_i U_j \sin(\delta_{ij}) \end{bmatrix}, \tag{2.9}$$

and the Hessian by,

$$\nabla_{xx}^2 \mathcal{P}_{ij}^{loss}(x) = 2g_{ij} \begin{bmatrix} 1 & -\cos(\delta_{ij}) & U_j \sin(\delta_{ij}) \\ -\cos(\delta_{ij}) & 1 & U_i \sin(\delta_{ij}) \\ U_j \sin(\delta_{ij}) & U_i \sin(\delta_{ij}) & U_i U_j \cos(\delta_{ij}) \end{bmatrix}. \tag{2.10}$$

Example

For an operating condition with voltage magnitudes fixed at 1 pu and a small angle difference of 0.05 rad the gradient is given by,

$$\nabla_x \mathcal{P}_{ij}^{loss} \left(\begin{bmatrix} 1 \\ 1 \\ 0.05 \end{bmatrix} \right) = 2g_{ij} \begin{bmatrix} 0.00125 \\ 0.00125 \\ 0.04998 \end{bmatrix}. \tag{2.11}$$

This supports the common hypothesis that voltage magnitudes have limited effect on the loss function since their sensitivities are close to zero. In contrast, the sensitivity of losses to angle difference is about 50 times larger.

If the operating condition deviates slightly, however, the effects of voltage magnitudes become more pronounced. Consider the case with $U_i = 1.02$ pu, $U_j = 1$ pu, and $\delta_{ij} = 0.1$ rad, which gives the gradient,

$$\nabla_x \mathcal{P}_{ij}^{loss} \left(\begin{bmatrix} 1.02 \\ 1.00 \\ 0.10 \end{bmatrix} \right) = 2g_{ij} \begin{bmatrix} 0.02500 \\ -0.01490 \\ 0.10183 \end{bmatrix}. \tag{2.12}$$

The sensitivity of losses to voltage magnitude has increased greatly, with the sensitivity of losses to the angle difference now only about 4 to 7 times larger. This suggests that inclusion of voltage magnitude effects into the loss formulation could result in nontrivial improvements in the model performance for conditions away from a flat voltage profile. □

Unfortunately, with the inclusion of voltage magnitudes, losses can no longer be expressed in a piecewise-linear form as is done when only angle difference is considered. In this situation, the formation of a set of linear inequalities becomes useful. As discussed previously, it is desirable to use a small number of constraints to capture the most important function characteristics, and to ensure tightness of the model by selecting linearization points from regions where the function exhibits convexity.

The (local) convexity/concavity of the loss function (2.1b), in terms of bus voltage magnitudes and the angle difference, is given by the eigenvalues of the Hessian (2.10). If all the eigenvalues are positive then the function is convex in a region around the operating point. If there are both positive and negative eigenvalues then the function is a saddle, exhibiting convexity in some directions and concavity in others. This motivates the following theorem.

Theorem 1. *The Hessian matrix* (2.10) *of the line loss function* (2.1b) *will have exactly two positive eigenvalues over the region given by* $U_i > 0$, $U_j > 0$, $\delta_{ij} \in [-\frac{\pi}{2}, \frac{\pi}{2}]$.

Proof. The (scaled) Hessian matrix, $H = \frac{1}{2g_{ij}} \nabla^2_{xx} \mathcal{P}^{loss}_{ij}(x)$, can be expressed symbolically as,

$$H = \begin{bmatrix} a & b & c \\ b & d & e \\ c & e & f \end{bmatrix}. \tag{2.13}$$

This matrix is symmetric and may be decomposed into factors $H = LDL^\top$ where,

$$L = \begin{bmatrix} 1 & 0 & 0 \\ L_{21} & 1 & 0 \\ L_{31} & L_{32} & 1 \end{bmatrix}, \qquad D = \begin{bmatrix} D_1 & 0 & 0 \\ 0 & D_2 & 0 \\ 0 & 0 & D_3 \end{bmatrix}.$$

If the factorization exists, the signs of the diagonal elements of D will match the signs of the eigenvalues of H [67]. The elements of D can be expressed in terms of the entries in H as

$$\begin{aligned} D_1 &= a \\ D_2 &= d - \frac{b^2}{a} \\ D_3 &= f - \left(\frac{c^2}{a} + \frac{(ae - bc)^2}{a^2 d - ab^2} \right). \end{aligned}$$

Substituting for terms from (2.10) and simplifying gives,

$$D_1 = 1 \tag{2.14a}$$

$$D_2 = \sin^2(\delta_{ij}) \tag{2.14b}$$

$$D_3 = -(U_i^2 + U_j^2 + U_i U_j \cos(\delta_{ij})), \quad \delta_{ij} \neq 0. \tag{2.14c}$$

When $\delta_{ij} \neq 0$, (2.14) provides a well-defined decomposition of H, with D_1 and D_2 both positive and D_3 negative. This implies that H has two positive eigenvalues and one negative eigenvalue. When $\delta_{ij} = 0$, D_3 is ill-defined due to a $\frac{0}{0}$ term and the decomposition does not exist. However, in this case substituting $\delta_{ij} = 0$ into (2.10) gives,

$$H = \begin{bmatrix} 1 & -1 & 0 \\ -1 & 1 & 0 \\ 0 & 0 & U_i U_j \end{bmatrix},$$

which has eigenvalues 0, 2 and $U_i U_j$. Since the voltage magnitudes are assumed to be strictly positive, the Hessian will have two positive eigenvalues and a single zero eigenvalue. □

The eigenvalues λ and eigenvectors v of the Hessian matrix $\nabla^2_{xx}\mathcal{P}^{loss}_{ij}(x)$ can be used to establish conditions which ensure the second-order term of the Taylor-series expansion (2.8) is positive,

$$\Delta x^\top \nabla^2_{xx}\mathcal{P}^{loss}_{ij}(x_0)\Delta x \geq 0. \tag{2.15}$$

Let Δx be expressed as a linear combination of the eigenvectors,

$$\Delta x = av_1 + bv_2 + cv_3.$$

Then (2.15) becomes,

$$(av_1 + bv_2 + cv_3)^\top \nabla^2_{xx}\mathcal{P}^{loss}_{ij}(x_0)(av_1 + bv_2 + cv_3) \geq 0. \tag{2.16}$$

Since v_1, v_2, and v_3 are the eigenvectors of $\nabla^2_{xx}\mathcal{P}^{loss}_{ij}(x_0)$, this gives,

$$(av_1 + bv_2 + cv_3)^\top (a\lambda_1 v_1 + b\lambda_2 v_2 + c\lambda_3 v_3) \geq 0. \tag{2.17}$$

Because $\nabla^2_{xx}\mathcal{P}^{loss}_{ij}(x)$ is symmetric, the eigenvectors can be expressed orthonormally so that $v_i^\top v_i = 1$ and $v_i^\top v_j = 0$ for $i \neq j \in \{1, 2, 3\}$. Accordingly, (2.17) becomes,

$$a^2\lambda_1 + b^2\lambda_2 + c^2\lambda_3 \geq 0. \tag{2.18}$$

Since one of the eigenvalues is nonpositive while the other two are positive, equality in (2.18) describes an elliptic cone in the eigenbasis coordinates a, b, c. When the inequality is strictly greater than zero, it describes an elliptic hyperboloid. Any directions lying outside the cone will cause the second-order term in (2.8) to be positive. The centerline of the cone is given by the eigenvector associated with the negative eigenvalue. The minor and major axes of the elliptic cross-section of the cone are defined by the eigenvectors associated with the positive eigenvalues. The span of the two eigenvectors associated with the positive eigenvalues defines a plane which is perpendicular to the centerline of the cone. Figure 2.2 shows these surfaces for a typical voltage realization.

The analysis of the Hessian motivates a loss model which (approximately) captures the variation in losses as voltages change from a given base voltage condition. This loss model comprises the loss linearization at the base voltage condition together with a set of loss linearizations formed by selecting neighboring voltage realizations. These neighboring points lie on the plane defined by the two eigenvectors associated with the positive eigenvalues. They are very likely to satisfy the convexity criterion necessary for a tight model as

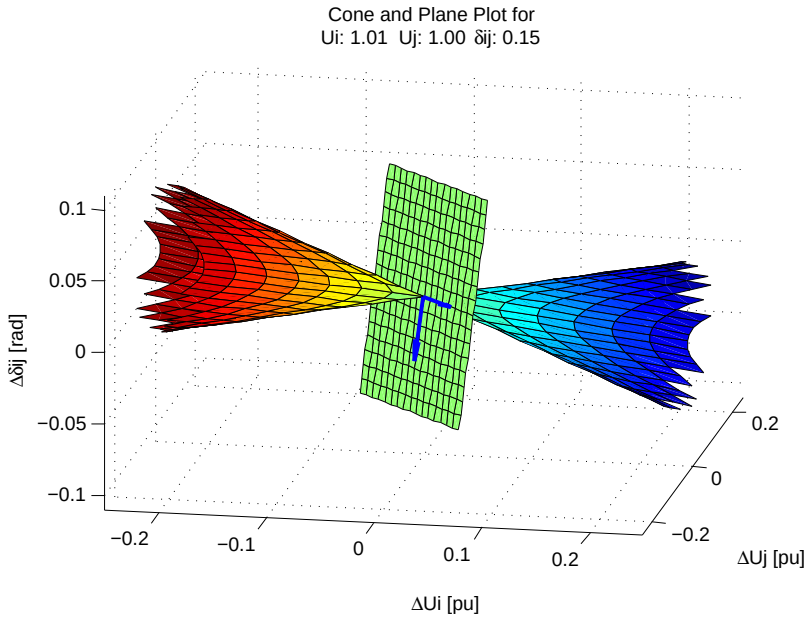

Figure 2.2: Cone and plane defined by the eigen-decomposition of the loss function Hessian matrix. The second-order term of the Taylor-series expansion is positive for points outside the elliptic cone. The plane describes the span of the eigenvectors associated with the two positive eigenvalues.

long as they remain sufficiently close to the original base operating point. This enables the model to capture the local convex nonlinearity of losses while largely eliminating the influence from the concave direction.

If prior knowledge of system behavior is available, the model can also be tuned to improve its accuracy for the likely changes. For instance, as shown in Figure 2.2, one of the eigenvectors with a positive eigenvalue points primarily in the direction of $\Delta\delta_{ij}$ with minimal changes to U_i and U_j. The other points primarily in the direction $+\Delta U_i$, $-\Delta U_j$ with minimal changes to δ_{ij}. If it is known that voltage magnitudes will not vary significantly, more linearization neighbors can be biased in the direction of the first eigenvector to better capture the nonlinearity in that direction.

2.2.3 Trends in the Eigendecomposition of Losses

When voltage conditions across the line change, the eigenvectors and eigenvalues of the Hessian matrix of the loss function will also change. For the greatest accuracy, the position of the neighboring linearization points relative to the base voltage condition should also be updated by finding the new eigenvectors of the Hessian. Doing so will ensure that the most significant nonlinearity of the function is captured by the loss model. However, if computational limits require more rapid implementation of loss model updates, the eigenvectors need not be recomputed for small changes in voltage conditions.

Over the range of typical power system voltages, $U_i,\ U_j \in [0.9, 1.1]$ pu and $|\delta_{ij}| \in [0, \pi/6]$ rad, the

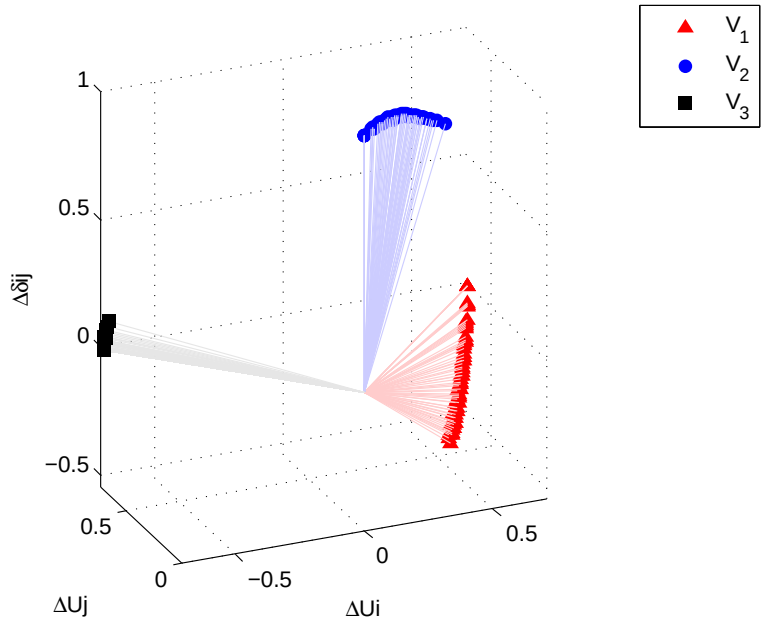

Figure 2.3: Eigenvectors of the loss Hessian for typical network voltages, $U_i,\ U_j \in \{0.9, 1, 1.1\},\ |\delta_{ij}| \in \{0, \pi/60, \pi/30, \ldots, \pi/6\}$. Eigenvectors are ordered by sorting the eigenvalues from negative to positive.

orientation of the eigenvectors of the loss Hessian remain relatively constant. Figure 2.3 shows the three eigenvectors over the set of voltages, $U_i,\ U_j \in \{0.9, 1, 1.1\},\ |\delta_{ij}| \in \{0, \pi/60, \pi/30, \ldots, \pi/6\}$. The eigenvector v_3 associated with the larger positive eigenvalue is identified by black squares. It remains almost unchanged in the direction $[\Delta U_i\ \Delta U_j\ \Delta\delta_{ij}] = [-\frac{1}{\sqrt{2}}\ \frac{1}{\sqrt{2}}\ 0]$. As the angle difference across the line increases in magnitude, the other two eigenvectors rotate slightly around v_3. Changes in voltage magnitude have negligible effect on the orientation of the eigenvectors. When $|\delta_{ij}| \approx 0$, the eigenvector v_2 with the smaller positive eigenvalue, identified by blue circles, points in the general direction $[\Delta U_i\ \Delta U_j\ \Delta\delta_{ij}] = [0\ 0\ 1]$, and the eigenvector v_1 with the negative eigenvalue, indicated by red triangles, points in the direction $[\Delta U_i\ \Delta U_j\ \Delta\delta_{ij}] = [\frac{1}{\sqrt{2}}\ \frac{1}{\sqrt{2}}\ 0]$.

Based on these observations, the eigenvectors of the loss Hessian may not need to be updated when changes in the voltage angle difference across the line are less than 10 degrees. Using the previous eigenvectors to define the directions of the neighboring linearizations will still adequately capture the nonlinearity of the new loss condition and will save time in the computation of the updated loss model.

Over typical operating voltages, the eigenvalues of the loss Hessian change in a predictable manner. Both positive eigenvalues are significantly larger in magnitude than the negative eigenvalue. Figure 2.4 shows the eigenvalues of the scaled loss Hessian, $\frac{1}{2g_{ij}}\nabla^2_{xx}\mathcal{P}^{loss}_{ij}(x)$, over the set of voltages, $U_i,\ U_j \in \{0.9, 1, 1.1\},\ |\delta_{ij}| \in \{0, \pi/60, \pi/30, \ldots, \pi/6\}$. The larger positive eigenvalue, λ_3 in Figure 2.4, remains relatively constant over all typical voltage conditions. The smaller positive eigenvalue, λ_2, increases as voltage magnitudes increase

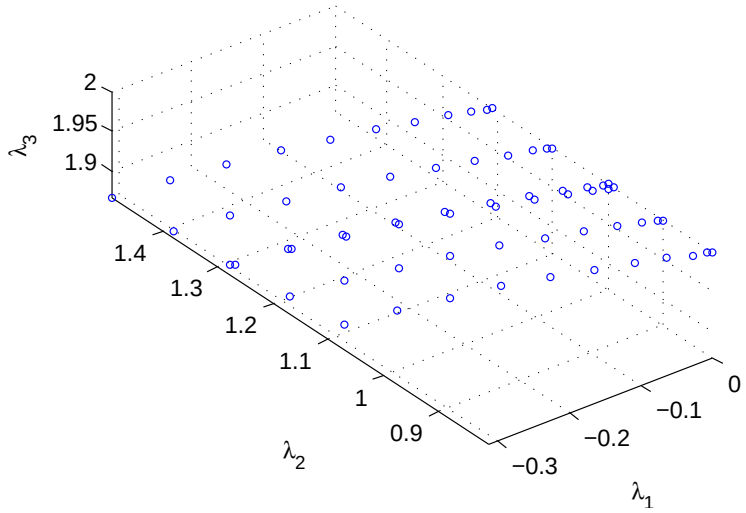

Figure 2.4: Eigenvalues of the scaled loss Hessian, $\frac{1}{2g_{ij}}\nabla^2_{xx}\mathcal{P}^{loss}_{ij}(x)$, for typical network voltages, $U_i,\ U_j \in \{0.9, 1, 1.1\},\ |\delta_{ij}| \in \{0, \pi/60, \pi/30, \ldots, \pi/6\}$. Eigenvalues are ordered by sorting from negative to positive.

while the negative eigenvalue, λ_1, remains mostly unchanged. When the angle difference across the line increases in magnitude, λ_1 decreases (becomes more negative) while λ_2 increases at almost the same rate. For small angle differences, the negative eigenvalue is approximately zero.

Although the proposed loss model does not include additional linearization neighbors in the direction of the eigenvector associated with the negative eigenvalue, the loss function exhibits very little nonlinearity in this direction. The negative eigenvalue, λ_1, is much smaller in magnitude than the two positive eigenvalues. This means that the linearization at the base voltage condition will sufficiently describe the behavior of the loss function in this direction and any overestimation of losses will be slight.

2.2.4 Application to Lower Dimensional Models

The model discussed so far assumes that both the voltage magnitudes and the angle difference between them are allowed to vary during the solution process. However, the presence of buses with fixed voltage magnitudes, such as generator buses, may mean that one or more of the voltage magnitudes in the line loss model remain constant. The effect of this modification is reflected in the eigenvalues of the Hessian in the resulting two-dimensional space.

Removing the row and column from (2.10) associated with a fixed voltage magnitude $U_{fix} \in \{U_i, U_j\}$ results in the Hessian matrix,

$$\nabla^2_{xx}\mathcal{P}^{loss}_{ij}(x) = 2g_{ij}\begin{bmatrix} 1 & U_{fix}\sin(\delta_{ij}) \\ U_{fix}\sin(\delta_{ij}) & U_{free}U_{fix}\cos(\delta_{ij}) \end{bmatrix} \tag{2.19}$$

where $x \equiv [U_{free}\ \delta_{ij}]^\top$. This matrix will always have at least one positive eigenvalue due to the '1' on the main diagonal and will be positive definite within the operating range $0.5 \leq U_i, U_j \leq 1.5$ pu, $|\delta_{ij}| \leq \frac{\pi}{6}$ rad. If the voltage magnitudes are closer to one, the angle difference criterion relaxes to about $\frac{\pi}{4}$ rad. The positive definite characteristic of the Hessian means that any direction can be used to establish neighboring linearizations for the line-loss relaxation.

When both bus voltage magnitudes are fixed and only the angle difference across the line is allowed to vary, the Hessian matrix reduces to a single term,

$$\nabla^2_{xx}\mathcal{P}^{loss}_{ij}(\delta_{ij}) = 2g_{ij}U_iU_j\cos(\delta_{ij}). \tag{2.20}$$

This term is positive in the operating region $0 < U_i, U_j$ and $|\delta_{ij}| < \frac{\pi}{2}$ rad. The resulting model in this situation is very similar to a typical piecewise-linear approximation except that it provides a better loss estimate around the specified baseline voltage condition by utilizing the true voltage magnitudes instead of assuming they are fixed at 1 pu.

2.3 Demonstration of Proposed Loss Model

The steps required to set up the proposed loss model for a single transmission line are outlined as follows:

1. Find the eigenvalues and eigenvectors of the Hessian matrix of the loss function, $\nabla^2_{xx}\mathcal{P}^{loss}_{ij}(x_0)$, for the base voltage condition.

2. Select neighboring voltage realizations, $x_1, \ldots, x_n$, within a relatively small ball on the plane spanned by the eigenvectors associated with the two positive eigenvalues of the Hessian matrix.

3. Define the linear inequality,

$$\mathcal{P}^{loss,app}_{ij}(x) \geq \mathcal{P}^{loss}_{ij}(x_k) + \nabla_x\mathcal{P}^{loss}_{ij}(x_k)^\top(x - x_k),$$

for the loss equation at each point $x_k \in \{x_0, x_1, \ldots, x_n\}$ using (2.1b) and (2.9). The complete loss model can then be expressed as,

$$\mathcal{P}^{loss,gen}_{ij}(x) = \max\left\{0, \max_{k\in\{0,\ldots,n\}}\left\{\mathcal{P}^{loss}_{ij}(x_k) + \nabla_x\mathcal{P}^{loss}_{ij}(x_k)^\top(x - x_k)\right\}\right\}, \tag{2.21}$$

where the outer 'max' ensures that the loss model cannot return a negative value. The superscript '*gen*' identifies this as the generalized loss model, which will be referred to in later discussions as AC-GEN.

4. Confirm that each inequality is the binding constraint at its own linearization point (i.e. $\mathcal{P}_{ij}^{loss,app}(x_k) = \mathcal{P}_{ij}^{loss}(x_k)$ for each $k = 0, ..., n$). Discard any constraints which do not satisfy this criterion.

If the neighboring voltage realizations conditions are selected well by remaining relatively close to the base voltage condition, step 4 should rarely discard any constraints.

This process can be tuned to improve performance when specific voltage changes are likely or more significant. For instance, in networks where voltage magnitudes change little, linearization neighbors can be biased in the direction of the eigenvector which emphasizes changes in angle difference.

The performance of the proposed approach (AC-GEN) is compared against two common linear loss models. The first is a simple first-order Taylor-series expansion of the line loss equation (2.1b) in terms of voltage magnitudes and angle difference (AC-LIN),

$$\mathcal{P}_{ij}^{loss,lin}(x) = \mathcal{P}_{ij}^{loss}(x_0) + \nabla_x \mathcal{P}_{ij}^{loss}(x_0)^\top (x - x_0). \tag{2.22}$$

The second is a piecewise-linear approximation of the squared angle difference which ignores voltage magnitudes (DC-PWL) [63]. Each loss modelling technique is employed to approximate the line loss equation (2.1b) for every line in a network.

Both the AC-GEN and DC-PWL models require various input parameters. DC-PWL requires the maximum possible angle difference across the line and the number of segments to use in the piecewise linear approximation. For this analysis, the maximum angle was set to 2.5 times the angle at the line rating, $\delta_{ij}^{max} = 2.5 X_{ij} P_{ij}^{lim}$ using the DC power flow approximation. This range was broken into 25 segments. AC-GEN requires the distance from the base voltage condition, x_0, to the neighboring voltage realizations, $x_1, \ldots, x_n$. For this analysis, eight evenly spaced neighboring realizations were selected from the edge of a circle on the plane spanned by the two eigenvectors associated with positive eigenvalues. The radius of this circle was chosen to be 0.005 pu. Figure 2.5 exemplifies how each of these modeling approaches sectionalizes the space of voltage variables, $[U_i \; U_j \; \delta_{ij}]$, to approximate the nonlinear losses.

To demonstrate the operational characteristics on a realistically large network, the MATPOWER [68] test case based on the 2383-bus Polish grid for the 1999-2000 winter peak was used for the discussions in this section. This test network provides a wide variety of realistic voltage and impedance characteristics. Since losses are only affected by series conductance, g_{ij}, the R/X ratios of the lines do not directly affect the various loss models. However, different impedance characteristics cause the voltages across lines to vary in different ways, providing a variety of test conditions for the three loss models.

Testing was undertaken for 25 different scenarios. Five random base-case power flow scenarios were generated and then five random demand deviations were established for each base-case. For each of the

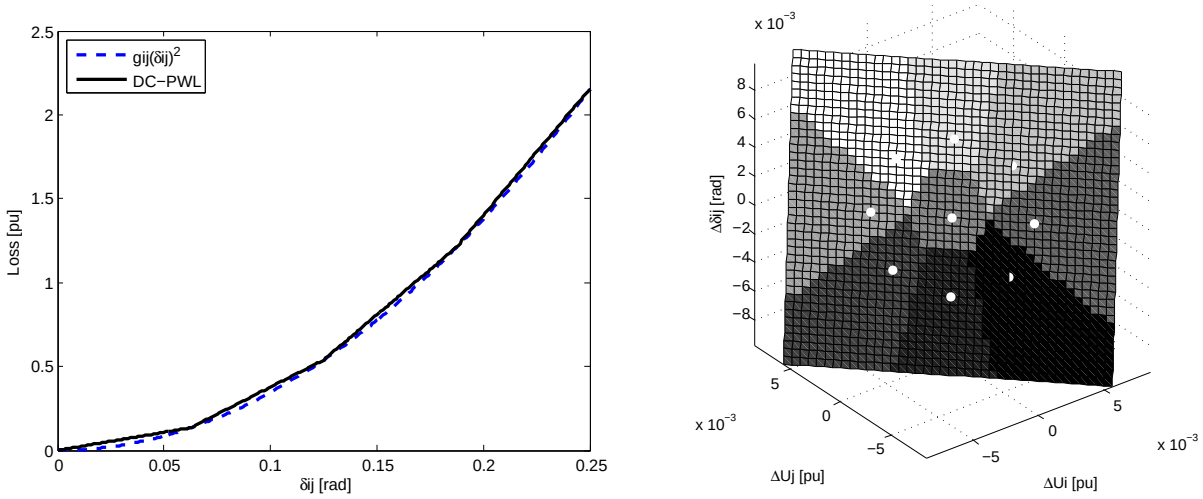

(a) (b)

Figure 2.5: Sample representations for DC-PWL and AC-GEN. (a) DC-PWL only considers variation in angle difference. (b) AC-GEN behavior on the plane spanned by the eigenvectors associated with the positive eigenvalues of the Hessian. White dots indicate linearization points. Shading indicates the regions where each linear inequality is binding.

25 scenarios, a power flow captured the true line losses and the voltage deviations from the corresponding base-case. The voltage deviations were applied to each loss model to calculate its estimated losses. The models for AC-GEN and AC-LIN require a starting voltage condition and were updated for each base-case scenario. The DC-PWL model does not depend upon initial voltages so was generated once at the start of testing. Each base-case scenario was created by randomly perturbing active and reactive power loads. Active power loads were uniformly distributed over the range $\pm 50\%$ of their values given in the MATPOWER case, while reactive power loads were uniformly distributed over the range $\pm 30\%$ of their MATPOWER values. The deviation cases were likewise created by randomly perturbing active and reactive power loads, in this case over the ranges $\pm 50\%$ and $\pm 30\%$, respectively, of their values in the corresponding base-case scenario.

The errors between the actual line losses and the losses predicted by each model, for all lines in the Polish network across all 25 tests, giving a total of $L = 2896 \times 25 = 72,400$ cases, are summarized in Figure 2.6 and Table 2.1. The results of Figure 2.6a show the loss prediction error, $\text{Err}_\ell = \text{est}_\ell - \text{act}_\ell$, in per unit, while Figure 2.6b provides additional perspective by normalizing these errors, $\%\text{Err}_\ell = 100 \times (\text{est}_\ell - \text{act}_\ell)/\text{act}_\ell$. Normalized errors were ignored for loss values less than 1×10^{-4} pu. The AC-GEN model (2.21) and the DC-PWL model [63] are structured such that they do not allow negative losses. Consequently, their normalized errors cannot fall below -100%. This limit is evident in Figure 2.6b. In contrast, losses computed by the AC-LIN model (2.22) are directly dependent upon voltage values and therefore may go negative. Figure 2.6b also highlights the tendency for AC-GEN and AC-LIN to underestimate the loss function since it is convex

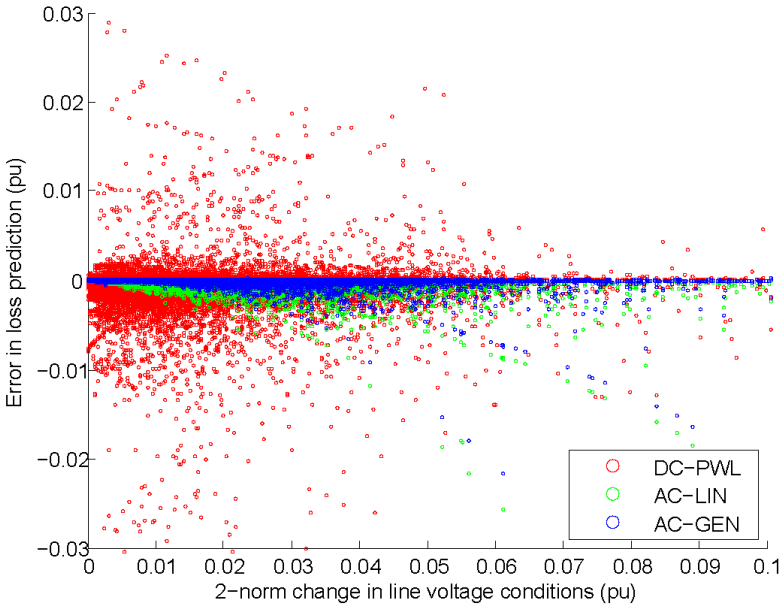

(a)

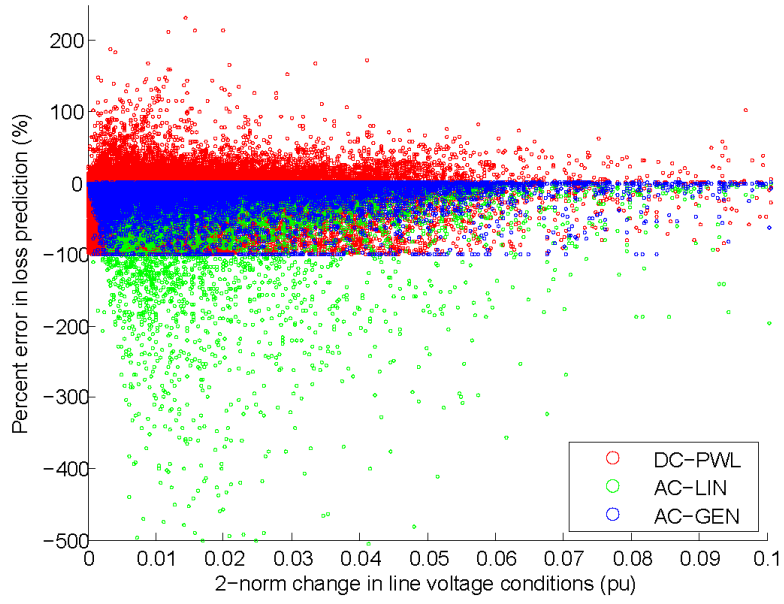

(b)

Figure 2.6: Errors between actual and estimated line losses for 25 tests on the Polish 2383-bus network. The x-axis position is determined using $\sqrt{\Delta U_i^2 + \Delta U_j^2 + \Delta \delta_{ij}^2}$. (a) Error in pu, Err = est − act. (b) Error in percent, %Err = 100 × (est − act)/act. Percent error for losses less than 1×10^{-4} pu is ignored.

in most directions and only weakly concave otherwise.

As expected, the AC-GEN and AC-LIN methods are both more accurate than the DC-PWL method for small changes in voltage conditions, as shown in Figure 2.6a for voltage changes between 0 and 0.02 pu. Both AC-GEN and AC-LIN start from a tight approximation of losses due to the linearization around the base-case

Table 2.1: Average loss error over 25 tests on the Polish 2383-bus network.

Method	$\frac{1}{L}\sum_{\ell=1}^{L} \text{Err}_\ell$, pu	$\frac{1}{L}\sum_{\ell=1}^{L} \lvert\text{Err}_\ell\rvert$, pu	$\frac{1}{L}\sum_{\ell=1}^{L} \lvert\%\text{Err}_\ell\rvert$, %
AC-GEN	-4.6×10^{-5}	4.6×10^{-5}	5.88
AC-LIN	-1.0×10^{-4}	1.0×10^{-4}	13.46
DC-PWL	-2.6×10^{-4}	4.4×10^{-4}	24.21

whereas DC-PWL has no mechanism for using base-case information. For voltage changes beyond 0.005 pu, AC-GEN improves upon AC-LIN due to the additional linearizations at neighboring voltage realizations, but both methods show quadratic growth in their error for large voltage deviations. This is due to their underlying local linearization structure. In contrast, the broader nonlinear characteristic of the DC-PWL method helps to suppress some of this behavior.

The summary in Table 2.1 assists in clarifying the overall performance of each method. The error summations given in the first column take into account the sign of the error and therefore provide an indication of the total system-wide error (with positive and negative errors partially canceling). The other columns consider the absolute value of the error, giving a better indication of the overall trend in line-by-line errors. In that sense, the right-most column is most relevant, providing a comparison of the average absolute value of the normalized errors. The AC-GEN method is more than twice as accurate as the AC-LIN method and more than four times as accurate as the DC-PWL method. Even though the 25 test cases exhibit significant variation in active and reactive power loads, and hence in network voltages, the AC-GEN loss model generally provides very good accuracy.

The results shown in Figure 2.6 and Table 2.1 indicate that even an untuned application of the proposed loss model can result in appreciable improvements in accuracy compared to existing methods. In those tests, the distance to the linearization neighbors was the same for every line. However, voltages change much more noticeably on some lines than others and the AC-GEN model can easily be tuned to capture this effect. Additionally, voltage changes tend to be much larger in the direction of the eigenvector with the smaller positive eigenvalue than in the direction of the eigenvector with the larger positive eigenvalue. This trend can also be used to better model the unique loss characteristics of each line.

The perturbations in voltages for each of the 25 tests can be transformed into the eigenbasis coordinates of the loss Hessian for each line, $[\Delta U_i \ \Delta U_j \ \Delta\delta_{ij}]^\top = \Delta v_1 \times v_1 + \Delta v_2 \times v_2 + \Delta v_3 \times v_3$ where Δv_i is the scalar coordinate associated with eigenvector v_i. Figure 2.7 shows this eigenbasis representation. It is apparent that voltage changes lie primarily in the direction of v_1, the eigenvector with a negative eigenvalue. Modest changes occur in the direction of v_2, the eigenvector with the smaller positive eigenvalue, and only limited

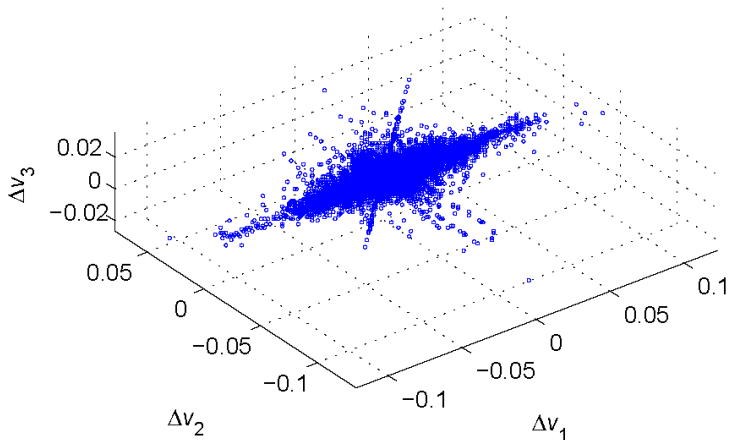

Figure 2.7: Change of line voltages in eigenbasis coordinates for 25 tests on the Polish 2383-bus network. Eigenvectors are ordered by sorting the eigenvalues from negative to positive on each line.

changes occur in the direction of v_3, the eigenvector with the larger positive eigenvalue. Although AC-GEN avoids linearization neighbors in the direction of v_1, the loss function is approximately linear in this direction and the base linearization sufficiently describes these changes.

Analyzing the results of Figure 2.7 reveals that voltage changes in the direction of v_2 are approximately five times larger than those in the v_3 direction. To better capture this pattern, the circle of white dots shown in Figure 2.5b was flattened into an ellipse whose axis in the direction of v_2 is five times the length of the axis in the direction of v_3. Additionally, two extra linearization neighbors were added in the direction of v_2 at twice the distance from the base condition. These helped capture even larger voltage changes in this direction.

The majority of voltage changes in Figure 2.7 are very close to the origin. However, some lines tend to experience much larger changes in voltage than others. Such prior knowledge can be used to establish, on a line-by-line basis, the length of the minor axis of the ellipse that describes the locations of the linearization neighbors.

The tuned AC-GEN model was tested on the same data as previously. The results are shown in Figure 2.8. Comparing with Figure 2.6a, it can be seen that tuning has resulted in additional improvements in overall accuracy and has eliminated the larger errors. The mean absolute error in the loss prediction, $\frac{1}{L}\sum_{\ell=1}^{L}|\text{Err}_\ell|$, is reduced to 3.0×10^{-5} pu or 2.55%. This type of tuning could easily be implemented in practice by using readily available historical data and performing more sophisticated data analysis.

In addition to considering the model accuracy, it is important to evaluate the influence of the loss model on the speed of optimization and control applications. To test this characteristic, each of the three models was applied within a simple QP which sought to drive voltage magnitudes and angles towards specified

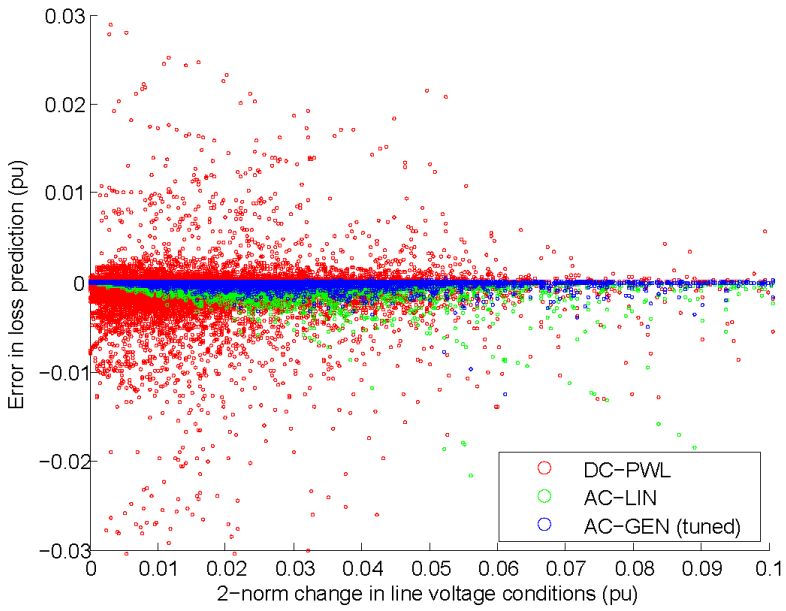

Figure 2.8: Errors between actual and estimated line losses for 25 tests on the Polish 2383-bus network. AC-GEN has been tuned for likely behavior on each line. The x-axis position is determined using $\sqrt{\Delta U_i^2 + \Delta U_j^2 + \Delta \delta_{ij}^2}$. The y-axis shows error in pu, err = est − act.

values while also minimizing total network losses.[1] This QP was run for each of the 25 test cases. The only constraints in each program were the loss models relating line losses to network voltages and a single summation of all line losses into total losses. Testing was performed on an HP ProBook 6470b with a 2.90 GHz Intel® i7 processor and 8 GB of RAM. The QP was formulated in MATLAB® and solved in Gurobi [69].

A summary of the QP constraint sets and the time required to build the loss model and solve each QP for each of the 25 test cases is presented in Table 2.2. The AC-LIN method has the smallest set of constraints and can be built and solved significantly faster than both the untuned AC-GEN and DC-PWL methods. The untuned AC-GEN method requires the most time to build and solve and takes about 46% longer to solve than the DC-PWL method. If the eigenvectors are not updated when building the AC-GEN model, the build time can be reduced by around 30%.

From the results of the case-study tests, it is apparent that trade-offs exist for each of the three methods. Subject to the formulation requirements discussed in Section 2.2, AC-GEN offers the greatest accuracy in predicting line losses. However, this improvement in accuracy requires an increase in the time to build and solve the model. Alternatively, if memory and time constraints are of primary concern, a simple linear model may provide acceptable accuracy depending on the application.

[1]The QP was not meant to address any real problem, but rather provide a means of establishing the relative computational costs of the three loss modelling formulations.

Table 2.2: QP test results for various loss models.

Method	Equalities	Inequalities	Variables	Build Time [μs/line]	Solution Time [s]
AC-GEN	1	26064	7663	167.	1.14
AC-LIN	2897	0	7663	3.14	0.02
DC-PWL	8689	0	85855	12.7	0.78

Several challenges may arise from incorporating a line-loss model into optimal power flow problems for both operational cost minimization and expansion planning. When negative prices are possible, any relaxation method (e.g. AC-GEN or DC-PWL) may cease to be tight as fictitious losses can reduce the overall cost [70, 71]. In this situation, a heuristic is necessary to remove the fictitious losses. For the AC-GEN method, the simplest solution is to use the AC-LIN model on any line connected to a bus with negative price. Also, [64] points out that the types of loss models discussed here can slow convergence by oscillating as they approach a solution. Unfortunately, the nonconvexity of the loss function when voltage magnitude variations are considered prohibits the extension of the method in [64] where successive "cutting planes" are added. However, to limit oscillation in the AC-GEN method, the distance to the linearization neighbors can be reduced as the solution is approached.

Another challenge with loss models which require updates as operating conditions change (e.g. AC-GEN and AC-LIN) is that these steps require additional computation. For the AC-LIN method, these costs are very small but AC-GEN may require some consideration depending on the application. For best results, AC-GEN should be updated whenever network voltages change. However, if these changes are small and remain within the region bounded by the linearization neighbors, it may be acceptable to retain the previous model. Ultimately, the design needs of the specific application will determine whether accuracy or speed is more important.

The application environments which are likely to benefit the most from the AC-GEN method are those which model losses on a small number of lines, require a linear constraint formulation, but also require good accuracy. Examples may include distributed or microgrid controllers or controllers such as the one studied in this work. In situations where line losses are predicting thermal behavior, small improvements in the line loss accuracy can result in amplified improvements in the temperature prediction.

Chapter 3

Accuracy and Simplicity in the Controller Model

The accuracy of the internal model of MPC when compared to the physical system determines the suitability of the control actions identified by MPC. Ideally, the model and real-world behavior would match perfectly, but the complexity of electric power systems makes this impossible and requires simplification of the internal model.

When determining how to simplify the internal model of MPC, the main objective is to adequately describe the most relevant behavior. As mentioned in Section 2.2.1, any constraints which are not binding at the solution add to the computational complexity of the problem but do not improve the solution quality. This chapter discusses improvements in the power flow, transmission temperature, and transformer models while attempting to find the appropriate balance between accuracy and simplicity in the problem formulation.

3.1 Power Flow

Capturing the relationship between power and voltage in electric power systems is a challenging requirement of optimal power flow applications. The physical relationship between network voltages and the flow of power is nonlinear and nonconvex. The formulation of (1.4) utilized by this work requires linear constraints. Therefore, any power flow relationship embedded into the constraints of the problem will be an approximation of the true nonlinear behavior.

The steady-state (nominal frequency) behavior of power systems is typically described in terms of complex-valued representations of power and voltage. Power, $S = P + \mathbf{j}Q$, is commonly stated in terms

of its rectangular coordinates of active power, P, and reactive power, Q. Voltage, $V = Ue^{\mathbf{j}\delta}$, is frequently given in polar coordinates with magnitude, U, and angle, δ. Following these conventions, the power flow relationship at each node in a network, $i \in \mathcal{N}$, with complex admittances, $Y = G + \mathbf{j}B$, is expressed as,

$$P_i = U_i \sum_{j \in \mathcal{N}} U_j (G_{ij} \cos(\delta_i - \delta_j) + B_{ij} \sin(\delta_i - \delta_j)), \tag{3.1a}$$

$$Q_i = U_i \sum_{j \in \mathcal{N}} U_j (G_{ij} \sin(\delta_i - \delta_j) - B_{ij} \cos(\delta_i - \delta_j)), \tag{3.1b}$$

and is referred to as AC power flow.

Throughout the years, different methods have been used to approximate (3.1) using linear expressions. Probably the most well known and commonly used method is the DC[1] power flow which ignores (3.1b); assumes voltage magnitudes are at unity, $U \approx 1$; assumes resistance is negligible, $0 \approx G \ll B$; and assumes voltage angles are small, $\sin(\delta) \approx \delta$ [72]. This results in a linear relationship between active power and voltage angle, $P_i = \sum_{j \in \mathcal{N}} B_{ij}(\delta_i - \delta_j)$. Unfortunately, this technique requires rather strong assumptions which mask important characteristics of real-world power systems. Other works have proposed alternative linear models of the AC power flow which do not require such strong assumptions [72, 73]. These works discuss hot-start models for linearized power flow which utilize off-nominal AC power flow conditions as linearization points. The models discussed in [72] follow the "MW-only" strategy of DC power flow by ignoring reactive power and fluctuating voltage magnitudes. Alternatively, [73] presents models which incorporate reactive power and changing voltage magnitudes. At the core of these models is a polyhedral relaxation of the cosine function capturing its nonlinearity for small voltage angles.

The previous formulation of (1.4) on which this work expands was developed using the DC power flow and will be referred to as DC-MPC [6–8]. That simplified model provides adequate accuracy under normal operating conditions but is less appropriate as the system becomes stressed. Furthermore, ignoring reactive power flows may underestimate line losses and impede MPC's ability to remove thermal overloads on lines with significant reactive power flows. Also, assuming voltage magnitudes remain fixed at 1 pu may mask unacceptable voltage deviations.

3.1.1 Linearized AC Power Flow Constraints

To improve MPC's ability to handle the variety of operating conditions present in practical power systems, the power flow model was expanded to include the effects of voltage magnitude and reactive power. The power flow relationship of (3.1) is approximated by a simple first-order Taylor expansion, $f(x_0 + \Delta x) \approx$

[1] Uppercase 'DC' refers to the simplified linearization of the AC power flow equations and should not be confused with the power flow equations in a direct current system.

$f(x_0) + (\partial f(x_0)/\partial x)\,\Delta x$. This approach was selected over the hot-start models of [72, 73] because the changes in operating conditions over the horizon of MPC will tend to be relatively small causing higher-order terms in the expansion to become negligible. Additionally, a practical implementation of this control process would have access to the state estimator data which provides the current operating condition of the network along with the first-order sensitivities at time l, the start of the prediction horizon. This linearized formulation of MPC will be referred to as LAC-MPC.

The measured operating condition at the start of the MPC prediction horizon is used as the linearization point for the model, x_0, and variables in (1.4) represent changes from the base conditions, Δx. This allows the power flow relationship in LAC-MPC to be linearly approximated as,

$$\sum_{n\in\Omega_i^G}\Delta p_{Gn}[k] + \sum_{n\in\Omega_i^R}\Delta p_{Rn}[k] - \sum_{n\in\Omega_i^D}\Delta p_{Dn}[k] - \sum_{n\in\Omega_i^S}\Delta p_{Sn}[k] = \sum_{j\in\mathcal{N}}\frac{\partial P_i}{\partial V_j}\Delta V_j[k] + \sum_{j\in\Omega_i^N}\frac{\partial P_i}{\partial t_{ij}}\Delta t_{ij}[k], \quad (3.2a)$$

$$\sum_{n\in\Omega_i^G}\Delta q_{Gn}[k] + \sum_{n\in\Omega_i^R}\Delta q_{Rn}[k] - \sum_{n\in\Omega_i^D}\Delta q_{Dn}[k] = \sum_{j\in\mathcal{N}}\frac{\partial Q_i}{\partial V_j}\Delta V_j[k] + \sum_{j\in\Omega_i^N}\frac{\partial Q_i}{\partial t_{ij}}\Delta t_{ij}[k], \quad (3.2b)$$

for $k \in \{0, \ldots, M-1\}$ and $i \in \mathcal{N}$.

The notation $\mathcal{N}$ represents the set of all nodes, and Ω_i^N, Ω_i^G, Ω_i^R, Ω_i^D, and Ω_i^S represent the sets of all neighboring nodes, generators, renewables, loads, and storage devices of node i, respectively. A condensed notation, $\Delta V_j = [\Delta\delta_j\ \Delta U_j]^\top$, is used for the voltage angle and magnitude at bus j, and $\partial P_i/\partial V_j$ is a shorthand expression of the first-order partial derivatives of (3.1a) with respect to voltage angle and magnitude. Similarly, $t_{ij} = a_{ij}e^{\mathbf{j}\psi_{ij}}$ represents the complex transformer tap ratio on branch ij with similar first-order partial derivatives, and the term $\Delta t_{ij} = [\Delta\psi_{ij}\ \Delta a_{ij}]^\top$ represents changes in the tap phase and magnitude from the condition at the start of the prediction horizon. The notation in (3.2b) is equivalent, and the first-order partial derivatives are derived with respect to (3.1b).

3.1.2 Voltage Magnitude Limits

Power system operation must ensure that voltage magnitudes remain within specified limits. These voltage limits are incorporated into the LAC-MPC formulation as soft constraints, where deviations above or below the acceptable range are penalized in the objective function. Two relaxation variables, U_n^+ and U_n^-, are defined for each bus with,

$$\Delta U_n[k] + U_n^{meas} - U_n^{max}[k] \le \frac{U_n^+[k]}{100}, \quad (3.3a)$$

$$U_n^{min}[k] - \Delta U_n[k] - U_n^{meas} \le \frac{U_n^-[k]}{100}, \quad (3.3b)$$

for $k \in \{0, \ldots, M-1\}$.

Both U_n^+ and U_n^- are (quadratically) penalized for deviating from zero. As U_n^+ and U_n^- are defined in percent, the division by 100 in (3.3) is necessary to convert units from percent to per unit. For buses with specified voltage schedules such as generator buses, U_n^{max} and U_n^{min} are both fixed to the scheduled voltage magnitude.

3.2 Transmission Limits

As mentioned in Section 1.2.3, transmission limits are typically designed to protect against excessive sag as the conductor heats up under heavy load. Directly modeling the temperature behavior of a transmission line allows more power to be transferred across the line because the conservative weather assumptions used when specifying the line power rating can be replaced with real-time weather data.

To control the line temperature from an electrical perspective, line power losses can be increased or decreased. The inclusion of voltage magnitudes into the formulation of (1.4) enables more accurate models for the losses on each line. This allows the controller to make predictions which better match the real-world behavior and bring it closer to the optimal control strategy.

3.2.1 Transmission Line Thermal Model

The thermal characteristics of a bare overhead transmission line are well understood. IEEE Standard 738 provides a useful description of the relationship between temperature and current in a transmission line [1]. The factors influencing conductor temperature include conductor material properties, conductor diameter, conductor surface conditions, conductor electrical current, and ambient weather conditions. This results in a nonlinear dynamic temperature characteristic,

$$\dot{T} = \frac{1}{mC_p}\left[R(T)I^2 + q_s - q_c(T) - q_r\left(T^4\right)\right], \tag{3.4}$$

with T representing the temperature of the conductor, mC_p the unit length heat capacity, $R(T)$ the temperature dependent conductor resistance, I the current in the conductor, q_s the solar heat gain rate, $q_c(T)$ the temperature dependent conductive heat loss, and $q_r\left(T^4\right)$ the radiative heat loss.

A strategy for grouping terms and simplifying the notation is given in [6]. This allows the thermal behavior to be expressed in terms of losses p_{ij}^{loss}, solar heat gain q_s, conductor temperature T, and ambient

temperature T_{amb},

$$\dot{T} = \frac{1}{mC_p}\left[p_{ij}^{loss} + q_s - \eta_c(T - T_{amb}) - \eta_r\left((T+273)^4 - (T_{amb}+273)^4\right)\right]. \tag{3.5}$$

The terms η_c and η_r are positive constants representing conductive and radiative parameters, and the temperatures are given in degrees Celsius. This nonlinear thermal characteristic is used to represent the true behavior of the physical system when testing MPC but must be linearized for use within MPC's internal predictive model.

The steady-state condition when the line operates at its rated current is the equilibrium point around which (3.5) is linearized with $T^* = T_{lim}$, $p_{ij}^{loss*} = p_{ij}^{loss,lim} = R(T^*)I_{lim}^2$, T_{amb}^*, and q_s^*. Changes away from this condition are represented by Δ terms[2] (e.g. $\Delta T = T - T^*$). If a transmission line's thermal limit is violated, it is easily detected with this notation as ΔT becomes positive. This linearization process is described in [6], and a summary of the discrete-time, linear internal model is presented below.

3.2.2 Thermal Model Constraints

Within MPC, thermal overloads on transmission lines (i.e. $\Delta T > 0$) are penalized to direct the controller toward a secure operating condition. The temperature dynamics in (1.4) are primarily driven by the line losses through the following constraints:

$$\Delta T_{ij}[k+1] = \tau_{ij}\Delta T_{ij}[k] + \rho_{ij}\left(p_{ij}^{loss}[k] - p_{ij}^{loss,lim} + \Delta q_{s,ij}[k]\right) + \gamma_{ij}\Delta T_{ij}^{amb}[k], \tag{3.6a}$$

$$\Delta T_{ij}[0] = \Delta T_{ij}^{meas}, \tag{3.6b}$$

$$\Delta T_{ij}[k+1] \leq \Delta\hat{T}_{ij}[k+1], \tag{3.6c}$$

$$0 \leq \Delta\hat{T}_{ij}[k+1], \tag{3.6d}$$

$$\Delta\hat{T}_{ij}[M] \leq 0, \tag{3.6e}$$

$$p_{ij}^{loss}[k] \geq \mathcal{P}_{ij}^{loss}(x_n) + \nabla_x\mathcal{P}_{ij}^{loss}(x_n)^\top\left(\Delta x[k] + x_0 - x_n\right), \qquad n \in \{0,\ldots,L\}, \tag{3.6f}$$

$$0 \leq p_{ij}^{loss}[k], \tag{3.6g}$$

for $k \in \{0,\ldots,M-1\}$.

These constraints are enforced for every transmission line ij in the network. Equation (3.6a) is a discretized linearization of the conductor temperature relationship [1] and is taken from [6, 7]. The term ΔT_{ij} describes the difference between the actual conductor temperature and the steady-state temperature when

[2]This differs from other 'Δ' variables within MPC which track changes from the start of the prediction horizon.

the line is operating at its current rating. The modeled losses on the line and the losses when the line is operating at its rating are given by p_{ij}^{loss} and $p_{ij}^{loss,lim}$, respectively. The terms $\Delta q_{s,ij}$ and ΔT_{ij}^{amb} indicate changes in the solar flux and ambient temperature from those used in the linearization. For this work, both of these values are assumed to remain constant, but could be used as external disturbances on the line temperature behavior. The coefficients τ_{ij}, ρ_{ij}, and γ_{ij} are defined in [6, 7] and are based on conductor material properties and weather conditions when the temperature equation is linearized.

The initial line temperature is set to its measured value at the beginning of the prediction horizon using (3.6b). Conductor temperatures are only penalized for deviations above their steady-state value at the line rating so equations (3.6c) and (3.6d) define a relaxation of the line temperature, $\Delta\hat{T}_{ij}$, which is penalized in the objective when the temperature increases above its rated steady-state value. For stability, (3.6e) enforces a terminal condition that all thermal overloads must be eliminated by the end of the prediction horizon. Equation (3.6f) represents the AC-GEN loss model described in Section 2.3. The loss function $\mathcal{P}_{ij}^{loss}(x)$, given by (2.1b), is linearized around the measured voltage condition at the start of the prediction horizon, x_0, and at L additional neighboring voltage conditions, $x_n,\ n \in \{1, \ldots, L\}$. The term $x \equiv [U_i\ U_j\ \delta_{ij}]^\top$ represents a shorthand notation of the voltage conditions on the line. Equation (3.6g) ensures that modeled losses remain nonnegative.

3.2.3 Thermal Model Validation

To demonstrate the performance of the linearized temperature model (3.6a), the case-study from Figure 2 in [1] has been reproduced. A 26/7 Drake ACSR conductor undergoes a step change in current from 800 amps to 1200 amps. The actual change in conductor temperature is simulated using the true nonlinear dynamical model of (3.5) with 60 second Euler integration steps. Starting from 81°C, it rises to 128°C, as shown by the solid blue curve in Figure 3.1.

The linear model (3.6a) was subjected to the same step change in current. The coefficients τ_{ij} and ρ_{ij} are determined at the steady-state conditions prior to the step change (i.e. the model is linearized at 800 amps and 81°C) using the technique presented in Section III-D of [7] and assuming a 60 second time-step. The terms $\Delta q_{s,ij}$ and ΔT_{ij}^{amb} are not incorporated into the test since ambient conditions do not change. The thermal behavior predicted by the linear model is shown as the dashed green curve in Figure 3.1.

It can be seen from Figure 3.1 that both models predict very similar behavior near the linearization conditions. However, the linear model cannot fully describe the variation of resistance and heat transfer with temperature.

Although the concept of a thermal time constant is not directly applicable to the nonlinear model of

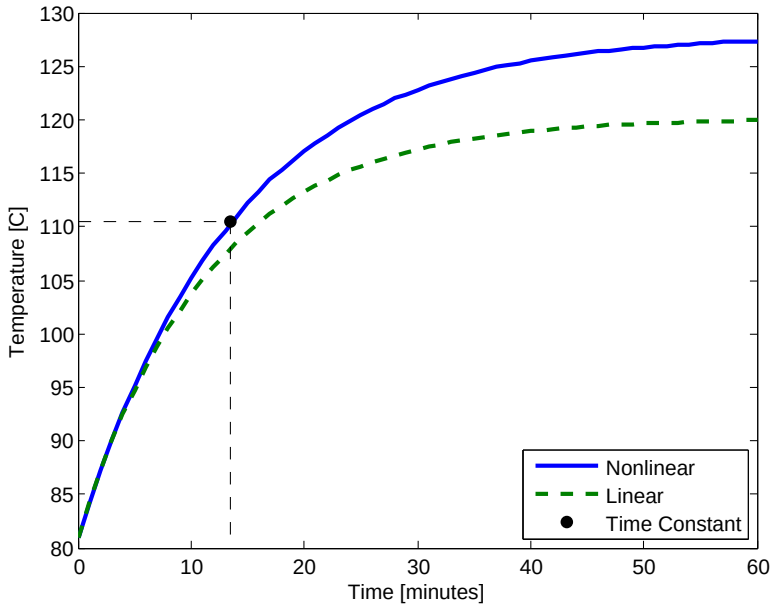

Figure 3.1: Temperature response of 26/7 Drake ACSR conductor to a step change in current from 800 A to 1200 A using both nonlinear and linear models. Test conditions are replicated from Figure 2 of [1].

thermal behavior, it can provide intuition regarding the rate of change for transmission line temperature dynamics. Assuming an exponential curve, the time constant denotes the time required to achieve 63% of the change from the initial temperature to the final value. For the example of Figure 3.1, the time constant is 13.4 minutes.

3.2.4 Demonstrating the Benefits of Accuracy

The benefits of using a linearized AC power flow description and the AC-GEN loss model of Section 2.3 are easily highlighted using a simple two bus power system. A constant load with 100 MVAr capacitive compensation is supplied by a single transmission line strung with 24/7 Peacock ACSR conductor. The network parameters are given in Table 3.1 and the steady-state condition is shown in Figure 3.2a. The losses are 4.80 MW, and the transmission line temperature settles at 88.2°C.

To disrupt the steady-state conditions, the load bus capacitor is disconnected from the system. The slack generator responds to the loss of 90.7 MVAr to balance the network. Both a DC model and a linearized AC model predict the new steady-state voltages and losses. The DC model ignores reactive power and predicts that voltage conditions remain unchanged. The linearized AC formulation of (3.2) predicts that the load voltage magnitude drops to 0.911 pu and the voltage angle changes to -7.22 degrees.

The voltage predictions of both the DC and linearized AC models are utilized to estimate the new steady-state losses. The DC model uses the DC-PWL formulation mentioned in Section 2.1 to describe losses in

Table 3.1: Two-bus network and thermal parameters

Parameter	**Value**	**Units**
Sampling Time, T_s	60	s
3-phase power base	100	MVA
Line-to-line base voltage	230	kV
Line length	14.5	mi
Line reactance, X_{ij}	0.042	pu
Line shunt susceptance, B_{ij}	0.088	pu
Thermal rating, f_{ij}^{lim}	303	MVA
Ambient Temperature, T_{amb}	35	°C
Wind speed, angle, $v_w \angle \theta_w$	0.61, $\pi/2$	m/s, rads
Conductor diameter, D_{ij}	24.2	mm
Heat capacity, $mC_{p,ij}$	958	J/m-°C
Ampacity, I_{ij}^{lim}	760	A
Resistance per unit length	113.5	$\mu\Omega$/m
Temperature limit, T_{ij}^{lim}	86	°C
Temperature coefficient, τ_{ij}	0.886	-
Loss coefficient, ρ_{ij}	0.063	°C-m/W
Solar heat gain rate, $q_{s,ij}$	22.5	W/m

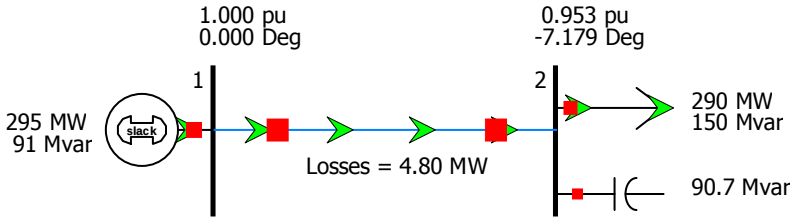

(a)

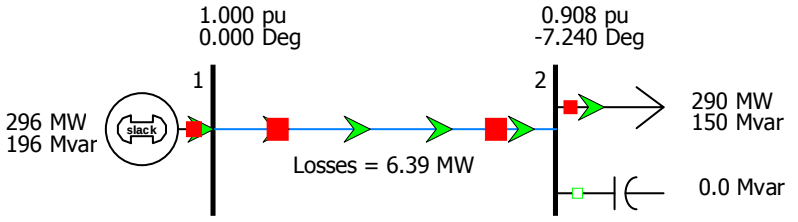

(b)

Figure 3.2: Steady-state conditions with a) capacitor connected and b) capacitor disconnected.

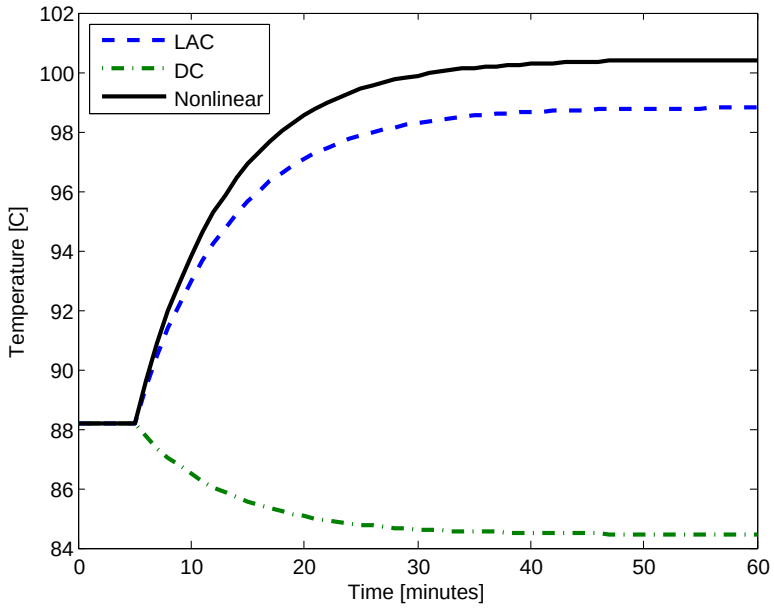

Figure 3.3: Temperature response of the transmission line in Figure 3.2 due to capacitor disconnection at minute five. The predictions of linear models based on DC and linearized AC (LAC) techniques are compared to the more accurate nonlinear model.

terms of the squared angle difference. The model discretizes the absolute angle difference across the line into 20 segments of width 0.728 degrees. The linearized AC model predicts losses using the AC-GEN formulation from Section 2.3. The (eight) additional voltage cases required for this formulation lie on a circle with radius 0.02 pu around the pre-contingency voltage case.

Although the DC model predicts that voltages remain unchanged, it estimates the new losses to be 4.39 MW instead of remaining at 4.80 MW. This underestimation is a result of ignoring the off-nominal voltage and reactive power flow which increase losses. The linearized AC model predicts that the new losses are 6.22 MW. The actual change in voltage and losses is found using a power flow and the results are presented in Figure 3.2b.

The actual temperature change of the transmission line is determined using the power flow losses and the nonlinear thermal dynamics in (3.5). The response is shown by the solid black curve of Figure 3.3, where the capacitor is disconnected at minute five. The losses given by the DC and linearized AC (LAC) models are used to predict the thermal response, with the results given by the dashed curves of Figure 3.3. The linearized AC estimation of losses is much closer to the actual losses than the DC estimation and provides a good approximation[3] of the thermal response. The DC method actually predicts a drop in temperature rather than a rise as it ignores reactive power and underestimates the losses.

This simple example highlights the importance of incorporating reactive power and voltage magnitudes

[3]The error in the linearized AC prediction of losses will be corrected through the feedback inherent in the MPC process.

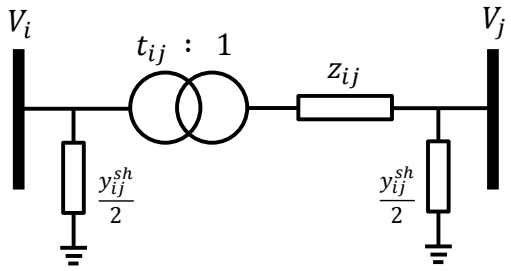

Figure 3.4: The Unified Branch Model allows both transformers and transmission lines to be described within a single framework.

into the MPC formulation. A DC implementation could predict that a transmission line is secure, even though emergency intervention is actually required. Such erroneous operation could later necessitate more extreme control action or lead to equipment damage or unnecessary tripping if the conductors reached a sufficiently high temperature. A linearized AC formulation avoids this situation by anticipating the temperature rise and directing the controller to take corrective actions immediately following the contingency.

3.3 Transformer Voltage Regulation

Transformers are vital components in electric power systems. They enable large power transfers over long distances by stepping up operating voltages to decrease current flow and losses. Many transformers are equipped to change their tap settings (turns ratio) while operating under load, and this enables them to regulate voltages across the network as loading patterns change. These devices are referred to as *load tap changers* (LTCs). If an LTC is set to automatically regulate voltage or power flow, the local feedback control process creates dynamics that can influence the behavior in other parts of the network.

Modern power dispatch processes coordinate these local control strategies to maximize the overall system benefit and avoid unstable operation. As mentioned in Section 1.2.3, voltage regulating transformers primarily interact with generator voltage regulators and reactive power compensation devices such as shunt capacitors or reactors. Without proper intervention during emergencies, the interaction of the control dynamics can exacerbate the situation and lead toward system collapse.

This section describes how LTC dynamics are incorporated into MPC's internal model. Though approximate, the model sufficiently captures the primary dynamic behavior and enables MPC to identify appropriate control actions during emergency situations.

3.3.1 Unified Branch Model

A commonly applied framework for modeling transmission networks is the Unified Branch Model. This approach easily incorporates both transmission lines and transformers into the network description and is discussed in [6]. Figure 3.4 summarizes the model parameters. An ideal (lossless) transformer with complex tap ratio, t_{ij}, is connected in series to complex impedance, z_{ij}. Any shunt admittance, y_{ij}^{sh}, is split evenly and lumped at the two end buses.

If the branch models a transmission line, the ideal transformer is ignored ($t_{ij} = 1$), and the series impedance and shunt admittance tend to be nonzero. If the branch models a transformer, the tap ratio will vary around 1, and the shunt admittance will tend to be zero. The series impedance may be purely imaginary if resistive effects in the transformer windings are ignored, but this is not generally the case. If the transformer is equipped with a voltage regulator, it will regulate V_j by adjusting the magnitude of t_{ij}.

Transformers may also be configured to regulate the power flow on branch ij. In this case, the power entering the branch from bus i is monitored. To regulate reactive power, the magnitude of t_{ij} is adjusted. To regulate active power, the angle of t_{ij} is adjusted.

Changing the tap magnitude, a_{ij}, or angle, ψ_{ij}, causes a nonlinear response in the effective admittances expressed in (3.1). Therefore, the linear sensitivities to both forms of tap changing are included in (3.2) to account for any tap changing behavior.

3.3.2 Transformer Tap-Changing Dynamics

Within the realm of power system dynamics, regulating LTCs operate slowly and in a discrete manner. Typically, they are designed to raise and lower their tap settings by 10 % from the neutral position over 32 additional positions. This produces individual step changes of 5/8 % or 0.00625 pu. The step change happens very quickly to minimize the current interruption and is modeled as instantaneous, but mechanical switching mechanisms typically require several seconds between subsequent tapping operations.

Because regulation happens through discrete changes, a deadband d is defined around the reference target to avoid oscillatory operation. This deadband is sized larger than the change in the regulated quantity resulting from a single tap operation. For example when regulating voltage, a tap operation typically produces an equivalently sized change in voltage magnitude (about 0.00625 pu). A common voltage deadband is specified as ± 0.01 pu. For the remainder of this discussion, transformer dynamics will be described with voltage as the regulated quantity since this is the most common configuration. The control dynamics are very similar when active or reactive power flow is regulated and these will be summarized as well when the internal model of MPC is presented in Section 3.3.3.

Intentional delays in addition to the mechanical delay between tapping operations are also built into the regulator control logic. Large disturbances in the network can cause voltage oscillations that require several seconds to subside. If these oscillations are sustained long enough, they could cause transformers to unnecessarily adjust their tap settings. This spurious behavior increases wear on the device and can shorten its lifespan. By intentionally delaying transformer operation, these effects are avoided.

Similarly, transmission networks typically have several layers of regulating transformers between generators and loads. Tap changes at one layer will influence the voltages at the other layers requiring coordination between the timescale of operation at different layers. For example, LTCs in the higher voltage transmission network may be set to operate more quickly than those in lower voltage sub-transmission networks. Changing the voltage in the transmission network tends to produce a similar change in the sub-transmission network. If both portions of the network have low voltages following a disturbance, increasing the transmission level voltage first may remove the deadband violation at the sub-transmission level as well and result in fewer tapping operations overall. Alternatively, a poorly coordinated system can produce oscillatory transformer behavior if tap changes at one layer push voltages at another layer outside their deadbands. Time delays and deadbands are typically set during system design and are modeled as fixed quantities in this analysis.

Discrete model of transformer tap-changing

The intentional delay between tapping operations can be a fixed quantity or vary with the severity of the deadband violation. In this way, the time between tapping operations is not an independent variable. A discrete time index s can be defined to increment whenever a tap change operation occurs. If a deadband violation is detected, an internal counter T_{vio} starts tracking the time over which the deadband violation is sustained. If it persists long enough to exceed the intentional delay T_d, a tap change operation occurs and $s \to s + 1$.

To account for the various intentional delay settings, a composite formulation can be used [74],

$$T_d = T_m + T_f + T_p \frac{d}{|U - U^{ref}|}. \tag{3.7}$$

Here, T_m is the mechanical delay required by the switching mechanism, T_f is any additional fixed delay specification, and T_p parameterizes the proportional delay term which varies with the severity of the deadband violation. Large deviations in the regulated voltage U away from its reference target value U^{ref} result in shorter delays between tapping operations.

After a deadband violation is sustained past the intentional delay ($T_{vio} > T_d$), a tap change is initiated.

Voltage regulating transformers adjust their tap magnitude a by step size Δa using the following logic [74],

$$a_{s+1} = \begin{cases} a_s + \Delta a, & \text{if } U > U^{ref} + d \text{ and } a_s < a^{max} \\ a_s - \Delta a, & \text{if } U < U^{ref} - d \text{ and } a_s > a^{min} \\ a_s, & \text{otherwise.} \end{cases} \tag{3.8}$$

This ensures that the tap remains within its upper and lower limits, a^{max} and a^{min} respectively. The tapping logic in (3.8) is appropriate for regulating the voltage at bus j in the circuit orientation shown in Figure 3.4. In order to regulate V_j, tap changes occur on the opposite side of the transformer closer to bus i. Therefore, increasing the tap magnitude a_{ij} will reduce voltage magnitude U_j and vice versa. If the regulated voltage is within its deadband or the tap is against a limit, a tap change will not occur.

The duration of T_d can vary quite significantly both over different systems and in different parts of a single system. However, it is fairly common for the delay to fall in the range of 30 seconds to two minutes [74, 75]. Sometimes a distinction will be made between the delay on the first tapping operation in a sequence and subsequent tapping operations. This is classified as a "sequential mode" of operation [74]. For instance the delay on the first operation may be defined normally as in (3.7), but subsequent delays may set $T_f = T_p = 0$ to permit faster operation during large voltage deviations. When no distinction of delays is made in the tapping sequence, it is referred to as a "non-sequential mode" of operation [74]. Though faster operation of transformers allows deadband violations to be resolved more quickly under normal conditions, it also reduces the intervention time available during voltage collapse conditions.

The transformer dynamics specified by (3.7) and (3.8) are highly nonlinear due to the variable time delay and discrete tap transitions. Figure 3.5 summarizes these dynamics. The delay T_d from (3.7) is shown in the solid black curves and assumes nonzero values for the fixed $(T_m + T_f)$ and proportional (T_p) time constants. These curves separate the three unique regions in (3.8). When transitioning from the central region to the upper-right or lower-right regions, a discrete tap change occurs. If the proportional time constant T_p is reduced to zero, the upper-right and lower-right regions become rectangular and are bounded on the left by $T_m + T_f$ and horizontally by the deadband (shown in the dashed gray lines).

If a voltage violation occurs outside the deadband, the counter T_{vio} begins increasing from zero (i.e. moving from left to right in Figure 3.5). If the voltage violation remains outside the deadband, T_{vio} continues to increase until it reaches one of the T_d curves and a tap change occurs. T_{vio} resets to zero if the voltage violation decreases in magnitude and moves back into the deadband while $T_{vio} < T_d$ or once a tap change has occurred.

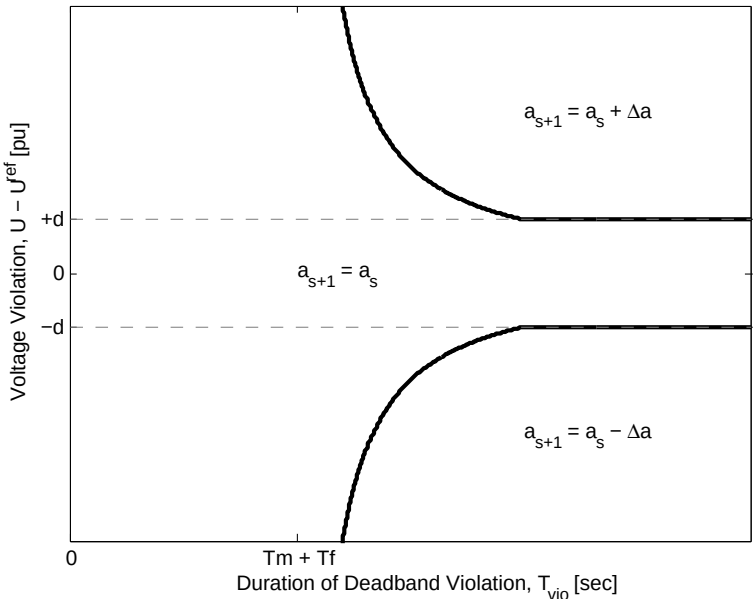

Figure 3.5: Transformer tap-changing dynamics (3.8) are discrete and depend on deadband and delay specifications. The delay T_d from (3.7) is shown in the solid black curves and bounds the upper-right and lower-right regions where tap changes occur. The dashed gray lines denote the voltage deadband. If a voltage violation occurs outside the deadband, T_{vio} begins increasing from 0 until it reaches T_d and a tap change occurs. If the voltage violation returns within the deadband while $T_{vio} < T_d$, T_{vio} resets to 0.

Continuous model of transformer tap-changing

To be applied within MPC, the transformer dynamics must be approximated into a linear formulation with continuous variables. A straightforward model is presented in [74] which ignores the deadband and fixed time constants and treats the transformer tap position as a continuous variable. This results in the dynamic relationship,

$$\dot{a} = \frac{1}{T_{dl}} \left(U - U^{ref} \right), \tag{3.9a}$$

$$a^{min} \leq a \leq a^{max}. \tag{3.9b}$$

This essentially turns the tap magnitude a into an integrator of the voltage error $U - U^{ref}$. The linear delay constant T_{dl} is given by

$$T_{dl} = \frac{T_p d}{\Delta a}. \tag{3.10}$$

The fixed delay constants T_m and T_f are assumed to be zero under this formulation [74].

However, it is possible that the transformer delay is only specified with fixed delay constants. When this occurs the model from [74] is ill-defined and the gain on (3.9a) goes to infinity. To resolve this condition,

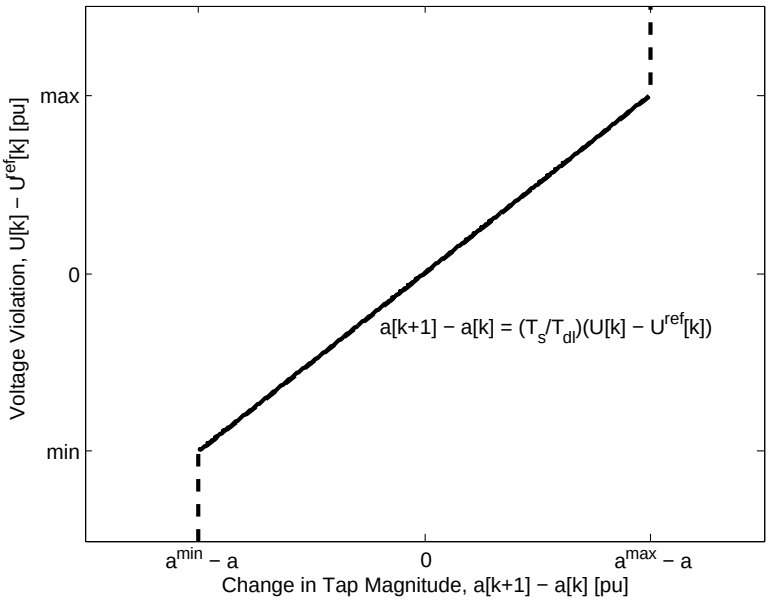

Figure 3.6: Transformer tap change dynamics within MPC (3.12) are continuous and linear. The linear delay constant T_{dl} is given by (3.11).

the linear delay constant is redefined here as

$$T_{dl} = \frac{(T_m + T_f + T_p)\, d}{\Delta a}. \tag{3.11}$$

Substituting (3.11) into (3.9) gives

$$\dot{a} = \frac{\Delta a \left(U - U^{ref}\right)}{d\,(T_m + T_f + T_p)}, \tag{3.12a}$$

$$a^{min} \leq a \leq a^{max}. \tag{3.12b}$$

The tap changing dynamics given in (3.12) are applied within MPC to approximate the true discrete behavior specified by (3.7) and (3.8). Instead of changing in discrete steps, the tap is assumed to vary continuously between its minimum and maximum values. Multiplying (3.12a) by the time-step T_s within MPC gives the discretized change in tap position from time k to $k+1$.

Figure 3.6 shows that continuous changes in the tap position result from voltage violations within the linear dynamics (3.12a). However, enforcing the tap limits (3.12b), introduces nonlinearities into the model (evidenced by the knee points on the curve in Figure 3.6). If the reference voltage U^{ref} is fixed, large voltage fluctuations could cause MPC to take drastic control measures as it attempts to enforce tap limits and remain on the solid linear portion of the curve.

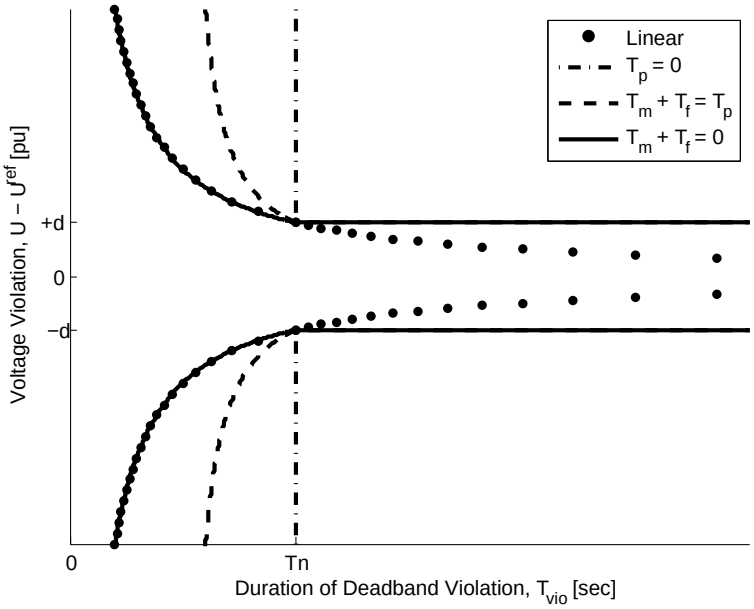

Figure 3.7: Transformer tap-changing dynamics under both the discrete and linear models. The curves represent the tap step under the discrete model with different delay characteristics. The linear model assumes the tap changes continuously from the origin, and the dots show where it predicts the tap change is equal to the step size $|\dot{a}T_{vio}| = \Delta a$.

This aggressive behavior to enforce transformer limits is unrealistic. In practice, an operator is not concerned if a transformer reaches its limit. Although this condition might be a signal that the system is stressed, it does not threaten the safety of the network. In fact, it may help to slow some situations of voltage collapse by preventing voltage dependent loads from recovering completely.

A straightforward method of ensuring that MPC can satisfy the linear tap change dynamics while enforcing tap limits is to allow the reference voltage U^{ref} to vary. Figure 3.6 shows how encountering a tap limit induces an artificial limit on the voltage error $U - U^{ref}$. Adjusting U^{ref} allows the voltage U to fluctuate arbitrarily while keeping the voltage error within its linear range.

Implementing (3.12) within the discrete time framework of MPC implies that any voltage violation will be sustained for the entire duration of each time-step. For example, each time-step within MPC has a duration of T_s. Therefore, the change in tap from one time-step to the next can be defined as,

$$\Delta a[k+1] - \Delta a[k] = \dot{a}[k]T_s = \frac{T_s}{T_{dl}}\left(U[k] - U^{ref}[k]\right). \tag{3.13}$$

The definition of T_{dl} given in (3.11) does not make any distinction between fixed and proportional time delays. Instead, it treats all delays as proportional which introduces some error into the model. Figure 3.7 shows the tap change under both the discrete model of (3.7) and (3.8) and the linear model of (3.12) for

a variety of time delay characteristics. The sum of the delay constants is equal for each curve to provide a normalized comparison, $T_n = T_m + T_f + T_p$.

The curves in Figure 3.7 show where the discrete model predicts the tap step will occur. When only fixed delays are modeled, $T_p = 0$, the delay is insensitive to the size of the voltage violation. As the delay shifts toward a proportional characteristic, $T_m + T_f = 0$, tap changes occur more rapidly for large voltage violations.

The linear model assumes that the tap changes continuously depending on the magnitude and duration of the voltage violation. The dots in Figure 3.7 show where the linear model predicts the tap change is equal to the step size, $|\dot{a}T_{vio}| = \Delta a$. If the delay characteristic is purely proportional, the linear and discrete models are fairly similar. Greater discrepancies arise when the delay characteristic is actually fixed. In this situation, the linear model predicts larger tap changes than the discrete model for the same duration of the voltage violation.

This overprediction of tap changes within the linear model of MPC has different implications depending on the operating situation. Under normal operating conditions, the tap changes restore system voltages to their desired levels. Overprediction of the tap change implies that this restoration will occur quickly and causes MPC to avoid taking additional control actions to restore voltages. Alternatively, during heavy load conditions, tap changing can cause undesirable voltage behavior. Overprediction of the tap changes in this scenario causes MPC to select more aggressive corrective measures than may be necessary to prevent the tap changing from driving the system unstable.

Numerical stability of transformer dynamics in MPC

The step-size, T_s, of MPC must be chosen small enough to ensure numerical stability of the transformer model. In a linear system with $\dot{a} = \lambda a$, where λ approximates the eigenvalues of the system, the system is stable as long as $\text{Real}(\lambda) < 0$. When using Euler discretization, the system dynamics are represented,

$$a[k+1] = a[k] + T_s \lambda a[k]. \tag{3.14}$$

This can be condensed to

$$a[k+1] = (1 + T_s\lambda)^{k+1}\, a[0]. \tag{3.15}$$

In order for this system to be stable, it must approach zero as k approaches infinity. This requires

$$|1 + T_s\lambda| < 1 \Leftrightarrow -1 < 1 + T_s\lambda < 1. \tag{3.16}$$

From this, the choice of T_s must satisfy two requirements:

$$T_s > 0, \tag{3.17a}$$

$$T_s < \frac{-2}{\lambda}. \tag{3.17b}$$

Assuming λ is negative, the conditions of (3.17) require that T_s be a small positive number for the numerical stability to match the underlying dynamic stability.

The tap dynamics of (3.13) are expressed in terms of voltage magnitude instead of the current tap position. To confirm numerical stability properties, (3.13) must be rearranged so that the tap position appears explicitly as in (3.14). The voltage behavior within MPC is driven by the linear power flow equations of (3.2). Rearranging these equations allows voltage magnitudes to be expressed in terms of transformer behavior and power injections across the network. Substituting for $U[k]$ in (3.13) gives,

$$\Delta a[k+1] = \Delta a[k] + \frac{T_s}{T_{dl}} \left(\left[\frac{dU}{da}\Delta a[k] + \frac{dU}{d\psi}\Delta\psi[k] + \frac{dU}{dp_G}\Delta p_G[k] + \ldots \right] - (U^{ref}[k] - U^{meas}) \right). \tag{3.18}$$

Grouping the coefficients of $\Delta a[k]$ in (3.18) allows an equivalent condition to that of (3.16) to be defined:

$$-1 < 1 + \frac{T_s}{T_{dl}} \frac{dU}{da} < 1. \tag{3.19}$$

Given that dU/da is negative, this implies that T_s must be chosen to satisfy,

$$T_s > 0, \tag{3.20a}$$

$$T_s < \frac{-2T_{dl}}{dU/da}. \tag{3.20b}$$

As system conditions change, the sensitivity dU/da will also change. Under normal conditions, this sensitivity is around -1. However, in a voltage collapse situation the sensitivity approaches zero [74]. This loss of sensitivity effectively relaxes the constraint of (3.20b). Therefore, selecting $T_s < 2T_{dl}$ will tend to satisfy numerical stability requirements for transformer models under all operating conditions. As mentioned previously, typical values for Δa, d, and $T_m + T_f + T_p$ are 0.00625 pu, 0.01 pu, and 30 seconds to two minutes, respectively. This causes T_{dl} to fall in the range of 48 to 192 seconds and agrees with the $T_s = 60$ seconds time-step typically chosen for thermal dynamics in MPC.

3.3.3 Transformer Constraints

The set of constraints describing the behavior of a voltage regulating transformer with the branch configuration shown in Figure 3.4 are

$$\Delta a_{ij}[k+1] = \Delta a_{ij}[k] + \frac{\Delta a_{ij} T_s}{d_{ij}(T_{m,ij} + T_{f,ij} + T_{p,ij})} \left(\Delta U_j[k] + U_j^{meas} - \frac{U_{ij}^{ref}[k]}{100} \right), \tag{3.21a}$$

$$\Delta a_{ij}[0] = 0, \tag{3.21b}$$

$$a_{ij}^{min} \leq \Delta a_{ij}[k+1] + a_{ij}^{meas} \leq a_{ij}^{max}, \tag{3.21c}$$

for $k \in \{0, \ldots, M-1\}$. The tap magnitude a_{ij} is driven by the dynamics of (3.21a) with Δa_{ij} describing changes from the measured tap magnitude at the start of the prediction horizon. MPC has the ability to influence this behavior by adjusting the voltage magnitude reference U_{ij}^{ref}. Changes to the reference are penalized quadratically in the objective function. The scaling of U_{ij}^{ref} by 100 is necessary for converting from units of percent to units of per unit. The tap position is initialized to the measured value using (3.21b). Equation (3.21c) ensures that the tap magnitude remains within its lower and upper limits.

If the transformer is configured to regulate its reactive power flow, the voltage terms in (3.21) are replaced with reactive power flow terms:

$$\Delta a_{ij}[k+1] = \Delta a_{ij}[k] + \frac{\Delta a_{ij} T_s}{d_{ij}(T_{m,ij} + T_{f,ij} + T_{p,ij})} \left(\Delta q_{ij}[k] + q_{ij}^{meas} - q_{ij}^{ref}[k] \right), \tag{3.22a}$$

$$\Delta a_{ij}[0] = 0, \tag{3.22b}$$

$$a_{ij}^{min} \leq \Delta a_{ij}[k+1] + a_{ij}^{meas} \leq a_{ij}^{max}, \tag{3.22c}$$

$$\Delta q_{ij}[k] = \frac{\partial q_{ij}}{\partial a_{ij}} \Delta a_{ij}[k] + \frac{\partial q_{ij}}{\partial V_i} \Delta V_i[k] + \frac{\partial q_{ij}}{\partial V_j} \Delta V_j[k], \tag{3.22d}$$

for $k \in \{0, \ldots, M-1\}$. Again, the tap magnitude a_{ij} is driven by the dynamics of (3.22a), and MPC has the ability to influence this behavior by adjusting the reactive power flow reference q_{ij}^{ref}. Any changes to q_{ij}^{ref} are quadratically penalized in the objective function. The tap position is initialized by (3.22b), and (3.22c) ensures that the tap magnitude remains within its lower and upper limits. The reactive power flow through the transformer q_{ij} is defined by (3.22d). The notation ΔV is a condensed representation of $[\Delta\delta \ \Delta U]^\top$.

A similar set of constraints is necessary for transformers regulating their active power flow:

$$\Delta\psi_{ij}[k+1] = \Delta\psi_{ij}[k] + \frac{\Delta\psi_{ij}T_s}{d_{ij}(T_{m,ij}+T_{f,ij}+T_{p,ij})}\left(\Delta p_{ij}[k] + p_{ij}^{meas} - p_{ij}^{ref}[k]\right), \tag{3.23a}$$

$$\Delta\psi_{ij}[0] = 0, \tag{3.23b}$$

$$\psi_{ij}^{min} \leq \Delta\psi_{ij}[k+1] + \psi_{ij}^{meas} \leq \psi_{ij}^{max}, \tag{3.23c}$$

$$\Delta p_{ij}[k] = \frac{\partial p_{ij}}{\partial \psi_{ij}}\Delta\psi_{ij}[k] + \frac{\partial p_{ij}}{\partial V_i}\Delta V_i[k] + \frac{\partial p_{ij}}{\partial V_j}\Delta V_j[k], \tag{3.23d}$$

for $k \in \{0, \ldots, M-1\}$. Here, the phase angle of the transformer tap, ψ_{ij}, is driven by the dynamics of (3.23a), and MPC can influence this behavior by adjusting the active power flow reference p_{ij}^{ref}. Changes to the reference are quadratically penalized in the objective function. The tap angle is initialized by (3.23b) and limits are enforced by (3.23c). The active power flow through the transformer, p_{ij}, is defined by (3.23d).

Chapter 4

Implementation Technique for Large Networks

Control areas in power systems can contain hundreds to thousands of buses and lines. Control processes such as the one presented in this work must therefore be capable of operating on large networks. While small test networks are often useful for developing a controller and understanding its behavior, they ultimately ignore the challenges that a process might face when operating in the real-world. In practice, controllers must be able to quickly process large amounts of data, communicate extensive control actions, and consider a vast set of network constraints while consistently reaching solutions that respect reliability criteria and match operator intuition.

This chapter addresses several of these considerations in the context of MPC. Specifically, techniques for reducing the number of constraints and variables in the problem formulation are discussed. Thermal models for transmission lines contribute significantly to the problem size but rarely affect the problem solution. Ignoring thermal models on lines far from their rated temperature is an easy exploitation of this characteristic. Additionally, many control devices have limited influence on an overloaded transmission line. Excluding these devices from the control set of MPC allows the problem size to be further reduced with limited detriment to the controller performance. The key ideas presented in this chapter were first published in [76].

4.1 QP Size Considerations

4.1.1 QP Solution Speed and MPC

As discussed in Section 1.4.2, MPC must solve a multi-period optimization problem every time it operates. Since each time period represents a unique operating condition, any growth in the number of variables and constraints used to model network devices is amplified by the M time-steps in the prediction horizon. Increasing problem size leads to longer solution times and greater potential for numerical challenges.

In order for MPC to operate reliably, it must determine the optimal control sequence very quickly relative to the dynamics of the underlying modeled process. Long delays between the time system measurements are taken and when control decisions are implemented will allow conditions to drift and introduce errors between the modeled and actual behaviors. In this work, the controller is assumed to solve instantaneously with the ability to instantaneously change any control inputs. However, large networks require solution times that strain this assumption and steps must be taken to reduce these solution times.

Techniques to reduce the size of a power system model have existed for quite some time. Historical computational abilities required models to be simplified in order to perform calculations. Some of these techniques for reducing the complexity of the network model are discussed in the next section.

4.1.2 Reduction of the Power Flow Constraints

The computational challenges experienced by MPC when operating on large networks bear similarity to the challenges of contingency analysis methods. A solution is desired for the system when it is in a stressed state. Operating conditions may be far from nominal. Results must accurately predict the extent of the problem. A solution must be found quickly. This provides an opportunity to apply the mature techniques used in contingency analysis to the MPC application of this work.

When a contingency occurs in a large network, the scope of the problem is often limited to a specific region. Early analysis introduced the idea of concentric relaxation [77]. If a line trips out of service, the end buses of the outaged line are designated as layer zero. Any bus connected to these buses through a line or transformer is in layer one, and the process continues outward until all buses in the network have been assigned to a layer. Outer layers are typically unaffected by the contingency while inner layers may change significantly. To solve a power flow quickly, an arbitrary cutoff is designated and outer layers maintain fixed voltage magnitude and angle while inner layers solve normally.

Unfortunately, some contingencies affect the network more broadly than others. Specifying an arbitrary layer cutoff may not capture the full extent of some changes for large events while unnecessarily modeling

unaffected buses for smaller events. Bounding and adaptive localization techniques address this issue by specifying a boundary region between the inner and outer layers which can expand or contract for different contingencies [77]. Contingency analysis is concerned with solving a power flow rapidly, so the adaptive localization starts from the pre-contingency solution and only updates voltages for buses with significant power mismatch. This starts at layer zero and slowly spreads outward while requiring fewer calculations than starting from a "flat start" voltage initialization.

These approaches offer a starting point for reducing the complexity of the problem solved by MPC, but miss several key considerations. First, MPC operates over a horizon, not just a single point in time. The power injections throughout the network are changing during this period and may have an important effect on the post-contingency behavior. Second, MPC must identify a sufficient number of controls to meet the terminality constraint (3.6e), requiring thermal overloads to be removed by the end of the prediction horizon, to ensure feasibility.

For now, assume that a method exists which addresses the second issue by identifying a sufficient set of controls. These techniques will be further addressed in Section 4.2. To address the first issue, the model in MPC must capture the evolving behavior outside the control set in combination with the influence of any control decisions. The Kron reduction method [78] offers a solution to this challenge.

Kron reduction utilizes the Schur complement of a matrix to reduce a set of linear equations to a smaller equivalent set. It has been applied in power systems to define reduced Ward-equivalents of large power systems [79] and to reduce differential-algebraic equations to simply differential equations [80]. The new reduced set of equations implicitly accounts for the requirements of any eliminated equations without loss of accuracy. The variables and constraints associated with the control set are maintained in MPC and some variables outside the control set are eliminated from the QP.

The power flow equations expressed in (3.2) can be written in matrix form as,

$$\begin{bmatrix} \frac{\partial P}{\partial \delta} & \frac{\partial P}{\partial U} & \frac{\partial P}{\partial \psi} & \frac{\partial P}{\partial a} & -I & 0 \\ \frac{\partial Q}{\partial \delta} & \frac{\partial Q}{\partial U} & \frac{\partial Q}{\partial \psi} & \frac{\partial P}{\partial a} & 0 & -I \end{bmatrix} \begin{bmatrix} \Delta\delta \\ \Delta U \\ \Delta\psi \\ \Delta a \\ \Delta P \\ \Delta Q \end{bmatrix} = \begin{bmatrix} 0 \\ 0 \end{bmatrix}, \tag{4.1}$$

where P and Q respresent the net active and reactive power injections, respectively. To reduce this set of constraints, the rows and columns of the matrix can be partitioned into two groups. The first group is

retained in the MPC model and the second group is eliminated from the model. The partitioned version of (4.1) can be written as,

$$\begin{bmatrix} A_{11} & A_{12} \\ A_{21} & A_{22} \end{bmatrix} \begin{bmatrix} x_1 \\ x_2 \end{bmatrix} = \begin{bmatrix} d_1 \\ d_2 \end{bmatrix}. \tag{4.2}$$

The variables included in set 2 are terms associated with reduced buses which are 'unknown' in a power flow sense. This includes voltage angles at PQ and PV buses, voltage magnitudes at PQ buses, and reactive power at PV buses. The constraints in set 2 are the equations for active and reactive power at reduced buses. Note that the same number of variables and constraints are eliminated, so A_{22} is square.

Applying the Kron reduction results in a smaller set of equations, $A_{red}x_1 = d_{red}$, with

$$A_{red} = A_{11} - A_{12}A_{22}^{-1}A_{21}, \tag{4.3a}$$

$$d_{red} = d_1 - A_{12}A_{22}^{-1}d_2. \tag{4.3b}$$

One of the drawbacks of this approach is that A_{red} is more dense than A. All of the boundary nodes of set 1 will be completely connected if any paths exist between them in set 2. Some of these connections will be very weak, resulting in very small nonzero values being created in A_{red}. Fill-in can be reduced by setting these terms to zero.

Initial testing on several networks seems to indicate that the number of nonzero entries in A_{red} remains similar to the number in A. No theoretical justification exists for this observed behavior. The detrimental increase in the density of the constraint matrix is far outweighed by the reduction in the problem size and allows the QP to be solved much more rapidly.

The reduction process of (4.3) only eliminates the variables outside the control set which are 'unknown' in a power flow sense. For those variables which are 'known' in a power flow sense but not under MPC's control, their values are assigned to their scheduled reference values, multiplied by their respective columns in A_{red}, and incorporated into the right-hand vector d_{red},

$$A_{red}(\cdot, c)x_1(c) = d_{red} - A_{red}(\cdot, \tilde{c})x_1(\tilde{c}). \tag{4.4}$$

Here, the notation c refers to the set of controllable variables, $\tilde{c}$ is the set of 'known' noncontrollable variables, and $A_{red}(\cdot, c)$ refers to the columns of A_{red} associated with set c.

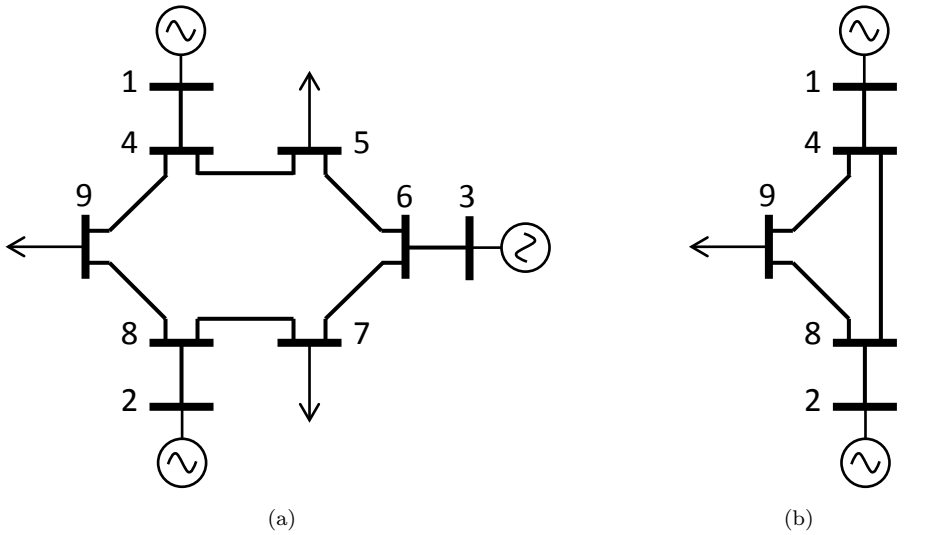

(a) (b)

Figure 4.1: MATPOWER 9-bus test system. (a) Full network. (b) Reduced network.

Example

A simple example of the power flow reduction process is demonstrated on the 9-bus MATPOWER [68] test system shown in Figure 4.1a. The buses in set 1 available to MPC are $S_1 = \{1, 2, 4, 8, 9\}$, indicating that the reduced buses in set 2 are $S_2 = \{3, 5, 6, 7\}$. The network controlled by MPC can effectively be visualized as the reduced network of Figure 4.1b. The boundary buses 4 and 8 have a path between them which is completely contained in the eliminated portion of the network. Therefore, they are connected by an equivalent impedance in the reduced network. The equivalent impedance is calculated as a byproduct of the reduction process.

The coefficient matrix of the linear power flow equations (4.1) for the full 9-bus network is shown in Figure 4.2a with nonzero entries indicated by blue dots. No regulating transformers exist in the network, implying that $\delta\psi$ and δa will be zero and can be ignored. The dashed lines separate the eight distinct portions of the matrix,

$$A = \begin{bmatrix} \frac{\partial P}{\partial \delta} & \frac{\partial P}{\partial U} & -I & 0 \\ \frac{\partial Q}{\partial \delta} & \frac{\partial Q}{\partial U} & 0 & -I \end{bmatrix}, \tag{4.5}$$

with variable vector $[\Delta\delta\ \Delta U\ \Delta P\ \Delta Q]^\top$. The righthand-side vector b is all zeros. There are 126 nonzero entries in the 18 rows and 36 columns of the full coefficient matrix A.

In order to eliminate the 8 rows of equations associated with buses in set S_2, 8 columns must also be selected for elimination to ensure that A_{22} is square. Bus 3 has a generator and can be represented as a PV bus while buses 5, 6, and 7 are represented as PQ buses. Therefore the columns associated with 'unknown' variables in set S_2, $x_2 = [\Delta\delta_3\ \Delta\delta_5\ \Delta\delta_6\ \Delta\delta_7\ \Delta U_5\ \Delta U_6\ \Delta U_7\ \Delta Q_3]^\top$, and the rows associated

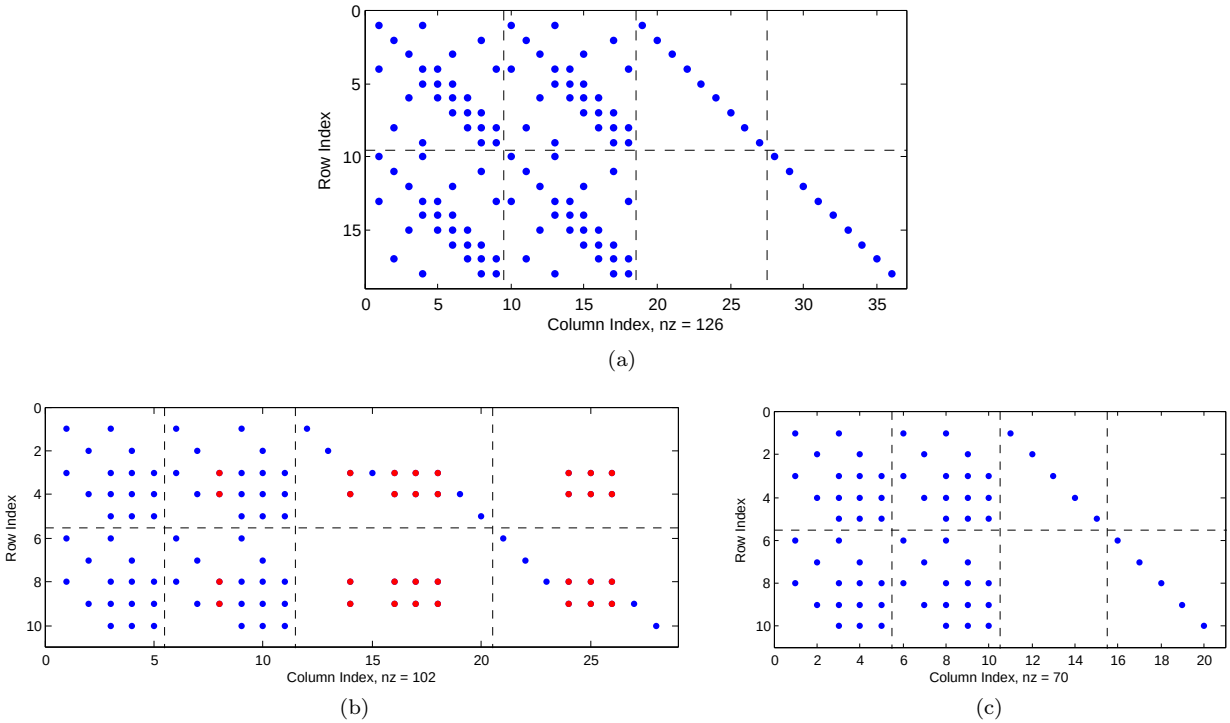

Figure 4.2: Nonzero entries of linear power flow matrix (4.1) for 9-bus example. (a) Full matrix. (b) Reduced matrix with columns in set $\tilde{c}$ shown in red (c) Final matrix in MPC. All columns are in set c.

with active and reactive power equations for buses 3, 5, 6, and 7 are selected for elimination. Removing this portion of the matrix using the Kron reduction of (4.3) produces the reduced matrix A_{red} shown in Figure 4.2b. This matrix has 102 nonzero entries in 10 rows and 28 columns. The columns which are still associated with 'known' variables for buses in set S_2 are shown in red. These variables are $x_1(\tilde{c}) = [\Delta U_3\ \Delta P_3\ \Delta P_5\ \Delta P_6\ \Delta P_7\ \Delta Q_5\ \Delta Q_6\ \Delta Q_7]^\top$. If any of these quantities is scheduled to change during the prediction horizon, the associated variable will be nonzero. Multiplying these variables by their coefficients and moving them to the righthand-side of the equations as in (4.4) will produce nonzero terms on the righthand-side vector, $b_{red} - A_{red}(\cdot, \tilde{c})x_1(\tilde{c})$. The nonzero entries are associated with equations for boundary buses, buses 4 and 8 in this example. The final coefficient matrix $A_{red}(\cdot, c)$ passed to MPC is shown in Figure 4.2c. It has 70 nonzero elements in 10 rows and 20 columns. All 20 variables in $x_1(c)$ are associated with the five buses in set S_1. □

4.2 Selecting a Set of Controls

As mentioned previously, techniques to reduce the size of the QP solved by MPC require the identification of a subset of controls most useful for achieving the controller objectives. Limiting the number of controls available to MPC reduces the number of device constraints and variables and allows the power flow constraints to be

condensed. This section discusses a sensitivity-based heuristic currently being used to identify the control set and outlines further opportunities for improvement in this process.

One of the primary objectives of the controller described in this work is the removal of thermal overloads on transmission lines. The thermal behavior is driven by losses on the line, and losses will tend to decrease as power flow across the line decreases. Sensitivity based methods for estimating line flow changes have been used for quite some time [77] and can easily be applied in this context to provide a rough prediction of the controller behavior.

Injection shift factors (ISFs) describe (to a linear approximation) how the flow on a line is affected by changing the power injection at a node in the network with a corresponding balancing injection at the slack node. For the flow on a line from bus i to bus j, the row vector of ISFs is given by,

$$s_{ij} = \frac{\partial f_{ij}}{\partial [\delta, U]} \left(\frac{\partial [P, Q]}{\partial [\delta, U]} \right)^{-1}, \tag{4.6}$$

where $\frac{\partial f_{ij}}{\partial [\delta, U]}$ is the row vector of partial derivatives of the power flow on line (i, j) with respect to the network voltages, and $\frac{\partial [P,Q]}{\partial [\delta, U]}$ is the power flow Jacobian. The only nonzero entries in $\frac{\partial f_{ij}}{\partial [\delta, U]}$ correspond to the end nodes i and j, so sparse matrix methods can be used to form s_{ij} very efficiently.

A simple equivalent problem can be defined to gain intuition for the behavior of MPC. At a basic level, the controller is a QP minimizing control deviations from scheduled values while seeking to eliminate line-flow overloads and maintain power balance across the network. This equivalent QP can be expressed as,

$$\min_{x} \ (x - x^{sp})^\top Q (x - x^{sp}) \tag{4.7a}$$

s.t.

$$0 = sx - b \tag{4.7b}$$

$$0 = \mathbf{1}^\top x \tag{4.7c}$$

where x is the vector of power injections, x^{sp} is the vector of scheduled injections, $Q \succ 0$ is a positive definite weighting matrix, s is the row vector of ISFs for a given line, b is related to the desired power flow on that line and $\mathbf{1}$ is the vector of ones. The program described by (4.7) seeks to minimize changes from scheduled injections (4.7a), while achieving a certain line flow (4.7b) and maintaining power balance (4.7c). The Lagrangian for this program is,

$$\mathcal{L}(x, u, v) = x^\top Q x - 2 x^{sp\top} Q x + x^{sp\top} Q x^{sp} - u(sx - b) - v(\mathbf{1}^\top x), \tag{4.8}$$

where u and v are scalar Lagrangian multipliers. The KKT conditions ($\nabla\mathcal{L} = 0$) require,

$$x = x^{sp} + \frac{1}{2}Q^{-1}s^\top u + \frac{1}{2}Q^{-1}\mathbf{1}v \tag{4.9a}$$

$$u = \left(s\frac{Q^{-1}}{2}s^\top\right)^{-1}\left(-s\frac{Q^{-1}}{2}\mathbf{1}v - sx^{sp} + b\right) \tag{4.9b}$$

$$v = \frac{\mathbf{1}^\top\frac{Q^{-1}}{2}s^\top\left(s\frac{Q^{-1}}{2}s^\top\right)^{-1}(sx^{sp} - b) - \mathbf{1}^\top x^{sp}}{\mathbf{1}^\top\frac{Q^{-1}}{2}\mathbf{1} - \mathbf{1}^\top\frac{Q^{-1}}{2}s^\top\left(s\frac{Q^{-1}}{2}s^\top\right)^{-1}s\frac{Q^{-1}}{2}\mathbf{1}}. \tag{4.9c}$$

Although (4.9) has rather involved expressions for the Lagrangian multipliers u and v, the intuition of the solution vector x is fairly straightforward, particularly if the objective weighting matrix is the identity matrix, $Q = I$. Expression (4.9a) indicates that the solution will seek to match the scheduled injections x^{sp}, but each injection will deviate in proportion to its influence over the flow on the controlled line $s^\top u/2$, and all injections will be shifted uniformly by an offset $\mathbf{1}v/2$ to ensure power balance.

In meshed networks, typically only a subset of buses have significant influence over the flow on a specific line. Consequently, the ISF vector s will often have a few dominant nonzero entries while the remaining entries are all relatively small. If a bus has a small entry in the ISF vector s for every line under consideration then varying the injection at that location will have negligible effect on all the flows of interest. Such buses can therefore be fixed to their scheduled injection values and removed from the set of controls.

The process of selecting which resources to include in the set of controls and which to ignore is undertaken prior to operation of MPC. Figure 4.3 provides an outline of the selection process currently being utilized. This algorithm runs sequentially for every overloaded line, with the aim of identifying the fewest devices necessary to remove the overload while respecting device injection limits. The final set of controls is the union of those identified for each individual overloaded line. If system conditions change significantly during MPC operation, the process reruns to update the set of controls.

In step 1 of Figure 4.3, the minimum and maximum injection limits of each control device are determined. These limits take into account ramp-rate limits and forecasted behavior of resources such as renewables and controllable loads.

Step 2 of the process calculates the ISF values for the overloaded line and then sorts the values from least to greatest (most negative to most positive) for each line. The outcome of this process is illustrated in Figure 4.4. If a certain bus k has a negative ISF value for line (i, j), then injecting power at bus k and absorbing it at the slack bus will cause power flow on line (i, j) to decrease in the direction from bus i to bus j. The reverse is true for positive ISF values.

At step 3, a bus is taken from the sorted list and any control devices at that bus are added to the

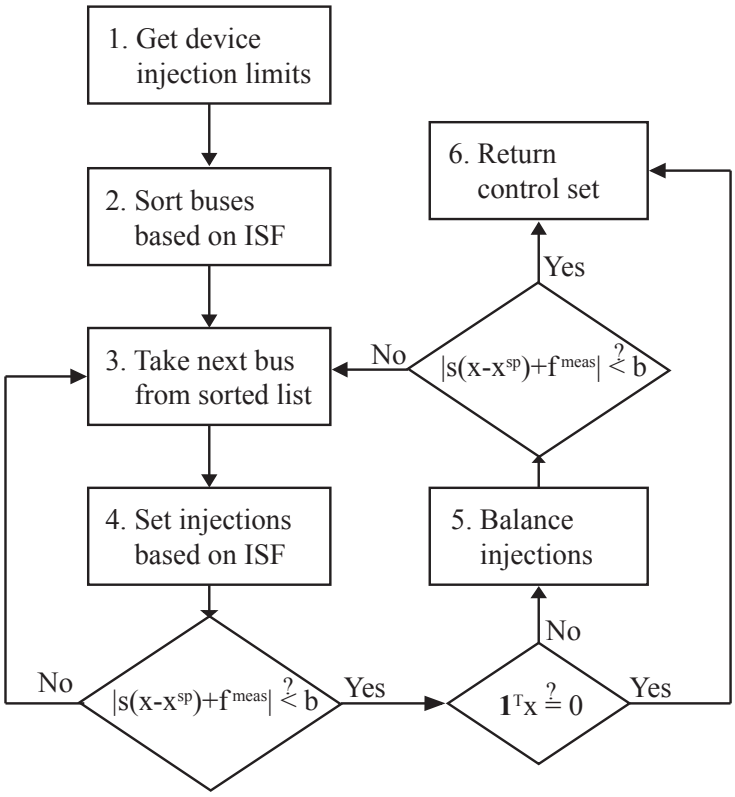

Figure 4.3: Process for selecting the set of control devices for each overloaded line.

set of control resources. The list was arranged in step 2 so that ISF values are sorted from negative to positive. Since the objective of this process is to identify the fewest resources necessary to resolve line flow overloads while maintaining power balance, control actions must be balanced between power injections and withdrawals. To achieve this balance, each subsequent bus is selected from alternating ends of the list. This helps to ensure that the most useful control devices are added to the control set while accounting for power balance.

In step 4, the injection capability of each control device is set to its minimum or maximum based on the sign of its ISF value and whether power flow should increase or decrease from bus i to bus j. The flow condition for overloaded line (i, j) is then checked to see whether,

$$|s_{ij}(x - x^{sp}) + f_{ij}^{meas}| < b_{ij}, \tag{4.10}$$

where s_{ij} is the vector of ISF values for line (i, j), x is the vector of device maximum/minimum injections, f_{ij}^{meas} is the actual (overloaded) line flow and b_{ij} is the maximum allowable flow. The entries of x include the control devices which are set to their injection limits and all other devices not in the control set which

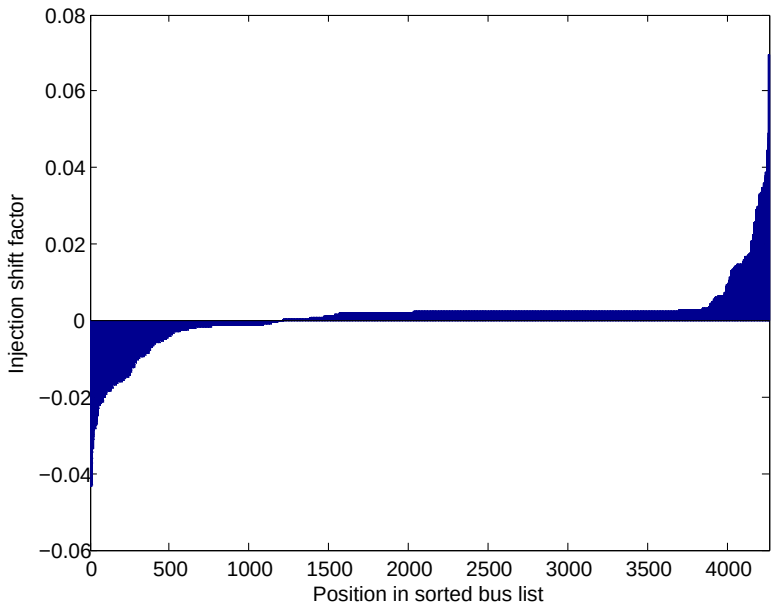

Figure 4.4: Injection shift factors ordered from least to greatest for a transmission line in the California electric grid.

are held at their scheduled injections x^{sp}. The value of b_{ij} is based on the line rating,

$$b_{ij} = \alpha f_{ij}^{lim}, \tag{4.11}$$

where α is in the range $(0, 1]$. Smaller values of α will cause the control set to be larger since more control capability will be required to reduce the flow to the more restrictive limit.

If the flow condition (4.10) is not satisfied, the process returns to step 3 and adds an additional bus to the control set. If the flow condition is satisfied, the power balance condition is checked. If power balance is achieved within a small tolerance, the process terminates and a sufficient set of control devices has been identified. If power balance has not been achieved, the process moves to step 5, and balances the injections.

To balance the power injections at step 5, the power injections of control devices added to the control set most recently are changed between injection and withdrawal until power balance is achieved. This allows power balance to occur while causing the least disruption to the line flow condition. Once power balance has been achieved in step 5, the flow condition is checked once more. If it is satisfied, the process is terminated. If the flow condition is not satisfied, the process returns to step 3 and adds an additional bus to the control set.

By running this process prior to the operation of MPC, a subset of control devices is identified. Only these control devices may be adjusted by MPC and all other devices in the network operate by following

their scheduled behavior. This greatly reduces the number of variables in the MPC problem allowing much faster solution.

4.3 Selecting a Set of Thermally Modeled Lines

Additional time-savings can be achieved during solution of the MPC optimization by limiting the number of lines which are represented by thermal models that predict their temperature behavior. Many lines in the network are far from their thermal rating and will remain well below their limit during control actions. If a line does not reach its thermal limit, the corresponding constraints will never be binding and so will have no effect on the objective cost or control decisions. Ignoring the thermal dynamics of these lines by not including them in the MPC formulation will not change the outcome but significantly reduces the number of constraints and variables.

At termination of the control set selection process, the predicted injections x^{pred} of every device in the network have been identified. These injections satisfy the line flow and power balance conditions used during the selection process. The ISF values for every line in the network can be calculated using (4.6) and the flow on each line can be predicted with,

$$f_{ij}^{pred} = s_{ij}(x^{pred} - x^{sp}) + f_{ij}^{meas}. \tag{4.12}$$

If the predicted flow on a line is sufficiently close to its rating (e.g. $|f_{ij}^{pred}| \geq 0.95(f_{ij}^{lim})$), it is included in the set of thermally modeled lines. Otherwise, the line does not receive a thermal model in MPC. All lines are still modeled in the network admittance information used in the power flow constraints. As MPC evolves, the predicted flow on each line is monitored. If any lines approach their rating they are added to the set of thermally modeled lines.

4.4 Identifying Critical Voltages

The control selection heuristic presented in Section 4.2 addresses transmission overloads but does not directly address voltage stability concerns. As such, the control set identified by this method may fail to provide sufficient control capabilities for correcting voltage limit violations. Additionally, the control actions predicted to correct the thermal overloads may cause voltages to deviate outside their limits. Any buses which experience high or low voltages due to the predicted injections x^{pred} should be identified and included within the internal model of MPC.

A rigorous method for identifying the relevant control set in a voltage collapse situation on a large network is not investigated in this work and remains an open opportunity for ongoing research. One of the challenges in addressing this question is attaining an appropriate data set for algorithm testing. Meaningful voltage collapse simulation requires a fairly detailed network model including information about regulating transformers. This data was not available for the network analyzed in Chapter 5, preventing realistic investigation of regional voltage collapse behavior.

A basic approach is suggested here as a first step in addressing the voltage control challenge. After the control set is selected, the predicted injections x^{pred} are available and the sensitivity of voltage magnitudes to changes in power injections is available from the inverse of the power flow Jacobian. The voltage response at each PQ bus due to the predicted injections can be calculated as,

$$U_n^{pred} = [\mathbf{0}, I] \left(\frac{\partial [P, Q]}{\partial [\delta, U]} \right)^{-1} (x^{pred} - x^{sp}) + U_n^{meas}, \tag{4.13}$$

where I is the identity matrix with dimension equal to the number of PQ buses in the network and $\mathbf{0}$ is a matrix of zeros appropriately sized to match the number of voltage angles δ. Buses with voltages U_n^{pred} or U_n^{meas} above or below their voltage limit should be added to the control set c retained within MPC. This enables MPC to consider the impact of the high or low voltages when selecting its control actions.

If voltage regulating transformers are included in the network model, the voltage they are set to regulate is necessary for the constraints of (3.21). If control actions do not significantly influence voltage magnitudes, it is possible that these devices could be ignored by MPC's internal model. However, without a relevant test network, it is difficult to determine how this may affect MPC. In this work, all regulating transformers are retained in the internal model of MPC. Therefore, any buses with voltages regulated by LTCs should also be added to the control set c and modeled within MPC.

As MPC operates on the network, the actual network response and the predicted response to control actions throughout the prediction horizon should be monitored. If any buses experience high or low voltages, they should be added to the control set for subsequent operations of MPC.

Chapter 5

Demonstration of Thermal Relief on a Large Network

5.1 Case-Study Description

To demonstrate the performance of the LAC-MPC formulation on a realistically sized network, a model of the Californian (CA) transmission grid was obtained together with hourly generation and load data. The resulting case-study presented in this chapter was first published in [76]. The model has 4259 nodes, 5867 lines/transformers, 2029 traditional and renewable generators and 1443 loads. Ten energy storage devices were added to the network using the approach described in [81]. To respect the limited use of storage in realistic networks, the cumulative power capacity of the storage devices was 0.5% of the generation capacity.

Modeling temperature behavior on transmission lines requires the use of detailed information regarding line length and conductor type. This information was not available for the CA network and was estimated based on the resistance, power rating and voltage base of each line.

A line trip during the morning ramp period causes an overload and initiates MPC operation. The overloaded line uses 30/7 Lark ACSR conductor with power flow at 138% of its normal rating immediately following the contingency. Without control intervention, the line temperature rises from 2°C below its rated value to 12°C above its rated value in four minutes and trips out of service.

During the first five minutes of operation, MPC seeks to limit thermal overloads while nominally following the pre-contingency schedule defined by the AC economic dispatch algorithm of [82]. After five minutes, a secure post-contingency dispatch becomes available and the new schedule is provided to MPC as its reference. MPC uses a prediction horizon of $M = 10$ steps and a time-step duration of $T_s = 1$ minute. As a comparison,

Table 5.1: Objective function coefficients for CA case-study

Term	MPC	Human
$\Delta\hat{T}_{ij}$	1	–
p_{Gn}	100	0.01
q_{Gn}	0.1	–
E_n	100	0.01
U_n^+, U_n^-	1000	–
Δp_{Gn}	0.05	0.05
p_{Rn}^{cur}	0.15	0.5
p_{Dn}^{red}	10,000	20,000
$p_{Sc,n}$, $p_{Sd,n}$	0.2	1000
ψ_{ij}	0.01	0.1
Rating violation	–	100

the "human operator" equivalent controller from Section IV-B of [8] is also employed to approximate operator response. This controller penalizes power flow rating violations but does not predict temperature behavior.

The objective coefficients for the MPC and approximate human controllers are given in Table 5.1. The high penalty applied to load reduction indicates that the controller should only utilize demand response if it is absolutely necessary. Additionally, the approximate human controller tends to ignore storage.

As mentioned previously, solving the QP defined by LAC-MPC can be computationally challenging for large networks. In this case study, multiple implementations of MPC were compared using different levels of control-set reduction. The algorithm developed in Section 4.2 was employed with various values of α in (4.11) to explore how reducing the retained set of controls affected the ability of LAC-MPC to respond to disturbances. For base-line comparison, the full network complete with all controllable devices was also considered.

Transmission lines with measured or predicted power flows within 70% of their rating were assigned thermal models within MPC. This resulted in 20 transmission lines having thermal models in all MPC implementations.

5.2 Thermal Response

Separate tests were undertaken for six different control implementations: base-line (full network), the reduced control set with $\alpha \in \{0.6, 0.65, 0.7, 0.9\}$, and the approximate human operator. In accordance with the interactions outlined in Figure 1.2, the controller guides the network response for at least 14 minutes and terminates once all physical line flows are within 2% of their rating. The maximum temperature of any overloaded line during this process is shown in Figure 5.1. No lines outside the thermally modeled set exceeded their power rating at any time.

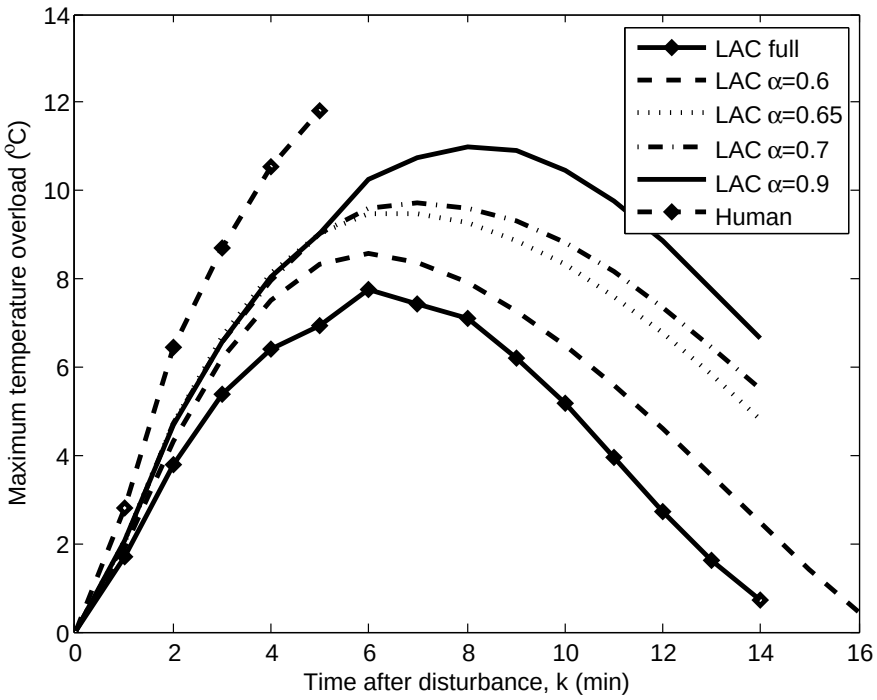

Figure 5.1: Maximum temperature overload $\hat{T}_{ij}$ response in the CA network for various control schemes.

Each of the LAC-MPC controllers successfully directs the network through the contingency and toward the updated economic dispatch once it becomes available after five minutes of operation. The approximate human controller is unable to suppress the initial temperature rise prior to the updated dispatch, and the overloaded line trips due to unacceptable heating.

In this example, a small amount of load reduction is necessary in addition to the other control options. Although it is expensive, MPC employs a small amount of demand response to satisfy the requirement that thermal overloads be minimized by the end of the prediction horizon. This small adjustment effectively limits the rapid initial temperature increase. The approximate human controller has no requirement that overloads be completely removed and does not recognize this need for demand response.

The LAC-MPC formulation with control across the full network attains the best temperature profile in Figure 5.1. The reduced formulations with $\alpha \in \{0.6, 0.65, 0.7, 0.9\}$ remain close to this trajectory and attain very similar performance to each other during the first five minutes. The variation in temperature at minute six is a result of MPC's balancing actions as network devices outside of the available control set rapidly move toward their new economic setpoints.

Smaller values of α require greater control effort to satisfy (4.11), resulting in MPC retaining control over a larger number of devices. Hence, as α decreases, the control decisions more closely resemble those of MPC with access to the full network. When α reaches 0.59 in this example, all devices in the network are

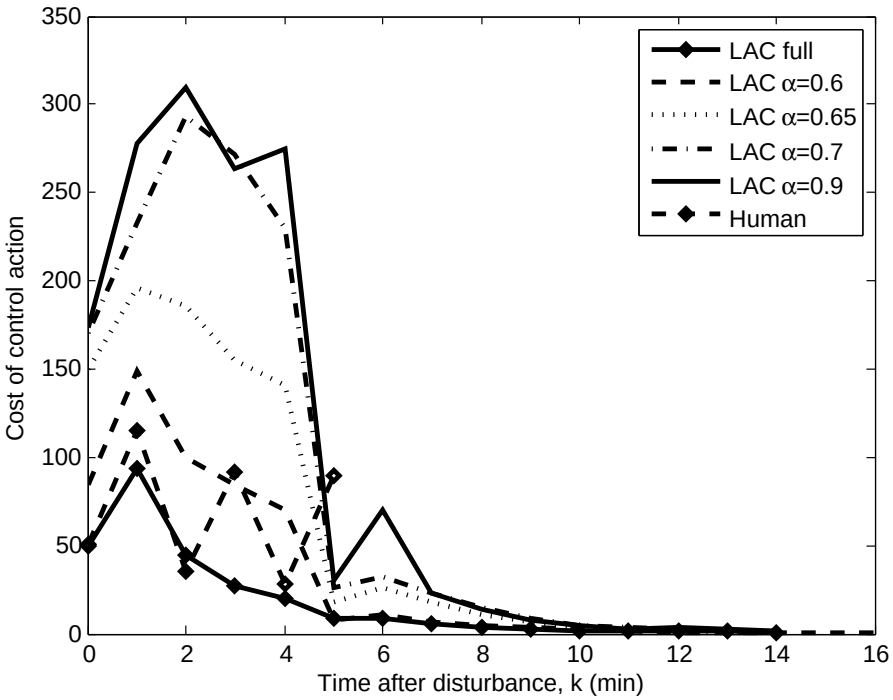

Figure 5.2: Cost of implemented controls $u[0|l]$ at each time-step for various control schemes.

included in MPC's control set. If α is too large, insufficient control is attained and MPC may have difficulty removing all thermal overloads by the end of the prediction horizon.

5.3 Control Cost

Figure 5.2 shows the objective cost of the controls implemented on the physical network at each time-step. Again, smaller values of α allow MPC to more closely match the base-line where the entire network is controlled. Only a relatively small number of devices have meaningful influence on the overloaded line as indicated by the injection shift factors in Figure 4.4. Values of α between 0.65 and 0.7 include all devices within the peaks at either end of the sorted ISF list for the overloaded line in this test. Below this value, the control set grows very rapidly for small changes in α because any additional devices have very limited influence on the line flow.

The control costs in Figure 5.2 when α is 0.7 or 0.9 are very similar. For α values in this range, controls obtained by decreasing α are effective but expensive and are not significantly utilized by MPC. Alternatively, decreasing α from 0.7 to 0.65 adds cheap but less effective controls. This allows MPC to decrease its costs by balancing the network with less expensive actions as evidenced in Figure 5.2, but does not significantly change the temperature response of the overloaded line in Figure 5.1.

Table 5.2: Computational aspects of LAC-MPC on the CA case-study

Version	Num. Bus	Mean Sol. Time (s)
full	4259	314
$\alpha = 0.6$	1569	488
$\alpha = 0.65$	934	324
$\alpha = 0.7$	470	10
$\alpha = 0.9$	379	20

5.4 Voltage Monitoring

Another benefit of utilizing a linearized AC formulation of MPC is the ability to manage voltage violations. LAC-MPC permits small voltage limit violations using the soft constraints of (3.3) if they are necessary for feasibility. Alternatively, unacceptable voltage violations are quickly detected and can be eliminated. This type of response is not possible in a DC formulation.

Bus voltages across the network are monitored each time MPC acquires updated information about the state of the system. In this demonstration, low voltages are experienced after the first control action of the LAC-MPC formulations operating on the full network and with $\alpha = 0.6$, and also for the approximate human controller. The voltage drop is larger than predicted by MPC at a peripheral bus and results in a 5% low voltage violation. Both MPC methods detect the violation and correct it in the following time-step. The approximate human controller is based on a DC power flow and does not recognize the violation, allowing it to persist. The LAC-MPC methods with smaller control sets do not experience any low voltage conditions.

Slight high voltage violations are experienced outside the control set of all reduced LAC-MPC formulations after the secure dispatch is introduced. The violations are insignificant at less than 0.7% and the buses are not added to the control set of MPC. If the violations were more severe, the buses could be added to the control set allowing the voltages to be considered in formulating subsequent control actions.

5.5 Solution Speed

For each of the LAC-MPC control implementations, Table 5.2 provides the number of retained buses and the average solution time required to solve the QP using Gurobi [69]. It is interesting to note that reducing the size of the QP by limiting the number of buses in the control set does not always result in a time reduction. This behavior is partially due to the fill-in effects of reducing the power flow constraints for the smaller α values. The sparsity of the full network equations is lost as constraints are eliminated. However, when enough constraints and variables are eliminated, the benefits of reducing the problem size outweigh the fill-in effects. For instance, the solution time when α is in the range of 0.7 to 0.9 is sufficiently rapid that computations could fit into the 60 second control window. That is not the case for the full network. The

increase in solution time when α increases from 0.7 to 0.9 is a result of feasibility challenges. The control set when $\alpha = 0.9$ is just sufficient to provide feasibility, whereas the larger control set when $\alpha = 0.7$ provides greater flexibility and finds a solution more easily.

For large networks where solution speed is a concern, several options are available. The control set and the resulting problem size can be reduced using the techniques presented in this work without significant loss of control capability. A second option is to increase the time-step duration T_s.

Chapter 6

Voltage Instability

One strength of a model-predictive control framework is its flexibility in modeling a wide variety of system behaviors. A controller operating in real-time must be able to respond to unplanned events and accurately account for the system response in these situations. Voltage instability is one such phenomena which has received significant attention during the past couple decades. Although voltage decay and instability may occur too quickly for a human operator to intervene, automatic control strategies such as MPC have the potential to rapidly identify and avoid these situations.

This chapter examines the voltage instability process and MPC's ability to correct detrimental behavior. The features and theoretical underpinnings of voltage instability are presented in Section 6.1. Sections 6.2 and 6.3 discuss MPC's performance on two networks commonly used as voltage instability case-studies. These demonstrations show that MPC can prevent voltage instability from occurring even in situations where a human operator would likely fail to do so. The interplay between thermal transmission limitation and load-based voltage instability is also discussed.

6.1 The Voltage Instability Process

Voltage instability is used to describe different behavior in different power system settings. While it may describe fast behavior when dealing with induction motors, this work considers the slower behavior driven by transformer tap changing and load recovery. Dynamics at the faster time scales are assumed to be secure so that the system settles back to the slower dynamic trajectory. Either way, voltage instability implies the lack of voltage stability. Voltage stability is generally defined as voltages recovering to a secure equilibrium condition following a disturbance [75]. For fast timescales, the equilibrium is described by the power flow equations with fixed taps in (3.1). For slower timescales, equilibrium implies that voltage regulation changes

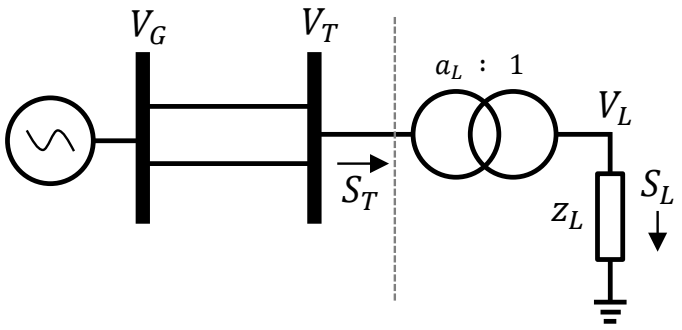

Figure 6.1: Simple network demonstrating load and voltage relationships.

(such as transformer tap-changing) have subsided.

The subtleties between voltage instability and other forms of instability (such as generator rotor angle instability) can be difficult to separate in faster settings. However, voltage instability on slower timescales typically is located near loads [74, 75]. As seen from the transmission network, loads are mostly voltage dependent. If the voltage magnitude drops, the power consumed by the loads will also drop. Transformers attempt to restore the voltage and therefore the power consumption of the loads. This restoration process may push the network and generators beyond their power capability limits causing voltage instability [74]. Two common symptoms of voltage instability are low voltages originating near load centers and emanating into the rest of the transmission network and generators reaching their reactive power limits and becoming unable to regulate their voltages.

6.1.1 Load Restoration

The implications of load restoration in power system networks can be demonstrated through a simple example. Consider the network shown in Figure 6.1 where a generator supplies power to a load (to the right of the dashed line) through two transmission lines. The load is represented by impedance z_L, and an ideal (lossless) transformer regulates the load voltage V_L by adjusting its tap position a_L. Since the transformer is lossless, the power drawn from the network S_T is equal to the power consumed by the load S_L,

$$S_T = S_L, \tag{6.1a}$$

$$= \frac{|V_L|^2}{z_L^*}. \tag{6.1b}$$

The term z_L^* denotes the complex conjugate of z_L. Employing the transformer voltage relationship $|V_L| = |V_T|/a_L$ allows further simplification,

$$S_T = \frac{|V_T|^2}{a_L^2 z_L^*}. \tag{6.2}$$

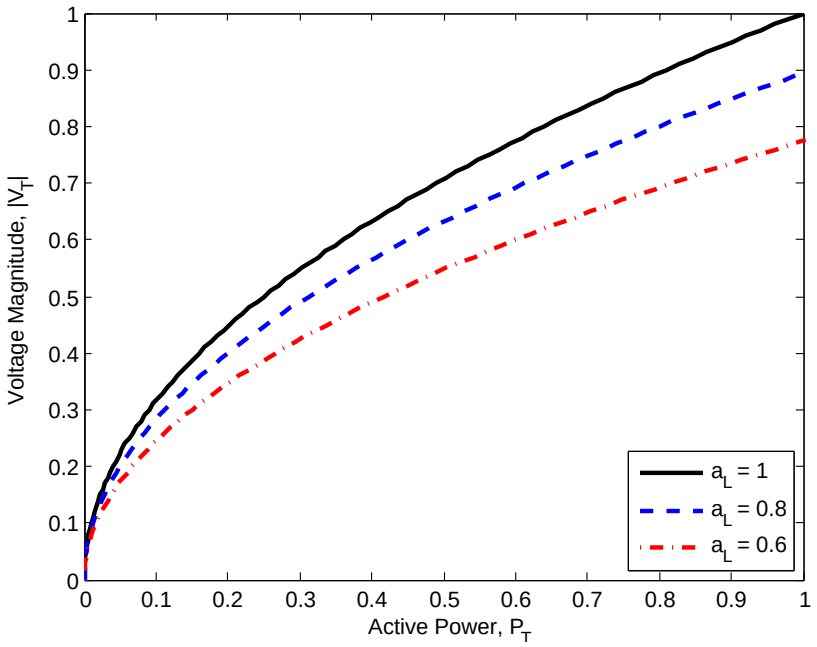

Figure 6.2: The load characteristic from the system of Figure 6.1 is influenced by the tap ratio of the load transformer. The active power from (6.2) is a quadratic function of the transmission voltage magnitude. Units assume $z_L = 1$.

Variations in the transformer tap position change the effective load impedance as seen from the transmission network. Figure 6.2 demonstrates the relationship between the active power drawn from the network P_T and the transmission network voltage magnitude $|V_T|$ assuming $z_L = 1$ pu. Reducing a_L increases the load on the transmission network (assuming that $|V_T|$ remains fixed as a_L changes). In the case of a low load voltage $|V_L|$, the transformer decreases its tap until the load voltage is restored to the desired level.

6.1.2 Network Characteristic

It is also possible to determine a network characteristic describing how V_T and S_T relate to each other over a range of loading conditions. Assuming that the network from Figure 6.1 has a purely inductive transmission impedance $X = 1$, Figure 6.3 shows the relationship between power and voltage. A derivation of this relationship is provided in [74].

Examining Figure 6.3, it becomes apparent that transmitting reactive power through the network is fundamentally difficult. In fact, the maximum reactive power that can be transmitted to the load is only a quarter of the short-circuit power at the load [74],

$$Q_T^{max} = \frac{V_G^2}{4X}. \tag{6.3}$$

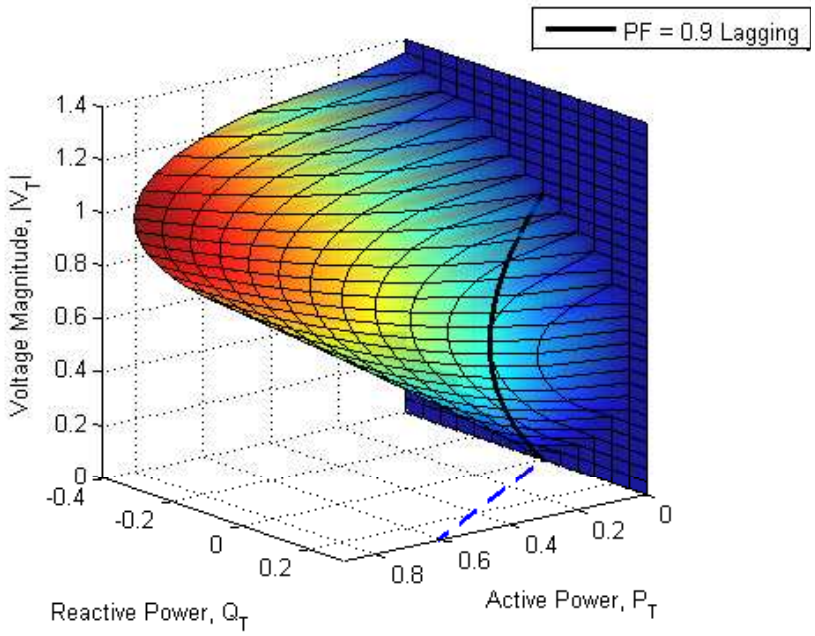

Figure 6.3: The network characteristic for the system shown in Figure 6.1. Units assume $V_G = 1$ and the transmission network impedance is purely inductive with $X = 1$.

This maximum occurs when no active power is consumed by the load ($P_T = 0$ in Figure 6.3). However, the active power supplied to the load can increase to any level as long as sufficient reactive compensation is provided at the load bus (e.g. Q_T becomes more negative in Figure 6.3). Unfortunately, significant reactive compensation will also cause unacceptable voltage rise as the load increases.

Typical operating conditions in a power system result in both active and reactive power being consumed. For example, the solid black curve in Figure 6.3 shows the network characteristic when the load operates at a power factor of 0.9 lagging. The ratio of active to reactive power consumption is fixed as the load level changes and is indicated by the dashed blue projection onto the power plane. The same network characteristic is represented in the (P_T,$|V_T|$) plane by the solid black curve in Figure 6.4.

If one of the transmission lines is disconnected, the network impedance doubles and reduces the maximum power that can be supplied to the load. The new network characteristic is shown by the dashed black curve in Figure 6.4. This decrease in transmission capability implies that voltage instability becomes much more likely under heavy load conditions.

If the load transformer is set to regulate the load voltage magnitude $|V_L|$, the tap changing behavior can degrade the transmission voltage V_T. At a long-term equilibrium condition with the load operating at its regulated voltage, the load consumes a certain amount of power (shown by the vertical dashed lines in Figure 6.4). It is important that this equilibrium power remains within the maximum power capability limit of the network characteristic.

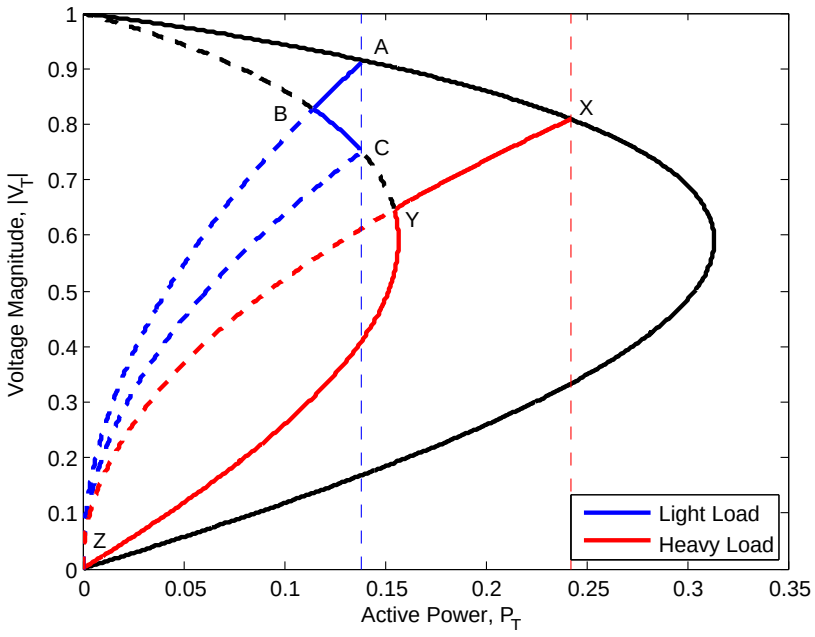

Figure 6.4: Transmission network characteristic (shown in the solid black curve) for the system of Figure 6.1 and assuming a purely inductive network $X = 1$. The load power factor is fixed at 0.9 lagging. If one of the transmission lines is lost, the transmission impedance doubles and the network characteristic is represented by the dashed black curve.

The system behavior during a contingency under light load is shown by the solid blue curve (A-B-C) in Figure 6.4. With both transmission lines in service and the load voltage at its setpoint value, the system operates at point A. Tripping one of the transmission lines causes a rapid transition to point B along the short-term load characteristic (i.e. the impedance characteristic with a given tap ratio from Figure 6.2). The low load voltage at point B causes the load transformer to begin decreasing its tap until the load voltage is restored to its setpoint value. This causes a slower transition from point B to point C, where the system rests at its new long-term equilibrium condition.

Under heavier load, a new long-term equilibrium condition does not exist at the desired load voltage after the loss of a transmission line. The system trajectory in this situation is shown by the solid red curve (X-Y-Z) in Figure 6.4. With both lines in service and the load voltage at its setpoint value, the system operates at point X. The system moves rapidly to point Y when a transmission line is lost, causing a low load voltage. As the load transformer attempts to restore the load voltage by decreasing its tap, the system moves from point Y toward point Z and experiences voltage collapse. In reality, transformer tap limits would prevent the system from reaching point Z implying an equilibrium condition along the lower portion of the red curve. However, in this condition other protective relays are likely to operate and could cause further system degradation. For example, significant reactive power losses in the network would exceed the reactive power capability of the generator and cause its voltage to also decay to unacceptably low levels.

6.1.3 Control Response to Voltage Instability

As mentioned earlier, voltage instability is closely tied to system loading conditions. Although the light load scenario in Figure 6.4 reaches a new long-term equilibrium condition within the maximum transmission capability of the network, this condition may be insecure due to unacceptably low voltages. The voltage collapse scenario under heavier load more obviously demonstrates voltage instability. In either situation, the voltage instability must be corrected by reducing the demand on the transmission network.

In the system of Figure 6.1, only one generation source and transmission path is available to supply the load. To reduce the demand on the network, load levels must be reduced. This can be directly accomplished by shedding load. If low load voltages are permissible, transformer tapping operations could also be blocked or the load setpoint voltage reduced. Improving the load power factor by increasing reactive power compensation could also increase the capability of the network to transmit active power and supply the load. In a more realistic meshed transmission network, other generating sources would also be available and could increase their power output to reduce the loading on the strained transmission corridor.

With these control actions at its disposal, MPC must predict the system behavior immediately following a disturbance (e.g. trajectories B-C or Y-Z in Figure 6.4). If it predicts insecure conditions, it must begin taking actions to address the situation. Transformer tap-changing tends to be the dynamic driver of this behavior and the models of Section 3.3.3 become vitally important for MPC to operate correctly. The case studies in Sections 6.2 and 6.3 examine the performance of these models and MPC's response to voltage instability.

6.2 Bonneville Power Administration Network

A small equivalent network developed by *Bonneville Power Administration* (BPA) offers useful insights into MPC's ability to correct voltage instability. The layout of this network is shown in Figure 6.5. Five high voltage transmission lines connect generation on the left to two loads partially offset by a local generator on the right. The system is loaded heavily so that tripping one of the high voltage transmission lines initiates a voltage instability sequence. A description of the network is provided in [75], but the relevant parameters used in this work are summarized here for completeness.

6.2.1 BPA Network Description

The general parameters for each bus in the BPA network are given in Table 6.1. The nominal operating voltages are shown in the second column. The power ratings of the shunt capacitors at nominal voltage are

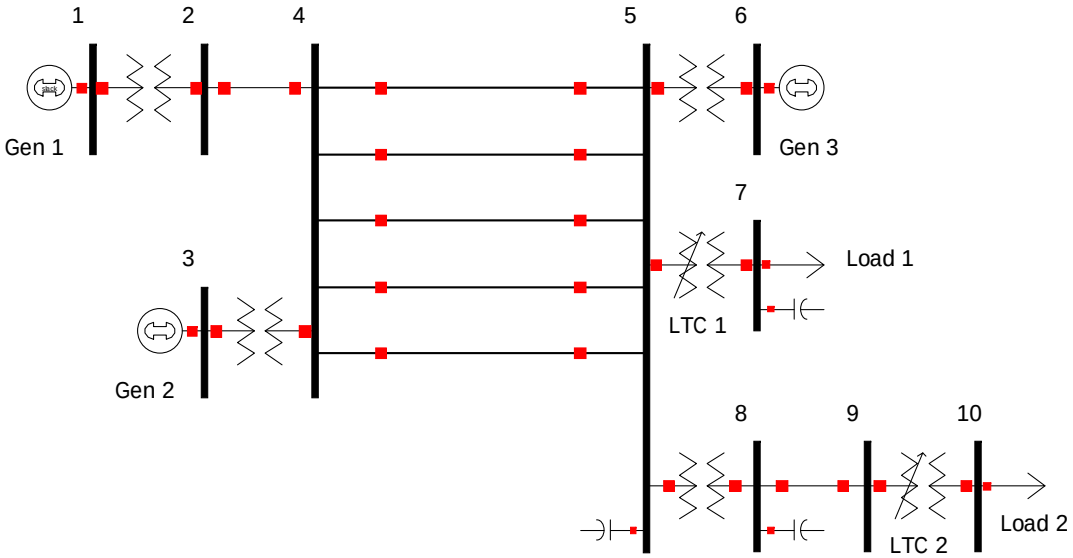

Figure 6.5: BPA network.

Table 6.1: BPA network bus parameters

Bus	**Nom. Volt.** [**kV**]	**Shunt Cap.** [**MVAr**]	**Min. Volt.** [**pu**]	**Max. Volt.** [**pu**]
1	13.8	0	0.98	0.98
2	500	0	1	1.15
3	13.8	0	0.964	0.964
4	500	0	1	1.15
5	500	868	1	1.15
6	13.8	0	0.972	0.972
7	13.8	1500	0.9	1.1
8	115	300	0.9	1.1
9	115	0	0.9	1.1
10	13.8	0	0.9	1.1

Table 6.2: BPA network branch parameters

Branch	Type	From	To	R [pu]	X [pu]	B [pu]	Tap [pu]
1	Xfrmr	1	2	0	0.002333	0	0.8857
2	Line	2	4	0	0.004	0	1
3	Xfrmr	3	4	0	0.005249	0	0.8857
4-8	Line	4	5	0.0015	0.0288	2.346	1
9	Xfrmr	5	6	0	0.005718	0	1.1082
10	LTC	5	7	0	0.003	0	-
11	Xfmr	5	8	0	0.003	0	1.0594
12	Line	8	9	0.000909	0.00303	0	1
13	LTC	9	10	0	0.001	0	-

given in the third column. The fourth and fifth columns specify the acceptable voltage ranges. Note that buses with generators have their voltage ranges fixed to the setpoint voltage of the generator.

Table 6.2 gives the branch parameters. The second column states the branch types: 'Xfrmr' references a fixed tap transformer, 'Line' references an overhead transmission line, and 'LTC' references a tap changing transformer which regulates its To bus voltage. Columns three and four provide the bus connections. Columns five and six give the series resistance and reactance, respectively. Column seven states the shunt susceptance. Finally, column eight gives the tap ratio. The tap ratios are not specified for the tap changing transformers since they vary with time. Thermal ratings are assumed to be sufficiently large and are ignored.

The voltage regulation characteristics for the tap changing transformers are given as follows. LTC 1 regulates its voltage between 0.99 and 1.01 pu by adjusting its tap between 1 and 1.1 pu with step size 0.003125 pu. It is set to operate non-sequentially with a fixed delay of 60 seconds. LTC 2 regulates its voltage between 0.99 and 1.01 pu by adjusting its tap between 0.9 and 1.1 pu with step size 0.00625 pu. It is set to operate sequentially with an initial fixed delay of 60 seconds and a subsequent fixed delay of 5 seconds.

The generators in Figure 6.5 regulate their terminal voltages and operate within a rectangular power capability region. Generators 1 through 3 can produce active power up to 50, 22, and 16 pu respectively on a 100 MVA system power base. Respectively, they can absorb reactive power up to 20, 2, and 2 pu and produce reactive power up to 20, 7.25, and 7 pu. Generator 1 operates as the slack generator and approximates a large remote system. Generator 2 is dispatched to produce active power at 15 pu, and generator 3 is dispatched at 10.94 pu. Output ramp rate limits on the generators are ignored.

The load power levels will be specified for the case studies in the following sections. Load 1 represents an industrial load connected directly to the transmission network with a constant power characteristic for its active power and constant current for its reactive power. It operates at a power factor of 0.8575 lagging. Load 2 represents a mixture of residential and commercial loads connected at the sub-transmission level. It operates at unity power factor with its active power split evenly between constant power and constant

Table 6.3: MPC objective coefficients for heavy BPA load

Term	Use Volt.	Use Power
p_{Gn}	100	1
Δp_{Gn}	1	1
q_{Gn}	1	1
p_{Dn}^{red}	1,000	10
U_n^+, U_n^-	1	100
U_{ij}^{ref}	1	100
a_{ij}	0.01	0.01

impedance characteristics.

6.2.2 Contingency Under Heavy Load

Tripping one of the high voltage transmission lines between buses 4 and 5 during heavy load causes a voltage instability event. Losing the transmission line significantly increases the reactive power losses and causes the voltage in the load area to drop. The voltage dependent portions of the loads decrease slightly, but the tap changing transformers begin to restore the load voltages. This restoration exceeds the reactive power capability of generator 3 and eventually drives the system unstable. The instability is identified by a lack of convergence in the power flow.

For this test case, load 1 demands $30 + \mathbf{j}18$ pu and load 2 demands 35 pu at nominal voltage. The loads remain at these levels over the entirety of the scenario. The system operates with all lines in service for five minutes. At minute five, one of the interarea transmission lines trips offline. Low voltage at bus 6 causes MPC to begin operating. The pre-contingency system conditions are used as the reference trajectory for MPC. The prediction horizon length is set to $M = 11$, and the period duration is $T_s = 1$ minute.

MPC can be tuned to emphasize certain types of controls. For instance, adjusting voltage settings may be preferable to changing the power dispatch. By assigning heavier objective penalties to changes in power, MPC will rely less on these controls. The objective coefficients emphasizing voltage control are given in the second column of Table 6.3.

Key system states are shown in Figure 6.6. The '$*$' markers show the behavior when MPC is not operating. The '$\circ$' markers show the behavior under MPC's control. Without intervention, collapse occurs before measurements become available at minute 7 due to rapid tap-changing on LTC 2.

The initial voltage drop in Figure 6.6a is quickly restored by MPC. Raising the voltage significantly increases the reactive power support available from the shunt capacitors. Voltage setpoint adjustments are inexpensive, and Figure 6.6b shows how MPC significantly raises the voltages at generators 1 and 2 and slightly adjusts settings in the load area.

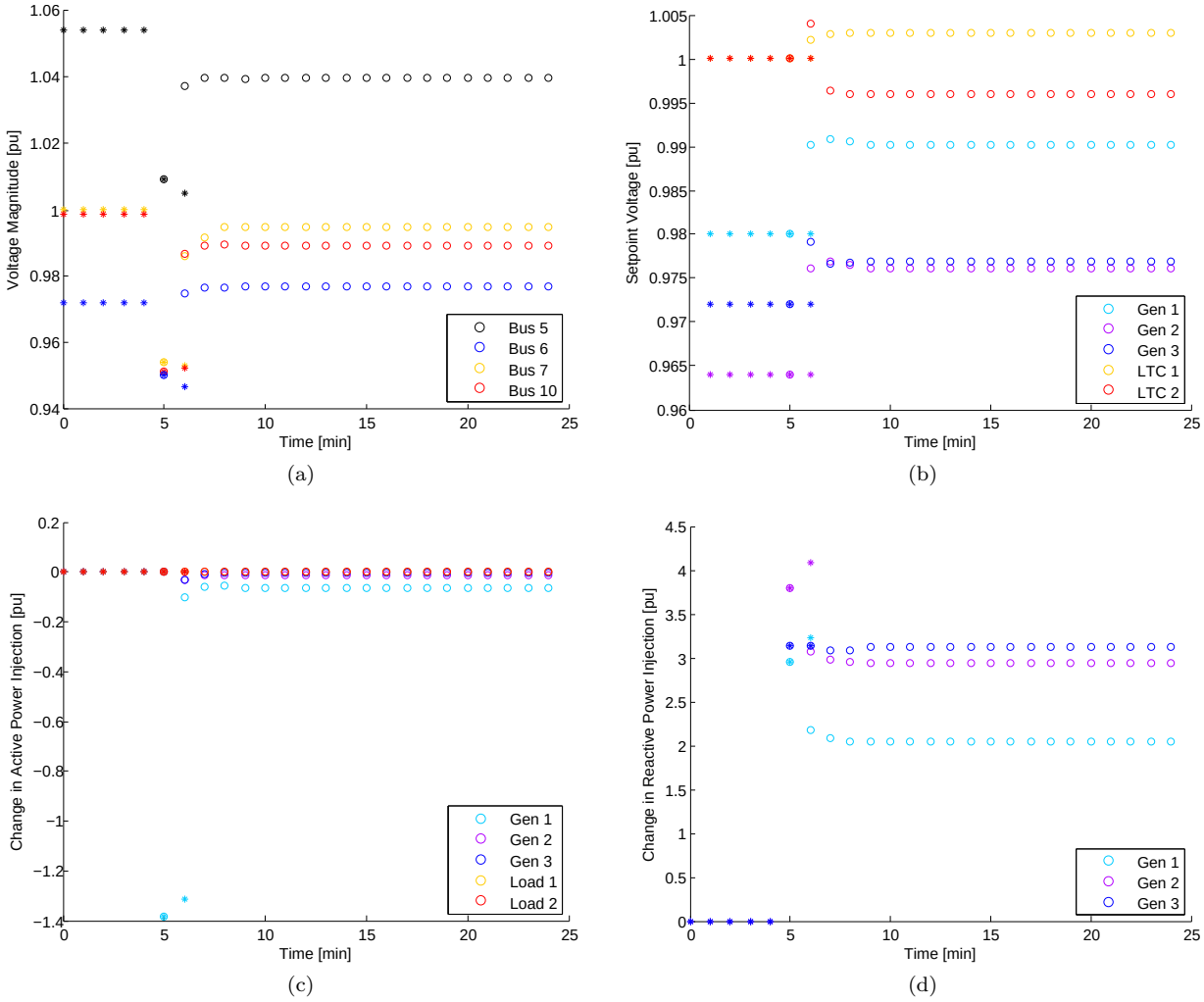

Figure 6.6: Conditions during a contingency at minute 5 under heavy load when voltage control is emphasized. Behaviors with and without MPC intervention are shown by '$\circ$' and '$*$', respectively. Changes in power are with respect to the conditions at time 0. (a) Voltage magnitudes drop sharply after losing a transmission line but are restored by MPC. (b) MPC increases voltage setpoints to better utilize shunt capacitors. (c) Active power remains mostly constant, and MPC returns the slack generator to its pre-contingency dispatch. (d) Reactive power requirements decrease as voltages recover at shunt capacitors.

Active power controls remain fairly constant at their pre-contingency dispatches in Figure 6.6c due to the high objective cost of deviations. The increase in output from the slack generator is the main driver of the voltage rise across the network. The reactive power required from generator 3 in Figure 6.6d remains consistent at its reactive power limit following the contingency. The reactive requirements from generators 1 and 2 decrease between minutes 5 and 6 as the active power output of generator 1 increases back toward its pre-contingency level.

This example demonstrates the importance of a coordinated voltage control strategy. Without intervention, the LTCs act as the primary drivers of load restoration and simultaneously lower the transmission voltages and drain generator reactive power reserves. However, MPC recognizes a solution that may not be immediately obvious to an operator and requests that all generators increase their voltage setpoints. Normally, increasing the voltage would require the generators to increase their reactive power outputs (even though they are already near their limits). Additionally, increasing active power from the sending area typically lowers voltages in the load area. In this situation however, the shunt capacitors in the load area balance these effects and provide the reactive power necessary to support the higher setpoint voltages. This atypical behavior is apparent through rapid computation, but would likely remain unnoticed using intuitive operating practices.

Alternatively, MPC can also be tuned to emphasize power adjustment and maintain the network voltage settings. The objective coefficients emphasizing power controls are shown in the third column of Table 6.3. The same contingency scenario is tested with these objective weights guiding MPC's decisions.

Figure 6.7a shows the voltage behavior when power adjustments are emphasized over voltage changes. Voltages drop sharply when the transmission line is lost at minute 5. MPC is able to partially restore the voltages by minute 6, but the voltage at bus 10 remains outside the deadband of the LTC. This initiates a rapid tap changing sequence on LTC 2 between minutes 6 and 7. The faster sequential operation is not modeled within MPC and is not predicted by the controller. This causes voltages to drop again at minute 7 (except at bus 10) and LTC 2 reaches its lower tap limit. MPC is then able to restore the voltages by minute 8. The voltage setpoints in Figure 6.7b remain unchanged due to the high objective cost of adjustments.

Active power production is shifted from generator 2 to generator 3 and demand response is enacted on both loads in Figure 6.7c. This reduces the strain on the transmission network while maintaining the voltage setpoints at their scheduled values. Reducing the transmission loading and restoring the load area voltage also decreases the amount of reactive power required from generators 1 and 2 in Figure 6.7d.

Both line trip scenarios demonstrate MPC's ability to detect and respond appropriately to sudden low network voltages. Major voltage instability is prevented even when voltages are governed less strictly by predicting the future voltage deterioration and better utilizing shunt compensation. MPC is able to safely

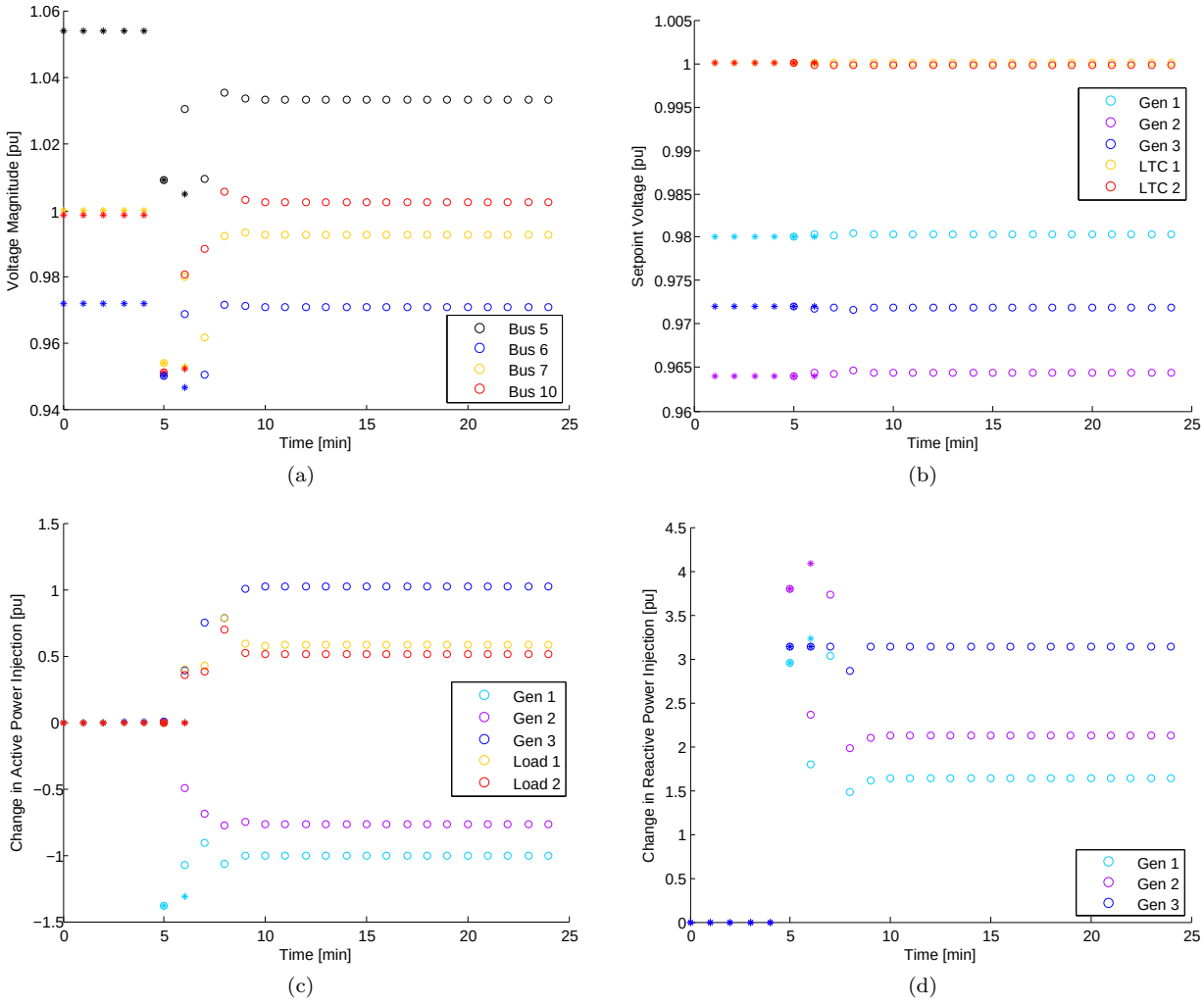

Figure 6.7: Conditions during a contingency at minute 5 under heavy load when power control is emphasized. Behaviors with and without MPC intervention are shown by '$\circ$' and '$*$', respectively. Changes in power are with respect to the conditions at time 0. (a) Voltage magnitudes drop sharply after losing a transmission line and rapid tap-changing not predicted by MPC causes deterioration at minute 7 before being resolved. (b) MPC avoids adjusting voltage setpoints on generators and LTCs due to cost. (c) Active power generation is shifted from the remote area to the load area, and demand response is enacted. (d) Initially large reactive power requirements are reduced as interarea transmission is relieved due to the redispatch of active power and restoration of shunt capacitor voltage.

guide the system using different objective strategies and corrects a situation that would likely be unavoidable for a human operator.

6.2.3 Load Pickup with Contingency

Voltage instability can also arise during periods of sustained load buildup. Consider the BPA network with one of the transmission lines between buses 4 and 5 removed from service. At moderate loading levels, the network is able to operate without any limit violations. However, if load 2 ramps up with generator 1 providing balancing adjustments, the transmission network becomes strained and eventually fails to supply the increasing load.

A continuation power flow [83] provides valuable insight in this type of scenario. A loading parameter incrementally increases the nominal power requested by load 2 until the maximum value of this parameter is identified. LTC taps are allowed to vary smoothly during this process to provide voltage regulation and the active power limits on generator 1 are ignored. Assuming nominal voltages, load 1 is set to $30 + \mathbf{j}18$ pu, and load 2 starts at 32 pu. The system behavior as load 2 increases is shown in Figure 6.8.

The maximum nominal power of load 2 is 34.98 pu and is clearly evidenced by the vertical slope on the voltage curves in Figure 6.8a. At this condition, both LTCs are at their respective lower limits in Figure 6.8b and generators 2 and 3 are both producing their maximum reactive power in Figure 6.8d. Figure 6.8c shows that the maximum active power which is actually delivered to load 2 is only 33.97 pu and occurs when the nominal demand is 34.19 pu.

The first indication that the system is strained occurs as generator 3 reaches its reactive power limit. As its terminal voltage begins to drop, a low voltage alarm signals that MPC should begin to operate. Subsequent warning signs include LTC 2 reaching its lower tap limit, closely followed by LTC 1 reaching its limit, and finally, generator 2 reaching its reactive power limit. After this point, system voltages degrade very quickly, and the reactive power output of generator 1 significantly increases.

The behavior shown in Figure 6.8 assumes that generator 1 supplies the active power required as load 2 increases. If generation is shifted into the load region, greater loading levels become possible. MPC is able to initiate this type of behavior to satisfy demand levels that cannot be supplied by generator 1 alone.

Consider similar conditions as those used in the continuation power flow. Load 1 is set to $30 + \mathbf{j}18$ pu, and load 2 increases from 32 pu to 36 pu at a rate of 6 pu/hr. The peak load is sustained for 5 minutes and then ramps back down to its starting level at an equal rate. Generator 1 balances the changes in active power. As was shown in Figure 6.8, the system will experience voltage collapse as load 2 approaches 35 pu. The objective weights used in MPC are given in Table 6.4.

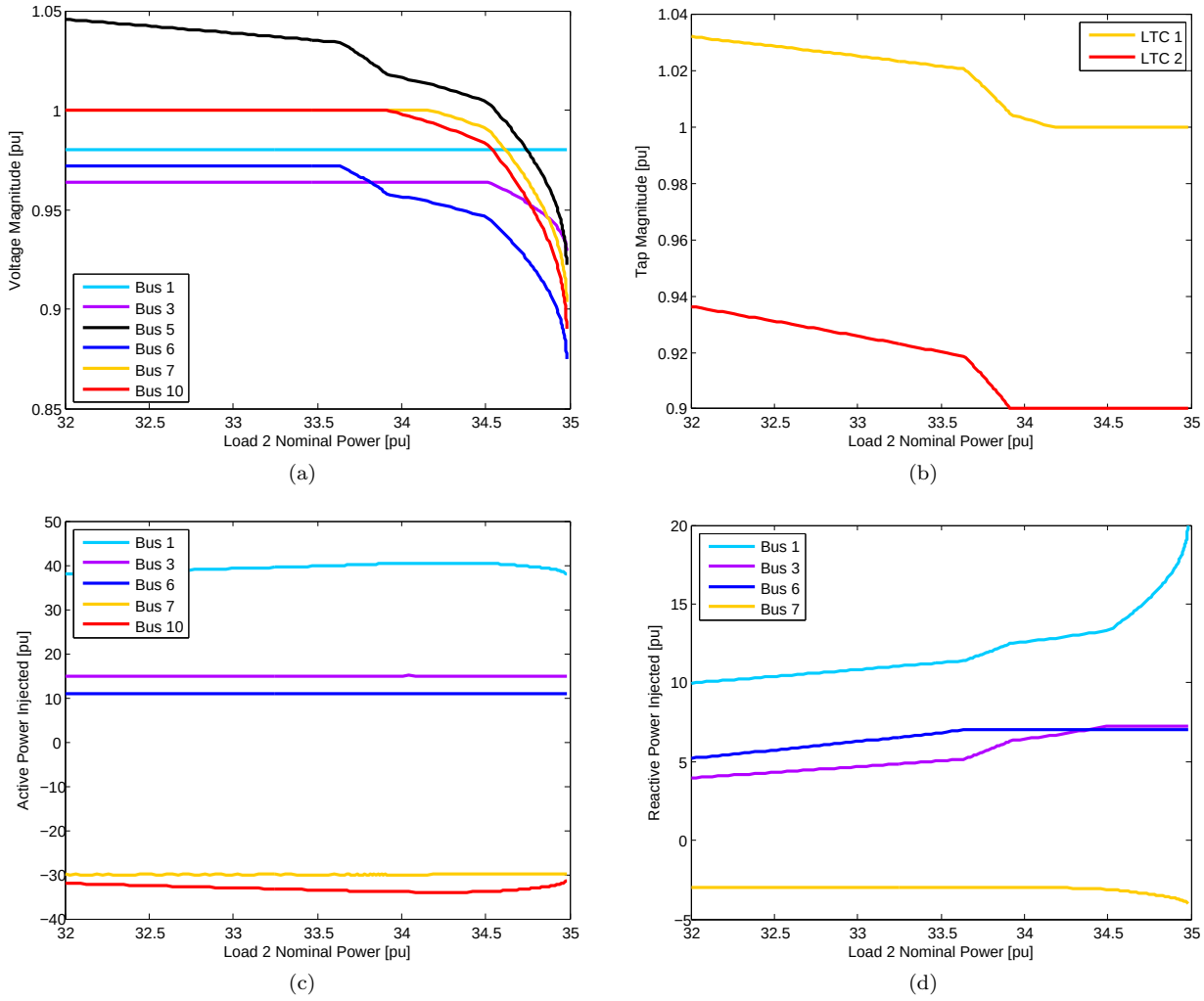

Figure 6.8: Behavior of the BPA network with one of the high voltage transmission lines removed and load 2 experiencing a slow ramp. (a) Voltages collapse quickly as the load approaches its maximum nominal value of 34.98 pu. (b) Tap changing transformer reach their limits as load increases. (c) Maximum power delivered to load 2 is 33.97 pu at nominal demand 34.19 pu. (d) Reactive power requirements increase sharply as the system approaches its power limit.

Table 6.4: MPC objective coefficients for ramping BPA load

Term	**MPC**
p_{Gn}	1
Δp_{Gn}	0.1
q_{Gn}	0.1
p_{Dn}^{red}	1,000
U_n^+, U_n^-	100
U_{ij}^{ref}	100
a_{ij}	0.01

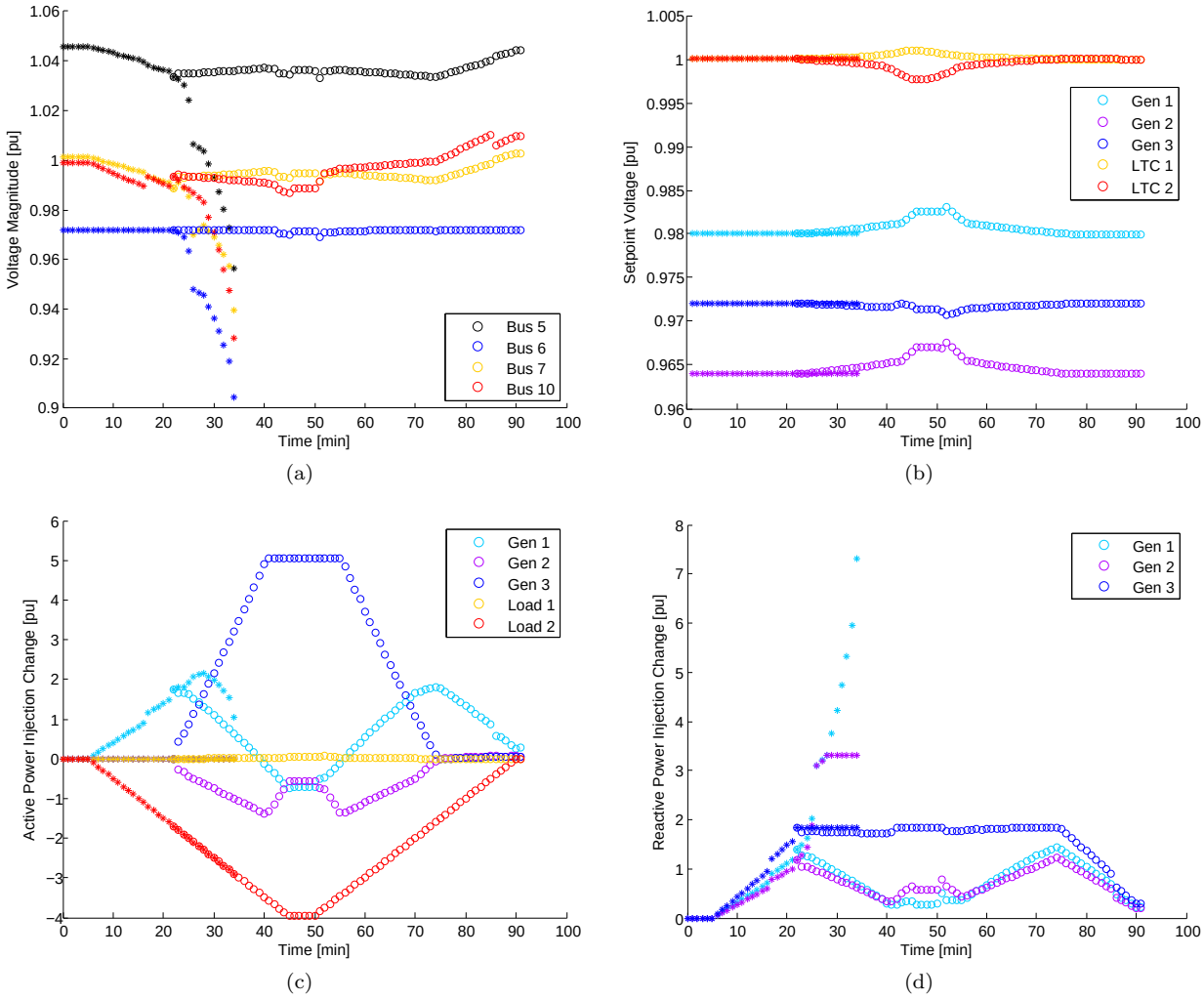

Figure 6.9: Conditions of the BPA network with one of the high voltage transmission lines removed and load 2 experiencing a slow ramp. Behaviors with and without MPC intervention are shown by '$\circ$' and '$*$', respectively. Changes in power are with respect to the conditions at time 0.

Figure 6.9 shows the system behavior during the ramp event. At minute 22 with load 2 at 33.7 pu, generator 3 reaches its reactive power limit, triggering a low voltage warning and causing MPC to begin operating. Without intervention, voltages decline in Figure 6.9a until the power flow eventually fails to converge between minutes 34 and 35 as load 2 reaches 34.9 pu. With MPC's intervention, voltage magnitudes remain fairly steady throughout the ramping event. The voltage setpoints in Figure 6.9b also remain fairly constant. Slight adjustments are made during the heaviest demand period from minutes 40 to 55.

MPC begins to shift the active power generation from generators 1 and 2 to generator 3 when it begins operating in Figure 6.9c. The inexpensive shift in generation allows it to minimize the more expensive costs of voltage deviations at generator buses. At minute 41, generator 3 reaches its active power limit, and generator 2 picks up the power changes during the peak load period. Only a very small amount (< 0.06 pu) of demand response is used during the peak load period. The reactive power needs shown in Figure 6.9d are also reduced by shifting generation into the load area. Without intervention, significant reactive power production is required.

The BPA network provides tractable examples of voltage collapse. With relatively few devices, behavior is easy to identify and useful insights into MPC's choices can be discussed. However, the lack of thermal constraints fails to demonstrate the benefits of a control formulation accounting for both transmission and transformer behaviors. Therefore, a case study which incorporates both conditions is presented in the following section.

6.3 Nordic Network

Another test network commonly used in voltage stability studies is the Nordic system [2]. This network is larger than the BPA network with 74 buses, 20 generators, and 22 loads. A diagram summarizing the 400 kV portion of the system is shown in Figure 6.10. The network is partitioned into four general regions. Generation in the Equivalent and North regions supplies demand in the Central region. The South region is loosely connected to the Central region. The North-Central power transfer occurs over five transmission lines at the 400 kV level. Voltage sensitive loads are connected to the system through tap changing distribution transformers.

A voltage instability event can be initiated by tripping one of the 400 kV lines connecting the North and Central regions. Generators in both regions approach their reactive power limits as LTCs restore the load voltages. Without intervention, transmission voltages eventually drop low enough that a power flow fails to converge.

Thermal aspects can be incorporated into the network behavior by further weakening the connection

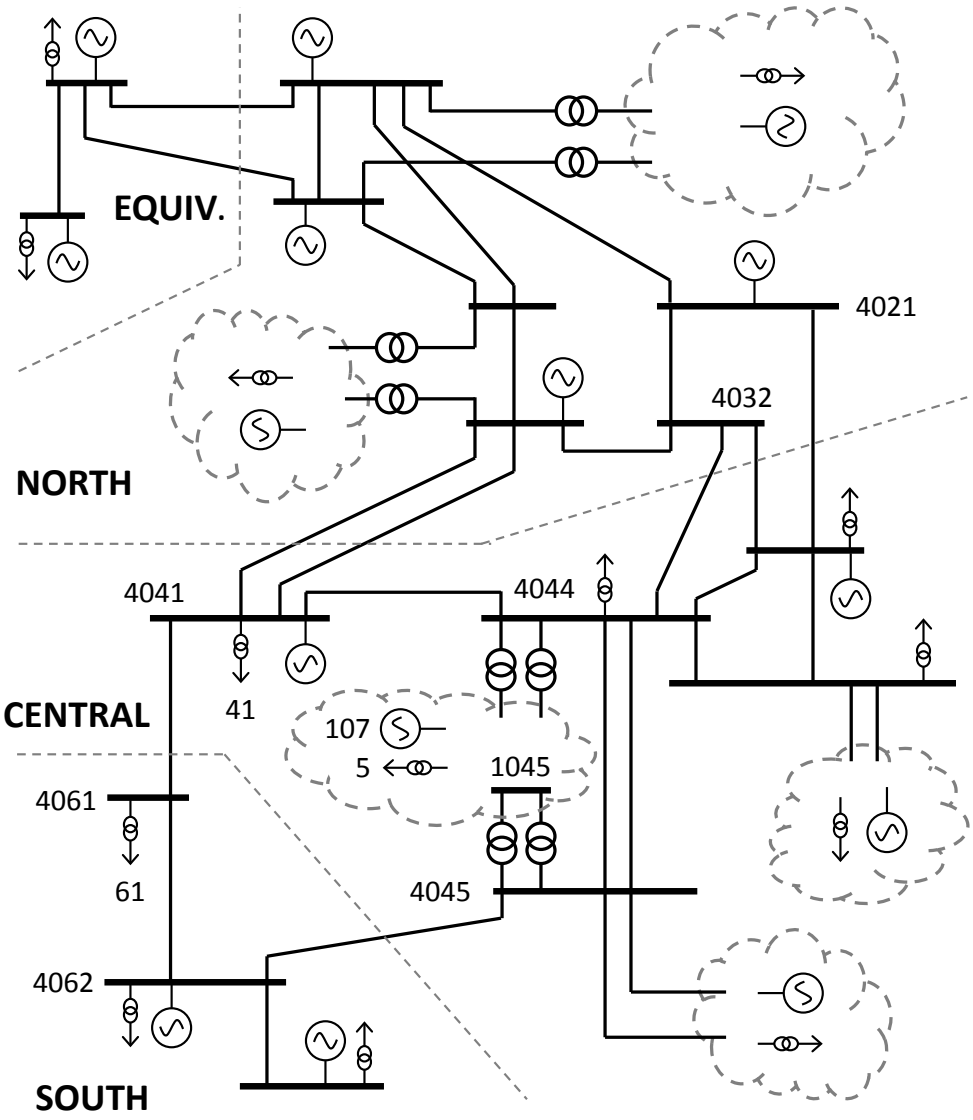

Figure 6.10: Summary of the 400 kV portion of the Nordic network adapted from [2]. The primary load center is the sub-transmission region connected to buses 4044 and 4045. Voltage instability occurs if a transmission line connecting the North and Central regions is lost.

Table 6.5: MPC objective coefficients for Nordic system

Term	MPC
(Equiv./South) p_{Gn}	1
(North/Central) p_{Gn}	100
Δp_{Gn}	0.1
q_{Gn}	0.1
p_{Dn}^{red}	1,000
U_n^+, U_n^-	100
U_{ij}^{ref}	100
a_{ij}	0.01
$\Delta\hat{T}_{ij}$	100

between the Central and South regions. Setting the objective coefficients so that generation changes are less expensive in the Equivalent and South regions than in the North and Central regions causes MPC to shift generation from the Equivalent to the South region to relieve the stress on the North-Central transmission corridor and restore voltages. The objective coefficients used in testing are shown in Table 6.5.

To test MPC's response to voltage instability, the system is set to operating point 'A' described in [2]. Loads remain at this level during the duration of the test. The Central-South transmission line connecting buses 4045 and 4062 is derated to 335 MVA. The system operates normally for two minutes before a double contingency occurs, and lines 4032-4044 and 4041-4061 are tripped out of service. MPC begins to operate with prediction horizon length $M = 11$ and period duration $T_s = 30$ seconds.

The system behavior during the test is shown in Figure 6.11. Conditions when MPC is not operating are denoted by '$*$' markers, and those when MPC is operating are shown by '$\circ$' markers. The slack generator in the Equivalent region accounts for active power changes as LTCs attempt to restore load voltages. This causes voltages to collapse before measurements become available at minute six. Alternatively, MPC quickly stabilizes voltages by shifting generation from the Equivalent to the South region while respecting the thermal rating of the remaining transmission line connecting the South and Central regions (line 4045-4062).

Several network voltages are shown in Figure 6.11a. The contingency occurs at minute 2, causing voltages across the network to dip. Without MPC, LTC operation begins to restore the voltage at load bus 5 at time 2:30. However, this increases the reactive power demand and causes generator 107 to drop below its setpoint voltage as it reaches its reactive power limit. Transmission and sub-transmission voltages also continue to decline as other generators reach their reactive power limits and load LTCs continue adjusting their taps. Finally, collapse occurs after time 5:30.

MPC begins operating at minute 2. It predicts the LTC operation and initiates corrective measures to prevent generator voltages from decreasing. This causes the voltage at load bus 5 to almost completely recover by time 2:30. However, the tap change predictions by MPC are larger than the actual changes which

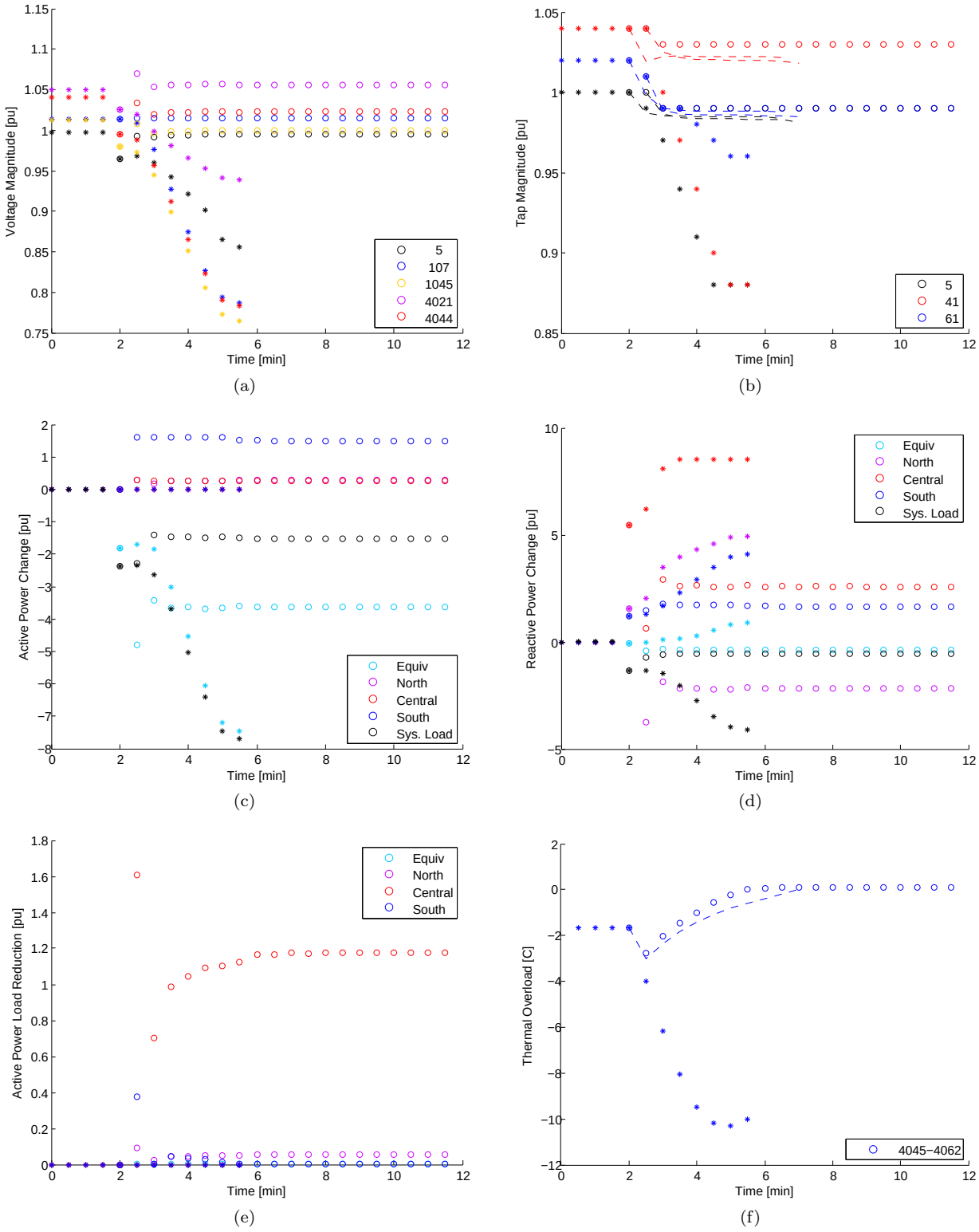

Figure 6.11: Conditions of the Nordic test. Behaviors with and without MPC intervention are shown by '$\circ$' and '$*$', respectively. Changes in power are with respect to the conditions at time 0. Dashed curves represent predictions by MPC.

occur by time 2:30 due to the discrepancies of the linear transformer model. This produces an overcorrection of transmission voltages at time 2:30. MPC resolves the overcorrection by minute 3 and the system settles into the post-contingency equilibrium identified by MPC between times 3:30 and 6.

The tapping behavior at several load LTCs is shown in Figure 6.11b. The predictions of tap behavior during the first two operations of MPC are shown by the dashed curves. The discrepancy between the predicted and actual behavior between times 2 and 2:30 is very apparent for the LTC connected to load 41. This device is configured to change its tap in steps of 0.01 pu with an initial fixed delay of 31 seconds and subsequent fixed delays of 9 seconds. MPC predicts that the tap will decrease by about 0.02 pu by time 2:30. However, the fixed delay prevents any tap changes from occurring by this point. Similar errors occur at other LTCs. The aggregation of these errors causes MPC to select more aggressive control than is actually required during the first period of operation. The predictions at the second operation of MPC better match the actual behavior and allow MPC to resolve the overcorrection. Despite the initial modeling errors during rapid changes at the beginning of the event, the general trend of tap behavior predicted by MPC over the horizon approximates the true response and allows MPC to identify useful control actions.

Changes in active and reactive power from the pre-contingency conditions are shown in Figures 6.11c and 6.11d, respectively. In both figures, the regional changes in generation and the total change in system load are shown. Without MPC, the slack generator in the Equivalent region tracks changes in load in Figure 6.11c. MPC shifts generation from the Equivalent region into the South region. The overcorrection in control is balanced by the slack generator at time 2:30 and resolved as time progresses. Figure 6.11d demonstrates how reactive power requirements on generation are significantly reduced by the controls identified in MPC.

Although load reduction control is expensive, Figure 6.11e shows that MPC employs it in the Central region. This allows voltage deviation penalties to remain small and satisfies the requirement that any thermal overloads be removed by the end of the prediction horizon. The aggressive control is also easily seen in this figure at time 2:30. The tap changes predicted within MPC would restore load voltages and load powers. Therefore, MPC employs load shedding to reduce the demand in the Central region. When the tap-induced load restoration does not materialize, load shedding is reduced over the time interval 2:30 to 3 minutes and then slowly increases to balance thermal overload conditions between the South and Central regions.

The thermal overload on the South-Central transmission interconnection is shown in Figure 6.11f. The discrepancies in voltage predictions at buses 4045 and 4062 are small enough that the accuracy of the thermal prediction on the transmission line is not significantly affected. Due to high penalties on thermal overloads, MPC respects the thermal limit at the new equilibrium condition. With smaller objective penalties, MPC would allow the thermal overload to settle at about 4 °C. The initial drop in temperature is due to a decrease in load before generation shifts into the South region. When MPC does not operate, the generation pattern

remains unchanged and the thermal limit does not present a concern to the system.

Chapter 7

Conclusions and Future Work

7.1 Conclusions

Electric power systems are rapidly changing. The energy supply, once primarily large dispatchable plants, is shifting toward smaller distributed renewable technologies. Demand for electricity continues to increase, and new control capabilities with storage and demand response are emerging. The physical transmission infrastructure continues to age while building new facilities becomes increasingly challenging due to land scarcity. At the same time, communication and computation technologies are experiencing significant improvements, facilitating a trend toward greater software utilization and autonomy.

These factors have collectively motivated the work discussed in this body of research. Historical operating strategies are likely to become obsolete in favor of more efficient practices which utilize emerging control capabilities. Strategies capable of identifying control choices during emergencies or periods of high strain on the network are of special interest due to the significant costs associated with system failure. Model-predictive control is well-suited to address this situation with its flexibility in modeling dissimilar system behaviors over a wide variety of operating conditions.

This work has investigated several important topics regarding MPC's application in practical power systems.

- The objectives of relieving transmission overloads and voltage collapse are combined into a single control formulation. This decreases the potential for control decisions addressing one concern to cause negative behavior in another portion of the network. It also increases the scope of situations LAC-MPC is capable of addressing. A case-study demonstrating the interaction between the two objectives is presented in Section 6.3.

- Realistic electric power systems are large, requiring long solution times for LAC-MPC. A heuristic for reducing the problem size and increasing the solution speed while minimizing the control impact is described in Chapter 4 and demonstrated on a model of the Californian network in Chapter 5.
- A linear relaxation of losses on an individual transmission line when expressed in terms of voltage magnitude and angle is presented in Chapter 2. The Hessian matrix of the loss function is proven to have exactly two positive eigenvalues over realistic operating conditions, and this eigenanalysis is used to justify the proposed loss-modeling strategy.
- The internal model of LAC-MPC is updated to include voltage magnitude and reactive power. Device models are expanded to include these effects in Chapter 1, and models for power flow, transmission line temperatures, and transformer tap-changing are presented in Chapter 3.

7.2 Future Work

During this work, several ideas for ongoing research have been identified. In particular, the strategy for increasing the computational speed on large networks prompts intriguing opportunities.

- The heuristic for selecting the control set of MPC in Chapter 4 considers the control of each overloaded line individually. It is possible that several lines may be overloaded simultaneously and feasible that control actions to address one overload may aggravate another. How should the control set be selected to account for this possibility while ensuring that sufficient control is available for MPC to guarantee feasibility?
- The process of selecting control devices for MPC currently uses a tuning parameter α in (4.11) to define a static power flow condition on the overloaded line. However, MPC is driven by the thermal behavior over the entire prediction horizon. A more appropriate tuning parameter would predict the thermal response of every overloaded line while accounting for the cost of controls to select an appropriate control set.
- Solution speed concerns motivate a reduced control set on large networks. A rigorous strategy for characterizing the solution speed as the control set changes should be determined and used to inform the number of controls retained in MPC.
- A method for selecting controls to address voltage collapse should be determined and tested on a realistically sized system. As shown in Section 6.2, the objective coefficients provided to MPC can significantly influence the type and location of controls and should be incorporated into the process.

Additionally, several practical implementation issues provide interesting opportunities for ongoing analysis.

- MPC must quickly transmit control commands to a wide variety of devices spread across the network. How might communication delays influence MPC's performance?
- MPC relies very heavily on the quality of its internal model. Controls will be less useful if the model fails to appropriately match the physical system. How might the model of MPC be tuned and updated in real-time based on system performance? If a control device does not respond to MPC, its future use could be discouraged by increasing the objective coefficient of that control variable. Additionally, load and weather forecasts significantly influence MPC's predictions of future behavior. How might inaccuracies in these models affect MPC?
- In the near-term, system operators may be hesitant to adopt an autonomous control strategy. How might the strategy of MPC be adjusted to provide decision support to a human operator? In the same way that personal navigation devices provide updated route information in response to driving decisions, could techniques from MPC be used to suggest a sequence of control actions implementable by a human operator?

Addressing these issues will provide further clarification of MPC's suitability for real-time electric power system operations. Regardless of the methods ultimately implemented, improving the efficiency and reliability of power systems offers interesting research opportunities with meaningful real-world impact.

Bibliography

[1] "IEEE standard for calculating the current-temperature relationship of bare overhead conductors," *IEEE Std 738-2012 (Revision of IEEE Std 738-2006 - Incorporates IEEE Std 738-2012 Cor 1-2013)*, pp. 1–72, Dec 2013.

[2] T. van Cutsem *et al.*, "Test systems for voltage stability analysis and security assessment," IEEE Power and Energy Society, Tech. Rep. 19, Aug 2015.

[3] J. Minkel, "The 2003 northeast blackout-five years later," *Scientific American*, Aug 2008. [Online]. Available: https://www.scientificamerican.com/article/2003-blackout-five-years-later/

[4] D. Kirschen and G. Strbac, *Fundamentals of Power System Economics*. West Sussex, England: Wiley, 2004.

[5] M. Almassalkhi, Y. Dvorkin, J. Marley, R. Fernandez-Blanco, I. Hiskens, D. Kirschen, J. Martin, H. Pandžić, T. Qiu, M. Sarker, M. Vrakopoulou, Y. Wang, and M. Xue, "Incorporating storage as a flexible transmission asset in power system operation procedure," in *19th Power Systems Computation Conference*, June 2016.

[6] M. Almassalkhi, "Optimization and model-predictive control for overload mitigation in resilient power systems," Ph.D. dissertation, University of Michigan, 2013.

[7] M. Almassalkhi and I. Hiskens, "Model-predictive cascade mitigation in electric power systems with storage and renewables part i: Theory and implementation," *IEEE Transactions on Power Systems*, vol. 30, no. 1, pp. 67–77, Jan 2015.

[8] ——, "Model-predictive cascade mitigation in electric power systems with storage and renewables part ii: Case-study," *IEEE Transactions on Power Systems*, vol. 30, no. 1, pp. 78–87, Jan 2015.

[9] *Large Power Transformers and the U.S. Electric Grid*, United States Department of Energy, Apr 2014.

[10] P. Ristanovic, O. Obadina, and M. Aganagic, "Security constrained optimal power flow method," U.S. Patent 6 775 597, Aug 10, 2004.

[11] *PJM Manual 03: Transmission Operations*, 49th ed., PJM, Jun 2016.

[12] U.S.-Canada Power System Outage Task Force, *Final Report on the August 14, 2003 Blackout in the United States and Canada: Causes and Recommendations*, United States Department of Energy, April 2004.

[13] *PJM Manual 11: Energy & Ancillary Services Market Operations*, 85th ed., PJM, Nov 2016.

[14] S. Tam, "Real-time security-constrained economic dispatch and commitment in the PJM: Experiences and challenges," Jun 2011, unpublished. [Online]. Available: https://www.ferc.gov/CalendarFiles/20110629082452-Jun29-SesC1-Tam-PJM.pdf

[15] S. K. Chang, F. Albuyeh, M. L. Gilles, G. E. Marks, and K. Kato, "Optimal real-time voltage control," *IEEE Transactions on Power Systems*, vol. 5, no. 3, pp. 750–758, Aug 1990.

[16] H. Vu, P. Pruvot, C. Launay, and Y. Harmand, "An improved voltage control on large-scale power system," *IEEE Transactions on Power Systems*, vol. 11, no. 3, pp. 1295–1303, Aug 1996.

[17] D. S. Popovic, V. A. Levi, and Z. A. Gorecan, "Co-ordination of emergency secondary-voltage control and load shedding to prevent voltage instability," *IEE Proceedings - Generation, Transmission and Distribution*, vol. 144, no. 3, pp. 293–300, May 1997.

[18] P. Ristanovic, "Control applications of optimal power flow in EMS," *IEEE Transactions on Power Systems*, vol. 12, no. 1, pp. 451–455, Feb 1997.

[19] X. Wang, G. C. Ejebe, J. Tong, and J. G. Waight, "Preventive/corrective control for voltage stability using direct interior point method," *IEEE Transactions on Power Systems*, vol. 13, no. 3, pp. 878–883, Aug 1998.

[20] E. F. Camacho and C. Bordons, *Model Predictive Control*, 2nd ed. London, UK: Springer-Verlag, 2007.

[21] J. B. Rawlings, "Tutorial overview of model predictive control," *IEEE Control Systems*, vol. 20, no. 3, pp. 38–52, Jun 2000.

[22] M. Larsson, D. Hill, and G. Olsson, "Emergency voltage control using search and predictive control," *International Journal of Electrical Power and Energy Systems*, vol. 24, no. 2, pp. 121 – 130, 2002. [Online]. Available: http://www.sciencedirect.com/science/article/pii/S0142061501000175

[23] M. Larsson and D. Karlsson, "Coordinated system protection scheme against voltage collapse using heuristic search and predictive control," *IEEE Transactions on Power Systems*, vol. 18, no. 3, pp. 1001–1006, Aug 2003.

[24] M. Larsson, "A model-predictive approach to emergency voltage control in electrical power systems," in *2004 43rd IEEE Conference on Decision and Control (CDC)*, vol. 2, Dec 2004, pp. 2016–2022 Vol.2.

[25] I. A. Hiskens and M. A. Pai, "Trajectory sensitivity analysis of hybrid systems," *IEEE Transactions on Circuits and Systems I: Fundamental Theory and Applications*, vol. 47, no. 2, pp. 204–220, Feb 2000.

[26] M. Zima, P. Korba, and G. Andersson, "Power systems voltage emergency control approach using trajectory sensitivities," in *Proceedings of 2003 IEEE Conference on Control Applications, 2003. CCA 2003.*, vol. 1, June 2003, pp. 189–194 vol.1.

[27] M. Zima and G. Andersson, "Model predictive control employing trajectory sensitivities for power systems applications," in *Proceedings of the 44th IEEE Conference on Decision and Control*, Dec 2005, pp. 4452–4456.

[28] I. A. Hiskens and B. Gong, "Mpc-based load shedding for voltage stability enhancement," in *Proceedings of the 44th IEEE Conference on Decision and Control*, Dec 2005, pp. 4463–4468.

[29] A. G. Beccuti, T. Demiray, M. Zima, G. Andersson, and M. Morari, "Comparative assessment of prediction models in voltage control," in *2007 IEEE Lausanne Power Tech*, July 2007, pp. 1021–1026.

[30] L. Jin, R. Kumar, and N. Elia, "Model predictive control-based real-time power system protection schemes," *IEEE Transactions on Power Systems*, vol. 25, no. 2, pp. 988–998, May 2010.

[31] M. Glavic, M. Hajian, W. Rosehart, and T. V. Cutsem, "Receding-horizon multi-step optimization to correct nonviable or unstable transmission voltages," *IEEE Transactions on Power Systems*, vol. 26, no. 3, pp. 1641–1650, Aug 2011.

[32] M. Glavic and T. van Cutsem, "Some reflections on model predictive control of transmission voltages," in *2006 38th North American Power Symposium*, Sept 2006, pp. 625–632.

[33] M. Hajian, W. Rosehart, M. Glavic, H. Zareipour, and T. V. Cutsem, "Linearized power flow equations based predictive control of transmission voltages," in *2013 46th Hawaii International Conference on System Sciences*, Jan 2013, pp. 2298–2304.

[34] S. R. Islam, K. M. Muttaqi, and D. Sutanto, "Multi-agent receding horizon control with neighbour-to-neighbour communication for prevention of voltage collapse in a multi-area power system," *IET Generation, Transmission Distribution*, vol. 8, no. 9, pp. 1604–1615, Sept 2014.

[35] B. S. Howington and G. J. Ramon, "Dynamic thermal line rating summary and status of the state-of-the-art technology," *IEEE Transactions on Power Delivery*, vol. 2, no. 3, pp. 851–858, July 1987.

[36] D. A. Douglass and A. A. Edris, "Real-time monitoring and dynamic thermal rating of power transmission circuits," *IEEE Transactions on Power Delivery*, vol. 11, no. 3, pp. 1407–1418, Jul 1996.

[37] D. J. Morrow, J. Fu, and S. M. Abdelkader, "Experimentally validated partial least squares model for dynamic line rating," *IET Renewable Power Generation*, vol. 8, no. 3, pp. 260–268, April 2014.

[38] N. Balu, T. Bertram, A. Bose, V. Brandwajn, G. Cauley, D. Curtice, A. Fouad, L. Fink, M. G. Lauby, B. F. Wollenberg, and J. N. Wrubel, "On-line power system security analysis," *Proceedings of the IEEE*, vol. 80, no. 2, pp. 262–282, Feb 1992.

[39] A. P. Meliopoulos and A. G. Bakirtzis, "Corrective control computations for large power systems," *IEEE Transactions on Power Apparatus and Systems*, vol. PAS-102, no. 11, pp. 3598–3604, Nov 1983.

[40] L. Lenoir, I. Kamwa, and L. A. Dessaint, "Overload alleviation with preventive-corrective static security using fuzzy logic," *IEEE Transactions on Power Systems*, vol. 24, no. 1, pp. 134–145, Feb 2009.

[41] A. Vergnol, J. Sprooten, B. Robyns, V. Rious, and J. Deuse, "Line overload alleviation through corrective control in presence of wind energy," *Electric Power Systems Research*, vol. 81, no. 7, pp. 1583 – 1591, 2011. [Online]. Available: http://www.sciencedirect.com/science/article/pii/S037877961100071X

[42] F. Capitanescu, J. M. Ramos, P. Panciatici, D. Kirschen, A. M. Marcolini, L. Platbrood, and L. Wehenkel, "State-of-the-art, challenges, and future trends in security constrained optimal power flow," *Electric Power Systems Research*, vol. 81, no. 8, pp. 1731 – 1741, 2011. [Online]. Available: http://www.sciencedirect.com/science/article/pii/S0378779611000885

[43] A. A. Mazi, B. F. Wollenberg, and M. H. Hesse, "Corrective control of power system flows by line and bus-bar switching," *IEEE Transactions on Power Systems*, vol. 1, no. 3, pp. 258–264, Aug 1986.

[44] J. G. Rolim and L. J. B. Machado, "A study of the use of corrective switching in transmission systems," *IEEE Transactions on Power Systems*, vol. 14, no. 1, pp. 336–341, Feb 1999.

[45] W. Shao and V. Vittal, "Corrective switching algorithm for relieving overloads and voltage violations," *IEEE Transactions on Power Systems*, vol. 20, no. 4, pp. 1877–1885, Nov 2005.

[46] A. J. Wood, B. F. Wollenberg, and G. B. Sheblé, *Power Generation, Operation, and Control*, 3rd ed. Hoboken, NJ: Wiley-Interscience, 2014.

[47] W. Shao and V. Vittal, "Lp-based opf for corrective facts control to relieve overloads and voltage violations," *IEEE Transactions on Power Systems*, vol. 21, no. 4, pp. 1832–1839, Nov 2006.

[48] B. Otomega, A. Marinakis, M. Glavic, and T. V. Cutsem, "Emergency alleviation of thermal overloads using model predictive control," in *Power Tech, 2007 IEEE Lausanne*, July 2007, pp. 201–206.

[49] ——, "Model predictive control to alleviate thermal overloads," *IEEE Transactions on Power Systems*, vol. 22, no. 3, pp. 1384–1385, Aug 2007.

[50] J. S. A. Carneiro and L. Ferrarini, "Preventing thermal overloads in transmission circuits via model predictive control," *IEEE Transactions on Control Systems Technology*, vol. 18, no. 6, pp. 1406–1412, Nov 2010.

[51] H. Banakar, N. Alguacil, and F. D. Galiana, "Electrothermal coordination part i: theory and implementation schemes," *IEEE Transactions on Power Systems*, vol. 20, no. 2, pp. 798–805, May 2005.

[52] N. Alguacil, M. H. Banakar, and F. D. Galiana, "Electrothermal coordination part ii: case studies," *IEEE Transactions on Power Systems*, vol. 20, no. 4, pp. 1738–1745, Nov 2005.

[53] J. H. Lee, "Model predictive control: Review of the three decades of development," *International Journal of Control, Automation and Systems*, vol. 9, no. 3, p. 415, 2011. [Online]. Available: http://dx.doi.org/10.1007/s12555-011-0300-6

[54] A. Grancharova and T. A. Johansen, *Explicit Nonlinear Model Predictive Control: Theory and Applications.* Heidelberg: Springer Verlag, 2012.

[55] *PJM Manual 12: Balancing Operations*, 35th ed., PJM, Aug 2016.

[56] *Manual 12: Transmission and Dispatching Operations Manual*, 3rd ed., New York Independent System Operator, Feb 2016.

[57] *Manual 15: Emergency Operations Manual*, 7th ed., New York Independent System Operator, Apr 2016.

[58] J. A. Martin and I. A. Hiskens, "Generalized line loss relaxation in polar voltage coordinates," *IEEE Transactions on Power Systems*, vol. PP, no. 99, pp. 1–1, 2016.

[59] C. Coffrin, P. V. Hentenryck, and R. Bent, "Approximating line losses and apparent power in ac power flow linearizations," in *2012 IEEE Power and Energy Society General Meeting*, July 2012, pp. 1–8.

[60] G. L. Torres and V. H. Quintana, "An interior-point method for nonlinear optimal power flow using voltage rectangular coordinates," *IEEE Transactions on Power Systems*, vol. 13, no. 4, pp. 1211–1218, Nov 1998.

[61] R. A. Jabr, "Modeling network losses using quadratic cones," *IEEE Transactions on Power Systems*, vol. 20, no. 1, pp. 505–506, Feb 2005.

[62] H. Zhong, Q. Xia, Y. Wang, and C. Kang, "Dynamic economic dispatch considering transmission losses using quadratically constrained quadratic program method," *IEEE Transactions on Power Systems*, vol. 28, no. 3, pp. 2232–2241, Aug 2013.

[63] A. L. Motto, F. D. Galiana, A. J. Conejo, and J. M. Arroyo, "Network-constrained multiperiod auction for a pool-based electricity market," *IEEE Transactions on Power Systems*, vol. 17, no. 3, pp. 646–653, Aug 2002.

[64] T. N. dos Santos and A. L. Diniz, "A dynamic piecewise linear model for dc transmission losses in optimal scheduling problems," *IEEE Transactions on Power Systems*, vol. 26, no. 2, pp. 508–519, May 2011.

[65] H. M. Ayres, L. C. P. d. Silva, W. Freitas, M. C. de Almeida, and V. F. d. Costa, "Evaluation of the impact of distributed generation on power losses by using a sensitivity-based method," in *2009 IEEE Power Energy Society General Meeting*, July 2009, pp. 1–6.

[66] H. M. Ayres, D. Salles, and W. Freitas, "A practical second-order based method for power losses estimation in distribution systems with distributed generation," *IEEE Transactions on Power Systems*, vol. 29, no. 2, pp. 666–674, March 2014.

[67] G. Strang, *Linear Algebra and its Applications*, 3rd ed. Harcourt Brace Jovanovich, 1988.

[68] R. D. Zimmerman, C. E. Murillo-Sanchez, and R. J. Thomas, "Matpower: Steady-state operations, planning, and analysis tools for power systems research and education," *IEEE Transactions on Power Systems*, vol. 26, no. 1, pp. 12–19, Feb 2011.

[69] *Gurobi Optimizer Reference Manual*, 6th ed., Gurobi Optimization, Inc., 2015.

[70] O. W. Akinbode and K. W. Hedman, "Fictitious losses in the dcopf with a piecewise linear approximation of losses," in *2013 IEEE Power Energy Society General Meeting*, July 2013, pp. 1–5.

[71] H. Zhang, G. T. Heydt, V. Vittal, and J. Quintero, "An improved network model for transmission expansion planning considering reactive power and network losses," *IEEE Transactions on Power Systems*, vol. 28, no. 3, pp. 3471–3479, Aug 2013.

[72] B. Stott, J. Jardim, and O. Alsac, "Dc power flow revisited," *IEEE Transactions on Power Systems*, vol. 24, no. 3, pp. 1290–1300, Aug 2009.

[73] C. Coffrin and P. Van Hentenryck, "A linear-programming approximation of ac power flows," *INFORMS Journal on Computing*, vol. 26, no. 4, pp. 718–734, May 2014.

[74] T. van Cutsem and C. Vournas, *Voltage Stability of Electric Power Systems*. Norwell, MA: Kluwer Academic, 1998.

[75] C. Taylor, *Power System Voltage Stability*. McGraw-Hill, 1994.

[76] J. Martin and I. Hiskens, "Corrective model-predictive control in large electric power systems," *IEEE Transactions on Power Systems*, vol. PP, no. 99, pp. 1–1, 2016.

[77] A. Wood, B. Wollenberg, and G. Sheblé, *Power Generation, Operation, and Control*, 3rd ed. Wiley, 2013.

[78] F. Dorfler and F. Bullo, "Kron reduction of graphs with applications to electrical networks," *IEEE Transactions on Circuits and Systems I: Regular Papers*, vol. 60, no. 1, pp. 150–163, Jan 2013.

[79] J. B. Ward, "Equivalent circuits for power-flow studies," *Transactions of the American Institute of Electrical Engineers*, vol. 68, no. 1, pp. 373–382, July 1949.

[80] M. Pai, *Energy Function Analysis for Power System Stability*. Kluwer Academic, 1989.

[81] H. Pandžić, Y. Wang, T. Qiu, Y. Dvorkin, and D. S. Kirschen, "Near-optimal method for siting and sizing of distributed storage in a transmission network," *IEEE Transactions on Power Systems*, vol. 30, no. 5, pp. 2288–2300, Sept 2015.

[82] J. K. Felder and I. A. Hiskens, "Optimal power flow with storage," in *Power Systems Computation Conference (PSCC), 2014*, Aug 2014, pp. 1–7.

[83] V. Ajjarapu and C. Christy, "The continuation power flow: a tool for steady state voltage stability analysis," *IEEE Transactions on Power Systems*, vol. 7, no. 1, pp. 416–423, Feb 1992.